
Masters Theses

Student Theses and Dissertations

1969

Anodic behavior of semiconducting InSb single crystals in acidic solutions

Lih-da Hu

Follow this and additional works at: https://scholarsmine.mst.edu/masters_theses



Part of the [Chemical Engineering Commons](#)

Department:

Recommended Citation

Hu, Lih-da, "Anodic behavior of semiconducting InSb single crystals in acidic solutions" (1969). *Masters Theses*. 7070.

https://scholarsmine.mst.edu/masters_theses/7070

This thesis is brought to you by Scholars' Mine, a service of the Missouri S&T Library and Learning Resources. This work is protected by U. S. Copyright Law. Unauthorized use including reproduction for redistribution requires the permission of the copyright holder. For more information, please contact scholarsmine@mst.edu.

ANODIC BEHAVIOR OF SEMICONDUCTING InSb SINGLE CRYSTALS
IN ACIDIC SOLUTIONS

BY

LIH-DA HU, 1942-

A

THESIS

submitted to the faculty of the

UNIVERSITY OF MISSOURI-ROLLA

in partial fulfillment of the requirement for the

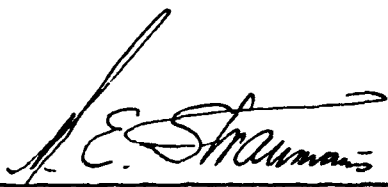
Degree of

MASTER OF SCIENCE IN CHEMICAL ENGINEERING

Rolla, Missouri

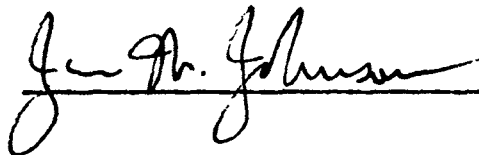
1969

Approved by



(Advisor)





ABSTRACT

Undoped, semiconducting single, n-type, InSb crystals were used to study the different etching behavior of the inverse {111} planes, to determine the apparent electron number of InSb under anodic dissolution (which corresponds to the sum of the absolute values of the oxidation numbers) and to investigate whether or not the inverse {111} planes show potential differences.

The In{111}, Sb{ $\bar{1}\bar{1}\bar{1}$ }, {110} and {100} faces were highly polished, etched and immersed in various acidic solutions. Several new etch patterns of the inverse {111} faces were observed giving other possibilities to distinguish both of these planes. The significant differences in potentials between the inverse {111} faces are exhibited in some acidic solutions. The potential of Sb{ $\bar{1}\bar{1}\bar{1}$ } is always less noble than that of In{111}. The addition of oxidizing or reducing agents does not shift the sequence in potentials of the inverse {111} faces within at least a certain range of current density.

The apparent electron number of InSb dissolving anodically in acidic solutions is close to 6 at low current densities. The deviation from the value of 6, for InSb dissolving anodically in 2 N HCl at current densities higher than $\sim 40 \text{ ma/cm}^2$, is found to be due to surface disintegration after a dark protective film (mainly $\text{Sb}_4\text{O}_5\text{Cl}_2$) is formed on the surface of the specimen. Sb particles, colloidal in origin and embedded in this corrosion product, are responsible for the dark color.

It is also found that the dissolution potentials of the inverse {111} faces of InSb are much closer to that of metallic Sb than to metallic In, indicating that the latter undergoes a larger chemical change during the InSb formation than Sb.

From the observed Tafel behavior and the calculated activation energies of InSb undergoing anodic dissolution in 2 N HCl, within the current density range of $\sim 3 \times 10^{-2}$ to ~ 30 ma/cm², it is concluded that the rate determining step is a one electron discharge and is the same on all four low-indexed crystallographic planes.

ACKNOWLEDGEMENTS

The author wishes to thank Dr. M. E. Straumanis, Research Professor of Metallurgy, and Dr. J. W. Johnson, Professor of Chemical Engineering for their advice, support, and encouragement during the course of this investigation. He also wishes to thank Dr. W. J. James, Professor of Chemistry and Director of the Graduate Center for Materials Research, for his assistance in this study.

Thanks are extended to the Graduate Center for Materials Research for the use of its facilities and equipment.

The author is also grateful to the New Enterprise Division of the Monsanto Company, St. Louis, especially to Mr. J. B. McNeely, for donation of the InSb crystals and to the Office of Naval Research and the University of Missouri-Rolla for financial assistance.

TABLE OF CONTENTS

	page
LIST OF FIGURES.....	viii
LIST OF TABLES.....	xii
I. INTRODUCTION.....	1
II. LITERATURE REVIEW.....	2
A. Crystal Structure and Surface Character- istics.....	2
B. Chemical and Anodic Etching.....	6
C. Anodic Dissolution and the Relationship Between the Current Density and Potential.....	8
III. MICROSCOPIC STUDIES OF InSb SINGLE CRYSTALS... ..	11
A. Materials.....	11
B. Apparatus and Procedure.....	11
C. Results.....	15
1. The determination of the inverse InSb{111} planes by chemical etching.....	15
2. The microscopic observation of etch patterns on the inverse InSb{111} planes by chemical etching in other etchants.....	17
3. Etch patterns on the inverse InSb{111} planes obtained by anodic etching in some acids.....	19
4. Etch pattern on the In{111} face obtained anodically in 2 N HCl and then etched chemically with HCl-Fe ³⁺ etchant.....	23
IV. THE DETERMINATION OF THE ELECTRON NUMBER OF THE ANODIC DISSOLUTION REACTION FOR InSb SINGLE CRYSTALS.....	24

A. Materials.....	24
B. Apparatus and Procedure.....	24
C. Results.....	27
1. Self-dissolution rates of InSb in various electrolytes.....	27
2. Apparent electron number of InSb in various electrolytes.....	27
a. In 2 N HCl.....	27
b. In 1 N HNO ₃ -1 N H ₂ C ₄ H ₄ O ₆	34
c. In 2 N HCl with Fe ³⁺ additions...	35
3. Reason for the decline of the valency number at increased current densities.....	35
V. MEASUREMENTS OF DISSOLUTION POTENTIALS OF InSb SINGLE CRYSTALS.....	42
A. Materials.....	42
B. Dissolution Potential Without Anodic Current.....	42
1. Apparatus and procedure.....	42
2. Data and results.....	42
a. Measurements of dissolution potential without anodic current of the inverse {111} faces of an InSb single crystal in aqueous HCl solution.....	42
b. Measurements of dissolution potential without anodic current of the inverse {111} faces of an InSb single crystal in various concentrations of HCl with 0.1 N Fe ³⁺ additions..	44
C. The Anodic Potential-Current Density Relationship for an InSb Single Crystal	47
1. In 2 N HCl.....	48
2. In 1 N HNO ₃ -1 N H ₂ C ₄ H ₄ O ₆	49
3. In 2 N HCl with Fe ³⁺ additions.....	51

4.	In 2 N HCl with Fe^{2+} additions.....	54
5.	In 2 N HCl with $\text{K}_3\text{Fe}(\text{CN})_6$ and $\text{K}_4\text{Fe}(\text{CN})_6$ additions.....	56
VI.	EFFECT OF TEMPERATURE ON THE DISSOLUTION POTENTIAL-CURRENT DENSITY RELATIONSHIP OF InSb SINGLE CRYSTALS DISSOLVING ANODICALLY IN 2 N HCl.....	60
A.	Materials.....	60
B.	Apparatus and Procedure.....	60
1.	Galvanostatic experiments.....	60
2.	Potentiostatic experiments.....	60
C.	Data and Results.....	60
1.	The dissolution potential-current density relationship for InSb single crystals dissolving anodically at various temperatures.....	60
2.	Activation energy calculations.....	62
a.	E_a from galvanostatic measure- ments.....	65
b.	E_a from potentiostatic measure- ments.....	68
VII.	DISCUSSION.....	73
A.	Anodic Dissolution and Potentials.....	73
B.	Etching Behavior of the {111} surfaces... ..	78
C.	Coulometric Measurements and Disinte- gration.....	81
VIII.	SUMMARY AND CONCLUSION.....	84
	BIBLIOGRAPHY.....	86
	APPENDICES.....	88
A.	Materials.....	89
B.	Equipment.....	90
C.	Experimental Data (Tables VIII to XXXII and XXXV to XXXVI).....	92
	VITA.....	122

LIST OF FIGURES

Figure	page
1. Zinc-blende crystal structure.....	5
2. The interference rings show that the InSb wafer is highly polished.....	13
3. Distortion exhibited by mechanical polished wafer after chemical etching.....	13
4. Cross section of the InSb electrode.....	14
5. Etch patterns of an InSb{111} face, defined as In{111}.....	16
6. Etch pattern of an InSb{111} face, defined as Sb{ $\bar{1}\bar{1}\bar{1}$ }.....	16
7. Etch patterns on In{111} produced by HCl-Fe ³⁺ ..	17
8. Etch pattern on Sb{ $\bar{1}\bar{1}\bar{1}$ } produced by HCl-Fe ³⁺ ..	17
9. Etch patterns on In{111} produced by HNO ₃ -HF...	18
10. Etch pattern on Sb{ $\bar{1}\bar{1}\bar{1}$ } produced by HNO ₃ -HF....	18
11. In{111} face etched anodically in 2 N HCl.....	19
12. Sb{ $\bar{1}\bar{1}\bar{1}$ } face etched anodically in 2 N HCl.....	20
13. In{111} face etched anodically in 1 N HNO ₃ - 1 N H ₂ C ₄ H ₄ O ₆	22
14. Sb{ $\bar{1}\bar{1}\bar{1}$ } face etched anodically in 1 N HNO ₃ - 1 N H ₂ C ₄ H ₄ O ₆	22
15. In{111} face etched anodically in 2 N HCl and then chemically in HCl-Fe ³⁺	23
16. Sketch of the apparatus used for potential measurements or electron number determinations of InSb single crystals undergoing anodic dissolution.....	25
17. Calculated electron number of InSb single crystals as a function of current density of the faces In{111}, Sb{ $\bar{1}\bar{1}\bar{1}$ }, {110} and {100} dissolving anodically in 2 N HCl.....	33

Figure	page
18. Cross section of the black film normally to its surface.....	36
19. A piece of black film resulting from anodic dissolution of In{111} of InSb in 2 N HCl. Substrate side.....	37
20. The same as in Fig. 19. Electrolyte side.....	37
21. The particle of the annealed black film resulting from anodic dissolution in 2 N HCl. Reflected light.....	40
22. Same as shown in Fig. 21 but in transmitted light.	40
23. The white material sticking to the wall of the glass tubing after InSb black film was annealed. Reflected light.....	40
24. Same as shown in Fig. 23 but in transmitted light.	40
25. A selected particle of the residue of the annealed black film of InSb. Reflected light.....	41
26. The same as in Fig. 25 but in transmitted light...	41
27. Sketch showing the end of capillary tube in detail	43
28. Dissolution potentials without anodic current of the inverse {111} faces of InSb versus time in various concentrations of HCl at 25°C.....	45
29. Dissolution potentials without anodic current of the inverse {111} faces of InSb versus time in various concentrations of HCl with Fe ³⁺ additions at 25°C.....	46
30. Anodic dissolution potentials E_H' of InSb versus log of current density i of the planes In{111}, Sb{ $\bar{1}\bar{1}\bar{1}$ }, {110} and {100} at 25°C.....	49
31. Anodic dissolution potentials E_H' of the inverse {111} faces of InSb versus log of current density i in 1 N HNO ₃ -1 N H ₂ C ₄ H ₄ O ₆ at 25°C.....	50

Figure	page
32. Anodic dissolution potentials E_H' of the inverse {111} faces of InSb versus log of current density i in 2 N HCl with Fe^{3+} additions at 25°C.	53
33. Anodic dissolution potentials E_H' of the inverse {111} faces of InSb versus current density i in 2 N HCl at 25°C.....	55
34. Anodic dissolution potentials E_H' of the inverse {111} faces of InSb versus log of current density i in 2 N HCl with $K_3Fe(CN)_6$ and $K_4Fe(CN)_6$ additions at 25°C.....	57
35. Sketch of the apparatus used for potentiostatic studies of InSb single crystals undergoing anodic dissolution.....	61
36. Anodic dissolution potentials E_H' of the In{111} face of InSb versus current density i in 2 N HCl at three temperatures.....	63
37. Anodic dissolution potentials E_H' of the Sb{ $\bar{1}\bar{1}\bar{1}$ } face of InSb versus current density i in 2 N HCl at three temperatures.....	64
38. Arrhenius plot of the anodic dissolution of InSb single crystals in 2 N HCl. Galvanostatic measurements.....	67
39. Arrhenius plot of the anodic dissolution of InSb single crystals in 2 N HCl. Potentiostatic measurements.....	71
40. Two-dimensional representation of the zinc-blende structure with surface steps.....	74
41. Schematic diagram of the electronic structure of a single InSb crystal.....	75

Figure	page
42. Anodic dissolution potentials E_H' of metallic In, metallic Sb and the inverse {111} faces of an InSb single crystal versus log of current density i in 2 N HCl at 25°C.....	77
43. Representation of a {111} face with an atomic pit and kink.....	79

LIST OF TABLES

TABLE	PAGE
I. The Weight Loss of InSb Electrode in Various Electrolytes at 25°C with Zero External Current Applied.....	28
II. The Apparent Electron Number of an InSb Single Crystal with the In{111} Face in 2 N HCl at 25°C	29
III. The Apparent Electron Number of an InSb Single Crystal with the Sb{ $\bar{1}\bar{1}\bar{1}$ } Face in 2 N HCl at 25°C	30
IV. The Apparent Electron Number of an InSn Single Crystal with the {110} Face in 2 N HCl at 25°C..	31
V. The Apparent Electron Number of an InSb Single Crystal with the {100} Face in 2 N HCl at 25°C..	32
VI. The Apparent Electron Number of an InSb Single Crystal in 1 N HNO ₃ -1 N H ₂ C ₄ H ₄ O ₆ at 25°C.....	34
VII. The Apparent Electron Number of an InSb Single Crystal in 2 N HCl-0.005 N Fe ³⁺ at 25°C.....	35
VIII. Dissolution Potential of the Inverse {111} Faces of an InSb Single Crystal Versus Time without Anodic Current in 1 N HCl at 25°C.....	93
IX. Dissolution Potential of the Inverse {111} Faces of an InSb Single Crystal Versus Time without Anodic Current in 2 N HCl at 25°C.....	94
X. Dissolution Potential of the Inverse {111} Faces of an InSb Single Crystal Versus Time without Anodic Current in 4 N HCl at 25°C.....	95
XI. Dissolution Potential of the Inverse {111} Faces of an InSb Single Crystal Versus Time without Anodic Current in 2 N HCl-0.1 N Fe ³⁺ at 25°C....	96
XII. Dissolution Potential of the Inverse {111} Faces of an InSb Single Crystal Versus Time without Anodic Current in 4 N HCl-0.1 N Fe ³⁺ at 25°C....	97

TABLE	PAGE
XIII. Anodic Dissolution Potential of the In{111} Face of an InSb Single Crystal in 2 N HCl at 25°C....	98
XIV. Anodic Dissolution Potential of the Sb{ $\bar{1}\bar{1}\bar{1}$ } Face of an InSb Single Crystal in 2 N HCl at 25°C....	100
XV. Anodic Dissolution Potential of the {110} Face of an InSb Single Crystal in 2 N HCl at 25°C....	102
XVI. Anodic Dissolution Potential of the {100} Face of an InSb Single Crystal in 2 N HCl at 25°C....	103
XVII. Anodic Dissolution of the In{111} Face of an InSb Single Crystal in 1 N HNO ₃ -1 N H ₂ C ₄ H ₄ O ₆ at 25°C.....	104
XVIII. Anodic Dissolution Potential of the Sb{ $\bar{1}\bar{1}\bar{1}$ } Face of an InSb Single Crystal in 1 N HNO ₃ - 1 N H ₂ C ₄ H ₄ O ₆ at 25°C.....	105
XIX. Anodic Dissolution Potential of the In{111} Face of an InSb Single Crystal in 2 N HCl- 0.0004 M Fe ³⁺ at 25°C.....	106
XX. Anodic Dissolution Potential of the Sb{ $\bar{1}\bar{1}\bar{1}$ } Face of an InSb Single Crystal in 2 N HCl- 0.0004 M Fe ³⁺ at 25°C.....	107
XXI. Anodic Dissolution Potential of the In{111} Face of an InSb Single Crystal in 2 N HCl- 0.002 M Fe ³⁺ at 25°C.....	108
XXII. Anodic Dissolution Potential of the Sb{ $\bar{1}\bar{1}\bar{1}$ } Face of an InSb Single Crystal in 2 N HCl- 0.002 M Fe ³⁺ at 25°C.....	109
XXIII. Anodic Dissolution Potential of the In{111} Face of an InSb Single Crystal in 2 N HCl- 0.002 M Fe ²⁺ at 25°C.....	110
XXIV. Anodic Dissolution Potential of the Sb{ $\bar{1}\bar{1}\bar{1}$ } Face of an InSb Single Crystal in 2 N HCl- 0.002 M Fe ²⁺	111

TABLE	PAGE
XXV. Anodic Dissolution Potential of the In{111} Face of an InSb Single Crystal in 2 N HCl- 0.00125 M $K_3Fe(CN)_6$ at 25°C.....	112
XXVI. Anodic Dissolution Potential of the Sb{ $\bar{1}\bar{1}\bar{1}$ } Face of an InSb Single Crystal in 2 N HCl- 0.00125 M $K_3Fe(CN)_6$ at 25°C.....	113
XXVII. Anodic Dissolution Potential of the In{111} Face of an InSb Single Crystal in 2 N HCl- 0.00125 M $K_4Fe(CN)_6$ at 25°C.....	114
XXVIII. Anodic Dissolution Potential of the Sb{ $\bar{1}\bar{1}\bar{1}$ } Face of an InSb Single Crystal in 2 N HCl- 0.00125 M $K_4Fe(CN)_6$ at 25°C.....	115
XXIX. Anodic Dissolution Potential of the In{111} Face of an InSb Single Crystal in 2 N HCl at 35°C....	116
XXX. Anodic Dissolution Potential of the In{111} Face of an InSb Single Crystal in 2 N HCl at 45°C....	117
XXXI. Anodic Dissolution Potential of the Sb{ $\bar{1}\bar{1}\bar{1}$ } Face of an InSb Single Crystal in 2 N HCl at 35°C....	118
XXXII. Anodic Dissolution Potential of the Sb{ $\bar{1}\bar{1}\bar{1}$ } Face of an InSb Single Crystal in 2 N HCl at 45°C.....	119
XXXIII. Data Used to Make Arrhenius Plot for the Anodic Dissolution of InSb Single Crystals in 2 N HCl..	66
XXXIV. Data Used to Make Arrhenius Plot for the Anodic Dissolution of InSb Single Crystals in 2 N HCl at a Potential of 101 mv (SHE). Potentiostatic Measurements.....	69
XXXV. Anodic Dissolution Potential of Metallic Indium in 2 N HCl at 25°C.....	120
XXXVI. Anodic Dissolution Potential of Metallic Antimony in 2 N HCl at 25°C.....	121

I. INTRODUCTION

InSb is a III-V intermetallic compound with a cubic zinc-blende structure which is noncentrosymmetric. Such crystals (without a symmetry) are polar; the polarity shows up through differences in chemical and physical behavior of the inverse planes of the respective crystals.

Reports have been made in the literature that the various crystal planes react differently in aqueous media, such that the III{111} and V{ $\bar{1}\bar{1}\bar{1}$ } inverse planes can be distinguished by the development of specific etch patterns. However, there are major disagreements especially concerning whether or not there is a significant difference of the electrode potential between the two inverse {111} faces.

The intention of the present investigation was to use high purity InSb crystals and try to establish mainly: (1) the different etching behavior between the inverse {111} faces in order to develop some new etch patterns for identifying the inverse {111} planes and also to prove that polarity does exist in the [111] direction, (2) the charge of cations going into solution in order to have some clarity regarding anodic dissolution reactions, and (3) the electrode potentials exhibited in various solutions by the inverse {111} faces and also by the {110} and {100} planes in order to see whether or not the potentials relate to the orientation of the single crystals.

II. LITERATURE REVIEW

This literature review on semiconducting InSb single crystals is divided into three parts: (1) crystal structure and surface characteristics, (2) chemical and anodic etching, and (3) anodic dissolution and the relationship between the current density and potential.

A. Crystal Structure and Surface Characteristics

Atoms from group IIIA of the periodic table combine with atoms from VA to form cubic semiconducting compounds of diamond structure called "III-V compounds". They may be considered as chemical compounds with very close to 1:1 atomic ratios between the III and V atoms, which occupy alternate sites in the crystal lattice. For example, if we melt a mixture of indium and antimony, the compound InSb is formed, and, upon solidification any excess of either constituent appears as a second phase.

III atoms have one valence electron less, and V atoms one electron more than those atoms of the group IV of the periodic table which form semiconducting crystals such as diamond, germanium, silicon and grey tin. III-V compounds have, therefore, the same average number of electrons per atom as the group IV semiconductors, and it is found that the former indeed have a crystal structure and electronic properties which are in many respects similar to those of the group IV semiconductors. Nevertheless, III-V compounds possess characteristic properties which distinguish them

from the group IV semiconductors. These differences arise chiefly from the fact that the compound crystals have a lower symmetry than the group IV semiconductors. The latter possess covalently bound neutral atoms, whereas the III-V compounds contain in part, positive and negative ions at the lattice sites. Though III-V crystals have a structure similar to that of diamond, there are two kinds of atoms in the unit cell. Nevertheless the compounds sometime show a simpler behavior than the monatomic group IV semiconductors.

There are two types of semiconductors, n- and p-type. The term "n-type" is used to describe material in which there are more conductive electrons than holes, and p-type to describe material with more holes than electrons¹⁾. Most engineering applications of semiconductors involve pure semiconductor materials (the impurity content is generally less than 1 p.p.m.) which have been doped with specific impurities to produce higher conductivity²⁾.

Nearly all the III-V compounds crystallize in an arrangement where each atom is at the center of a regular tetrahedron with the other kind of atoms at the corners. These tetradra can be arranged in the cubic "zinc-blende" and the hexagonal "wurzite"* structures. The cubic zinc-blende structure is identical to that of diamond except that the two different kinds of atoms occupy alternate positions in the lattice. Each of the III and V atoms lie on a separate face-centered-cubic sub-lattice, displaced relative to each

*In some articles the word "wurtzite" is used.

other by one quarter of the body diagonal of the cube. The wurzite structure is similar to zinc-blende except that alternate $\{111\}$ layers are rotated through 180° about the $\{111\}$ axis, giving a structure of hexagonal symmetry³⁾.

Because of the lack of a symmetry center the $[111]$ directions form polar axes, and there is a distinction between $[111]$ and $[\bar{1}\bar{1}\bar{1}]$ directions. There is also a distinction between $\{111\}$ and $\{\bar{1}\bar{1}\bar{1}\}$ faces of a crystal. If we define the direction from a III atom to a neighboring V atom as the $[111]$ direction, and from V to III atom as the $[\bar{1}\bar{1}\bar{1}]$ direction, we may consider a crystal bounded by $\{111\}$ faces and define $\{111\}$ and $\{\bar{1}\bar{1}\bar{1}\}$ faces as follows: a $\{111\}$ face is that face which is crossed perpendicularly, going from the inside to the outside of the crystal, by motion along a $[111]$ direction. Conversely a $\{\bar{1}\bar{1}\bar{1}\}$ face is crossed by motion along a $[\bar{1}\bar{1}\bar{1}]$ direction. Fig. 1 shows that a zinc-blende structure III-V crystal viewed perpendicularly to a $[111]$ direction appears as a series of double layers of III and V atoms. We see that $\{111\}$ faces contain either III atoms held to neighboring atoms of the other kind by three bonds or V atoms held by only one bond. On a $\{\bar{1}\bar{1}\bar{1}\}$ plane the binding of the two kinds of atoms is reversed. It is probable that the $\{111\}$ crystal surfaces are made up of atoms triply bonded to neighboring atoms of the other kind, so that $\{111\}$ faces consist of III atoms and $\{\bar{1}\bar{1}\bar{1}\}$ faces of V atoms⁴⁾. For such a structure the $[111]$ (or $[\bar{1}\bar{1}\bar{1}]$) direction is known as the polar axis.

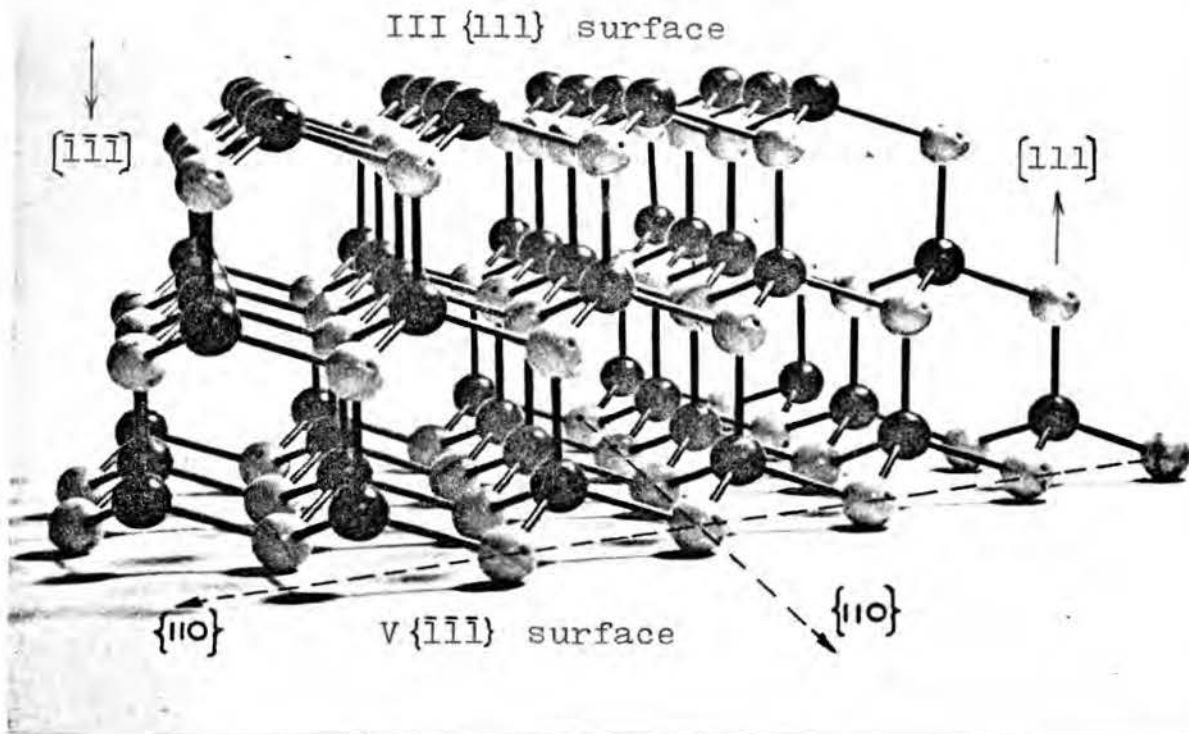


Fig. 1

Zinc-blende crystal structure. The bonds joining neighboring unlike lie along the $[111]$ directions. Lines joining nearest like atoms lie along $[110]$ directions. (Picture from the frontispiece of "Semiconducting III-V Compounds" by C. Hilsum and A. C. Rose-Innes. Pergamon Press, New York, Oxford, London, Paris. 1961).

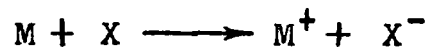
In principle $\{111\}$ and $\{\bar{1}\bar{1}\bar{1}\}$ faces can be distinguished either by X-ray measurements or by chemical or anodic etching⁵⁾. Once X-ray measurements and etch pit observations have been correlated for a certain compound, the methods may be used to distinguish between $\{111\}$ and $\{\bar{1}\bar{1}\bar{1}\}$ faces of other samples of the same compound. Warekois and Metzgen⁵⁾, White and Roth⁶⁾ and Gatos and Lavine⁷⁾ observed that, with etchants containing oxidizing agents, dislocation pits are produced on the $\{111\}$ but not on the inverse $\{\bar{1}\bar{1}\bar{1}\}$ faces of semiconducting III-V compounds single crystals, such as InSb, GaSb, AlSb, GaAs, InAs and InP. Dewald⁸⁾ reported in 1957 that, at low electric field, the rates of oxidation of the $\{111\}$ and $\{\bar{1}\bar{1}\bar{1}\}$ faces of InSb in a KOH electrolyte are quite different, a result of the different binding of the atoms to the neighboring ones in the lattice on these two faces. In 1960 Gatos et. al.⁹⁾ observed again that crystals of InSb grow more easily along the $[\bar{1}\bar{1}\bar{1}]$ direction than along the $[111]$. They suggested that this preferential growth and the formation of etch pits on $\{111\}$ faces only is a result of differential reactivity of the atoms on the $\{111\}$ inverse faces.

B. Chemical and Anodic Etching

The most common semiconductor materials--germanium, silicon, and III-V intermetallic compounds--are brittle. Wafers are normally cut and polished with abrasive materials. As a result, a layer with a disrupted crystal structure and with a large number of defects and dislocations is formed close to the surface. Either chemical or anodic etching is

used to removed this layer with the distorted structure.

Chemical etching is a dissolution of the surface layer with an etchant without the passage of an electric current. The name "chemical etching" can not be regarded as well-chosen, because this process has often an electrochemical nature. Upon etching, oxidation occurs and the overall equation of the process has the form



where M^+ (cation) is the oxidized form of M (atoms of the semiconductors) and X is the oxidant, changing to X^- after the reaction.

Many different etching agents have been described in the literature^{7,10,11,12}). Most contain nitric, hydrofluoric, acetic acids and hydrogen peroxide in various combinations with small amounts of iodine, bromine, and some metallic salts¹³).

The III-V semiconductors, with the zinc-blende type of crystal structure, have generally similar growth and etching characteristics as compared with diamond-type semiconductors. Generally the "Ga" and "In" $\{111\}$ faces normally show pits, while the "As" and "Sb" $\{\bar{1}\bar{1}\bar{1}\}$ faces do not. It was shown that the Group III and Group V $\{111\}$ faces behave similarly in all other III-V compounds⁷). Faust and Sagar¹⁰), Lavine, Gatos and Finn¹¹) have also shown that most etchants etch Sb $\{\bar{1}\bar{1}\bar{1}\}$ faster than In $\{111\}$ faces and, therefore, produce pits only at dislocation sites on In $\{111\}$. Inhibitors can slow down attack on Sb $\{\bar{1}\bar{1}\bar{1}\}$ ¹⁴).

In anodic etching both the current and the etching time can be readily controlled; the electrolytic treatment is obviously more flexible. This is a great advantage as compared to the chemical process. The cleanliness of electrolytic etching results from the fact that it produces soluble products (choosing the respective electrolytes) and therefore no residue is left on the surface. Anodic etching can be used to locate crystallographic directions, to bring out junctions, to expose crystal imperfections or inhomogeneous distributions of impurities¹⁵⁾.

Electropolishing is also a kind of electrolytic treatment for removing damaged material from the surface of the crystal. The main difference between anodic etching and electropolishing is that in the former usually a smaller current density is used than for the latter. InSb has been electropolished by Dewald⁸⁾ in a solution containing 10 parts of HClO_4 , 40 parts of acetic anhydride, and 2 parts of water used at 5°C at a current density of 50 ma/cm^2 . A black oxide film resulted, which spalled off in water. In this way a mirror-bright surface was obtained.

C. Anodic Dissolution and the Relationship Between the Current Density and Potential

All anodic processes on metal or semiconductor electrode are oxidation reactions. The reaction may involve dissolution of the electrode material or oxidation of ions in solution. This principle applies to anodes in electrolytic cell where current is forced through the cell by an external power source, e.g. battery. Under

certain conditions, anodic films may be formed which can grow to a considerable thickness provided that there is an adequate rate of ionic conduction through the film¹⁶⁾.

The chemical and anodic dissolution reactions of III-V semiconductors have been studied by Gatos et al.^{7,14)}, Pleskov¹⁷⁾, Gerischer^{18,19)}, Dewald⁸⁾, Harvey²⁰⁾ and Straumanis et al.²¹⁾ Dewald⁸⁾ reported that at low electric fields the rates of oxidation of the {111} and $\{\bar{1}\bar{1}\bar{1}\}$ faces of InSb in a KOH electrolyte are quite different. He also investigated the anodic film formation on single crystal InSb. He found that metallic oxides of unspecified composition were contained in the anodic film. Gatos et al.⁷⁾ reported significant differences in electrode potential (75 mv or greater) between the two inverse {111} faces in various etching media in the vicinity of 0°C. In addition, the electrode of In{111} was always more noble than that of Sb $\{\bar{1}\bar{1}\bar{1}\}$, consistent with the rate measurements²²⁾. Harvey²⁰⁾ found that the anodic dissolution reaction of GaAs proceeded quantitatively in well-stirred solutions of KOH and HClO₄ with the formation of soluble Ga³⁺ and As³⁺ compounds. He reported no potential difference between the two inverse GaAs {111} faces, but examination of his data reveals that the anodic potentials on Ga {111} are more noble than on As $\{\bar{1}\bar{1}\bar{1}\}$, at least up to to current densities of 50 ma/cm². Straumanis et al.²¹⁾ found definitely that in 1 N KOH electrolyte the Ga {111} face has a nobler rest and anodic potential than the As $\{\bar{1}\bar{1}\bar{1}\}$, and the anodic potentials of the

{110} and {100} planes lie in between those of the {111} planes. On the contrary, Gerischer^{18,19)} found no difference either in dissolution rates or in the current density-potential curves.

III. MICROSCOPIC STUDIES OF InSb SINGLE CRYSTALS

A. Materials

The single InSb crystals were obtained from the Monsanto Company (St. Louis, Mo.). They were grown in the {111} direction by the Czochralski or the gradient-freeze technique. They were of the n-type with no dopants. The impurity level was less than 1 p.p.m. The other specifications are as follows:

Face Orientation	Carrier Concentration atoms/c.c.	Mobility $\text{cm}^2/\text{volt-sec}$	Resistivity ohm-cm	Etch Pit Density EP/ cm^2
{111}	8×10^{15}	1.7×10^5	0.005	670
{110} & {100}	4.1×10^{14}	5.6×10^5	0.03	770

B. Apparatus and Procedure

Two different sizes of wafers, ~8 and ~12 mm in diameter, and ~2 mm thick, were cut from the single crystal rod with a wire-blade slicer using a SiC slurry. The orientation of the faces of these wafers was checked by means of Laue back-reflection patterns. The plane was aligned normally to the X-ray beam. The {111} plane could be recognized from the 3-fold symmetry of the Laue back-reflection patterns. The {110} or {100} planes showed a 2-fold or 4-fold symmetry respectively. If there were deviations from one of the faces mentioned, the respective

surface planes were so adjusted by successive grinding of the wafers at a certain angle with fine SiC paper, wetted with distilled water, so that the desired orientation appeared on the Laue patterns.

The damaged surface layer and the scratches present on the wafers were removed mechanically by grinding on 600 grit SiC paper and then by polishing on silk cloth, first with 3 micron SiC slurry then with 0.05 micron gamma polishing alumina. After these polishing procedures, the wafers had a mirror-like appearance (Fig. 2). In order to remove all the remaining mechanical surface irregularities, a chemical polisher, modified CP-4^{8,14)} (2 conc. HNO₃ + 1 conc. HF + 1 glacial CH₃COOH, in parts by volume), was used. The etching time was around 2 seconds depending on the temperature and the condition of the surface area. After this treatment the wafers were immediately transferred into the mixture of dilute aqueous tartaric acid and dilute nitric acid to prevent formation of a surface film. Finally the wafers were rinsed in distilled water and dried with acetone. Thus the surfaces were considered to be flat although slightly undulating²³⁾ as observed under the interference microscope (Fig. 3). After that the wafers were etched chemically by immersing them into a specific etchant for a certain time. Then after immediate rinsing in distilled water and drying with acetone, the wafers were ready for microscopic observation.

In anodic dissolution a good ohmic contact is of

importance. The rough, unpolished side of the wafer was used to make such a contact by pressing a Pt foil to the wafer in a Teflon electrode holder (Fig. 4). Teflon does not dissolve in acids and repels water. The cap of the Teflon electrode holder was sealed with a small amount of vaseline to prevent any electrolyte leaking into the holder. The pressure of the screw cap against the wafer was equalized by the use of an O-ring below the Pt foil. Thus only one side of the wafer was exposed to the electrolyte.

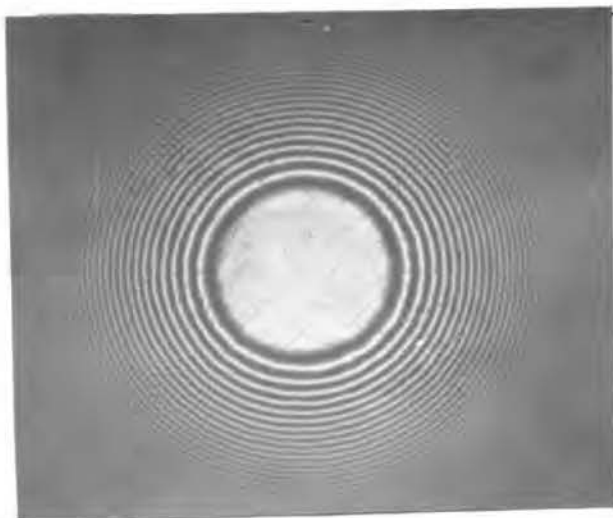


Fig. 2

The interference rings show that the InSb wafer is highly polished. 165X.

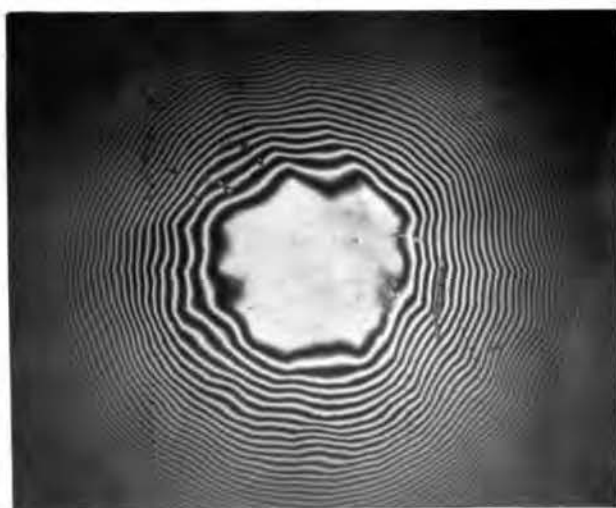


Fig. 3

Distortion exhibited by mechanically polished wafer after chemical etching. 165X.

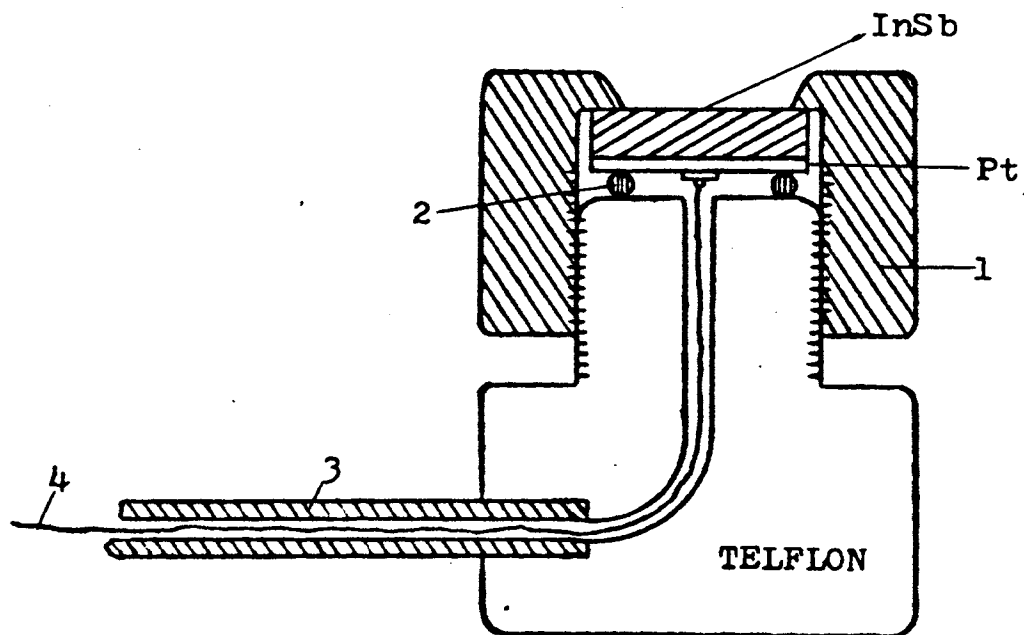


Fig. 4

InSb electrode, cross section. 1. Teflon screw cap; 2. O-ring; 3. Teflon tube (screwed in); 4. Cu lead wire.

C. Results

1. The determination of the inverse InSb{111} planes by chemical etching. A mark was placed on one face of the wafer with parallel {111} plane to distinguish this face from the other one. Both faces were etched anew by the modified CP-4 for 5 sec at about 25°C. The etch patterns are shown in Fig. 5 and 6, and it can be seen that they differ from each other.

Warekois and Metzga⁵⁾ using the X-ray technique of White and Roth⁶⁾ showed that for InAs, pits were produced on the {111} surface, containing In atoms on the surface. Once X-ray pictures and etch formation have been correlated for similar compounds, the etch patterns may be used to distinguish between {111} and {111} faces of other samples of III-V compounds of the same structure. It has been shown that in etchants containing oxidizing agents, pits are produced on the III-faces of III-V compounds but not on the V-faces. Examples are InSb, GaSb, AlSb, GaAs and InP^{5,6,7)}. Thus, from these three papers and from the present results which are shown in Fig. 5 and 6, it is evident that the In{111} face is that on which conical etch pits are developed (Fig. 5 a and b). The other {111} face which does not produce pits and is shown in Fig. 6, is hence defined as Sb{111} face.

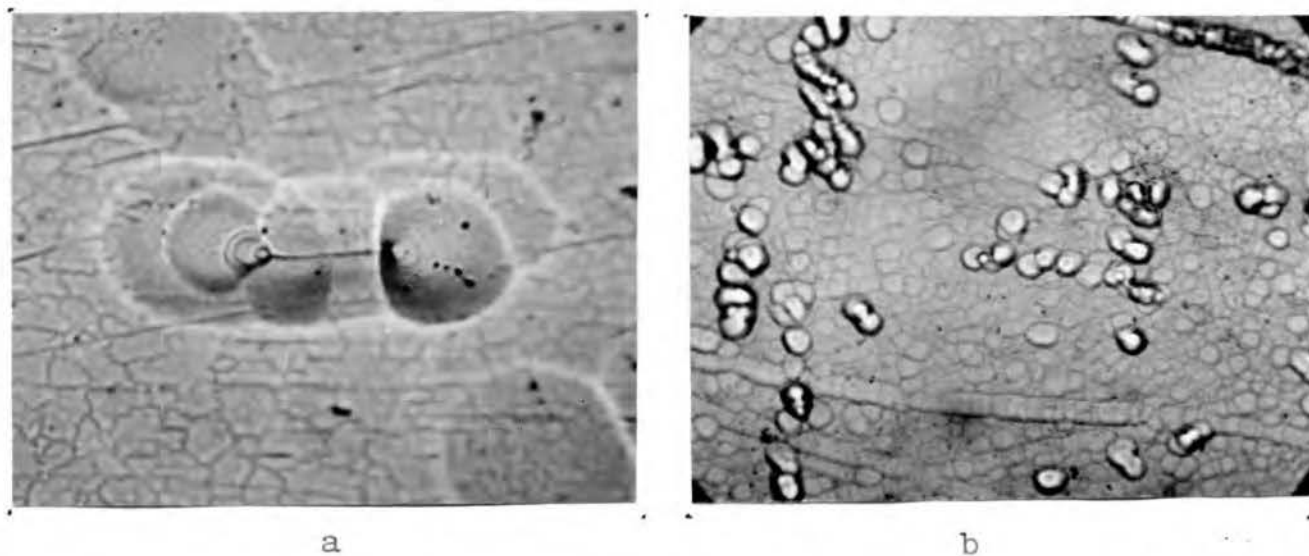
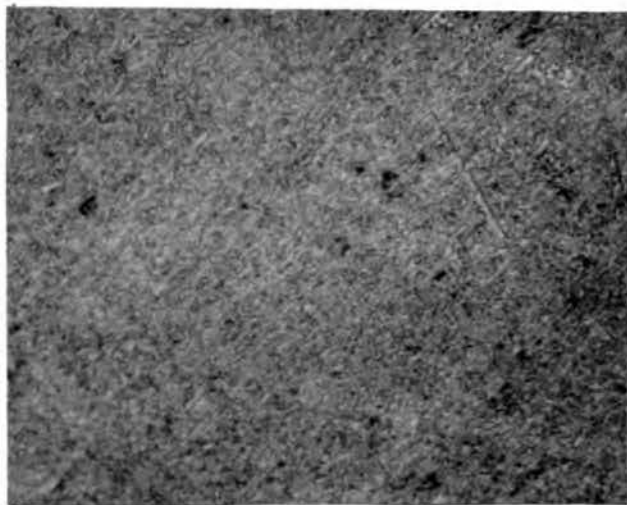


Fig. 5

Etch patterns of an $\text{InSb}\{111\}$ face, defined as $\text{In}\{111\}$.
 Etchant: modified CP-4; 5 sec; 25°C .
 a. 970X; b. 200X.

Fig. 6-

Etch pattern of an $\text{InSb}\{111\}$
 face, defined as $\text{Sb}\{\bar{1}\bar{1}\bar{1}\}$.
 Etchant: modified CP-4; 5 sec;
 25°C . 970X.



2. The microscopic observation of etch patterns on the inverse InSb{111} planes by chemical etching in other etchants. Since the inverse InSb{111} planes can now be identified, the etch figures on the two faces obtained with other etchants are as follows.

a. The etch patterns on the In{111} face produced by the HCl-Fe³⁺ etchant are shown in Fig. 7 a and b.



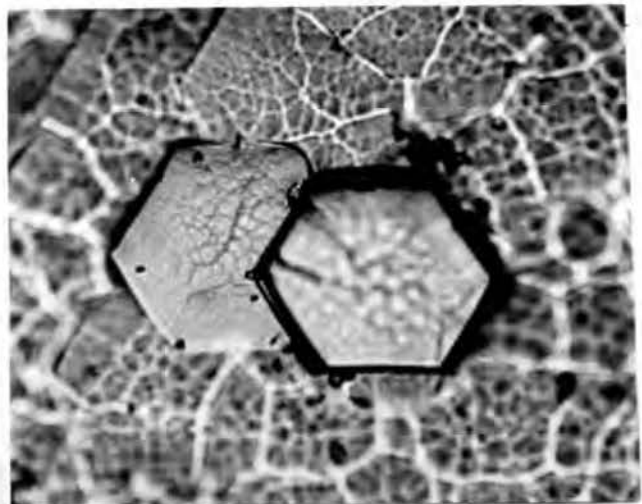
Fig. 7

Etch patterns on In{111} produced by: a. 6 N HCl-0.2 N Fe³⁺; 20 min; 80°C; 970X. b. 2 N HCl-0.5 N Fe³⁺; 24 hr; 25°C; 90X.

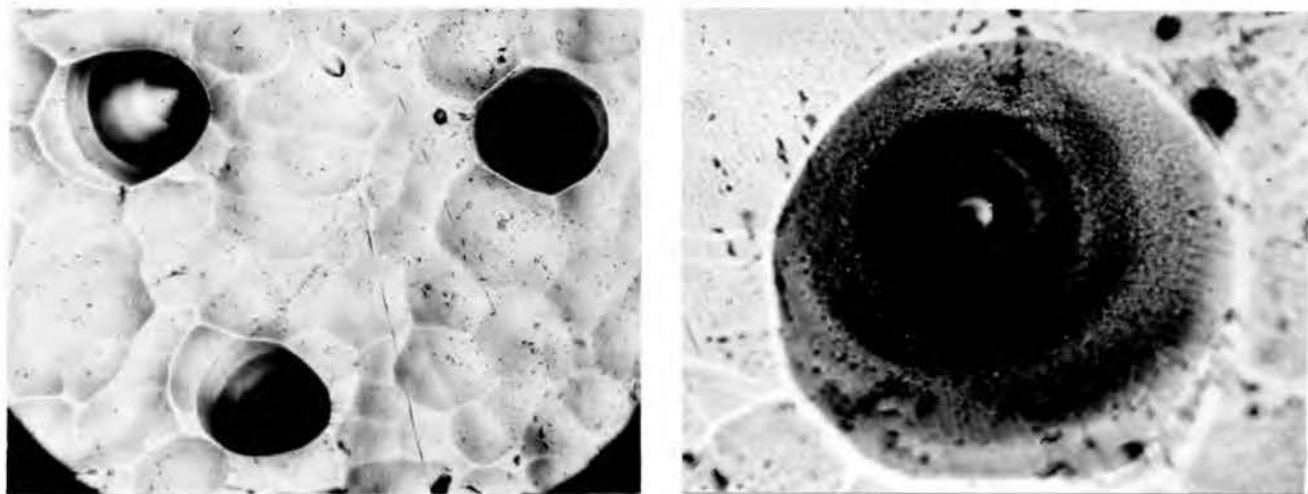
b. The etch pattern on the Sb{111} face in the same etchant. Hexagonal etch pits are formed as can be seen in Fig. 8.

Fig. 8

Etch pattern on Sb{111}.
Etchant: 6 N HCl-0.2 N Fe³⁺;
20 min; 80°C. 970X.



c. The HNO_3 -HF etchant (conc. HNO_3 -48% HF in parts by volume) produces on the $\text{In}\{111\}$ face round etch pits, (Fig. 9 a and b).



a

b

Fig. 9

Etch patterns on $\text{In}\{111\}$. Etchant: HNO_3 -HF; 25°C . a. 146X; b. 405X.

d. The same etchant forms triangular etch pits on $\text{Sb}\{\bar{1}\bar{1}\bar{1}\}$ (Fig. 10).

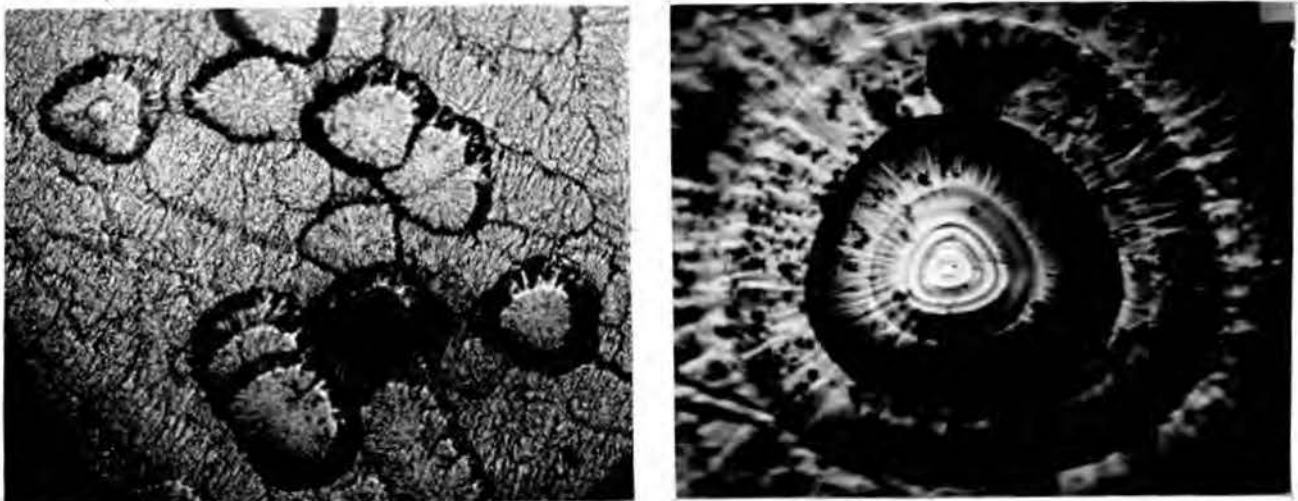
Fig. 10

Etch pattern on $\text{Sb}\{\bar{1}\bar{1}\bar{1}\}$.
Etchant: HNO_3 -HF; 15 sec; 25°C .
405X.



3. Etch patterns on the inverse InSb{111} planes obtained by anodic etching in some acids.

a. Anodic etching of the In{111} face in aqueous 2 N HCl leads to round-shaped or round triangular etch pits (Fig. 11 a and b). It seems that the etch pits grow in size and finally merge into each other. This agrees with the observation of Gatos and Lavine⁷⁾, who used the HCl-Fe³⁺ etchant for the In{111} faces.



a

b

Fig. 11

In{111} face etched anodically in 2 N HCl; 10 ma/cm²;

a. 15 min; 90X; b. 45 min; 405X.

b. As a result of anodic etching of the $\text{Sb}\{\bar{1}\bar{1}\bar{1}\}$ face in the same acid, fairly regular triangular etch pits are formed (Fig. 12 a), some of them developing etch pits within the etch pits (Fig. 12 b).



a



b

Fig. 12

$\text{Sb}\{\bar{1}\bar{1}\bar{1}\}$ face etched anodically in
2 N HCl; 10 ma/cm². a. 500X;
b. 970X.

c. Anodic etching of the In{111} face in an aqueous solution of a mixture of 1 N HNO_3 and 1 N $\text{H}_2\text{C}_4\text{H}_4\text{O}_6$ leads to round-shaped etch pits. Some of them appear separately, some in twins or in groups (Fig. 13 a, b and c). The etch pits in this solution appear clearer than those in 2 N HCl, which may be explained by the easier solubility of Sb in this solution rather than in pure HCl.



a

Fig. 13



b

Fig. 13



c

Fig. 13

In{111} face etched anodically in 1 N HNO_3 -
1 N $\text{H}_2\text{C}_4\text{H}_4\text{O}_6$; 10 ma/cm^2 ; 60 min.

a. a separate etch pit; 200X.

b. a twin etch pits; 500X.

c. a group of etch pits; 500X.

d. Anodic etching of the Sb{111} face in the same etchant produces triangular etch pits (Fig. 14), similar to those observed in aqueous 2 N HCl (Fig. 12).

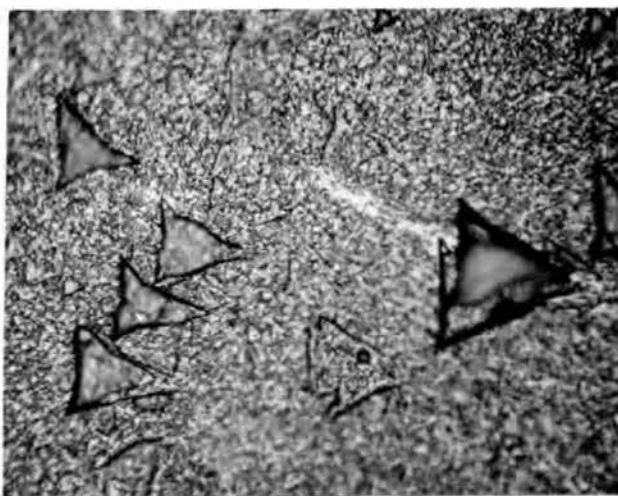


Fig. 14

Sb{111} face etched anodically in 1 N HNO_3 -
1 N $\text{H}_2\text{C}_4\text{H}_4\text{O}_6$; 10 ma/cm^2 ; 60 min. 500X.

4. Etch pattern on the In{111} face obtained anodically in 2 N HCl and then etched chemically with HCl-Fe³⁺ etchant. Anodic etching of In{111} in aqueous 2 N HCl leads to round-shaped etch pits (Fig. 11). This surface was etched again chemically with the HCl-Fe³⁺ etchant, and as the result the triangle-like pattern (of Fig. 7) was superimposed; now the walls of the deep etch pits (Fig. 11) were covered with triangular steps (Fig. 15 a and b). This proves that the In{111} face, which develops round-shaped etch pits under anodic current, does develop triangle-like etch pits on the same surface from chemical etching with the HCl-Fe³⁺ etchant.

The Sb{ $\bar{1}\bar{1}\bar{1}$ } face was usually rough after anodic etching, therefore if it was etched again chemically with the HCl-Fe³⁺ etchant, no clear superimposed pattern was observed.

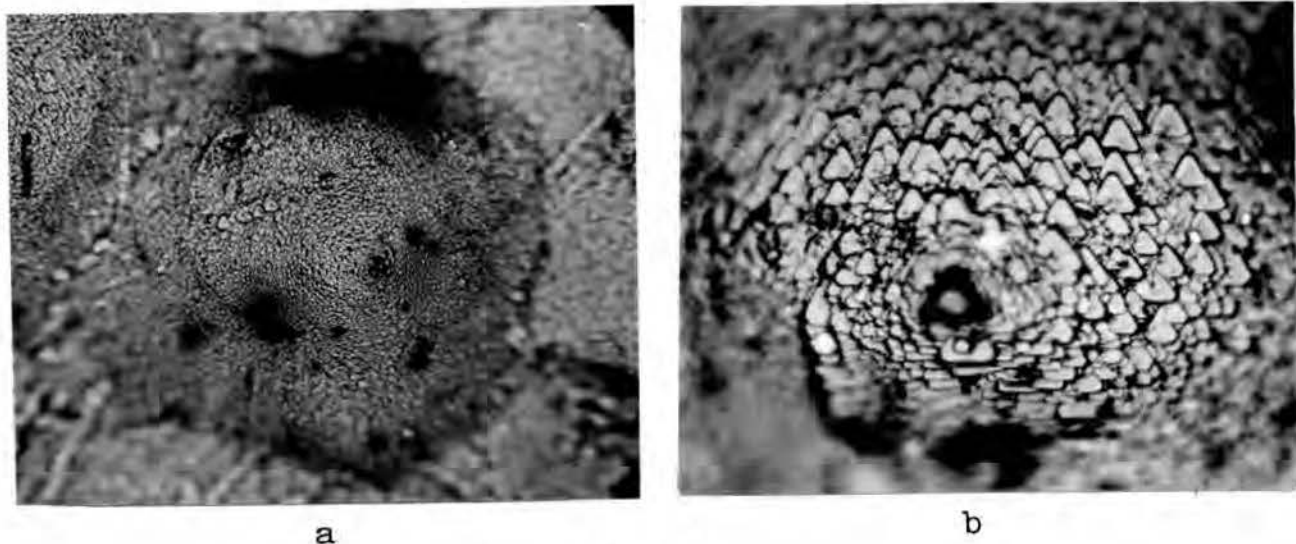


Fig. 15

In{111} face etched anodically (2 N HCl; 10 ma/cm²) and then chemically (6.N HCl-0.2 N Fe³⁺); 20 min; 25°C. a. 90X; b. 200X.

IV. THE DETERMINATION OF THE ELECTRON NUMBER OF THE ANODIC DISSOLUTION REACTION FOR InSb SINGLE CRYSTALS

A. Materials

The materials were the same as described in Section III.

B. Apparatus and Procedure

If one wishes to have some clarity regarding anodic dissolution reactions a very important point is the knowledge of the charge of the cations going into solution. It is not so self evident what the valencies of In and Sb ions of InSb are undergoing anodic dissolution. The apparatus used for the purpose of charge or electron number determination of an InSb single crystal anode has been described in Section III: a platinized-platinum cathode was arranged in series with a sensitive milliammeter, a millirecorder, a power source, which was a 12-volt storage battery, and a decade type of power resistor. The list of apparatus used in this study is given in Appendix B, and the sketch of the arrangement in Fig. 16. (The calomel electrode and the potentiometer, for the purpose of potential measurements, were not connected here). The time was measured with a second-timer. Approximately 200 milliliters of electrolyte were transferred into the cell which remained in the water bath for about 30 minutes to bring the system to constant temperature before starting a run. Then the InSb single crystal anode with a known exposed area and the platinum cathode were put into the cell and connected with external current.

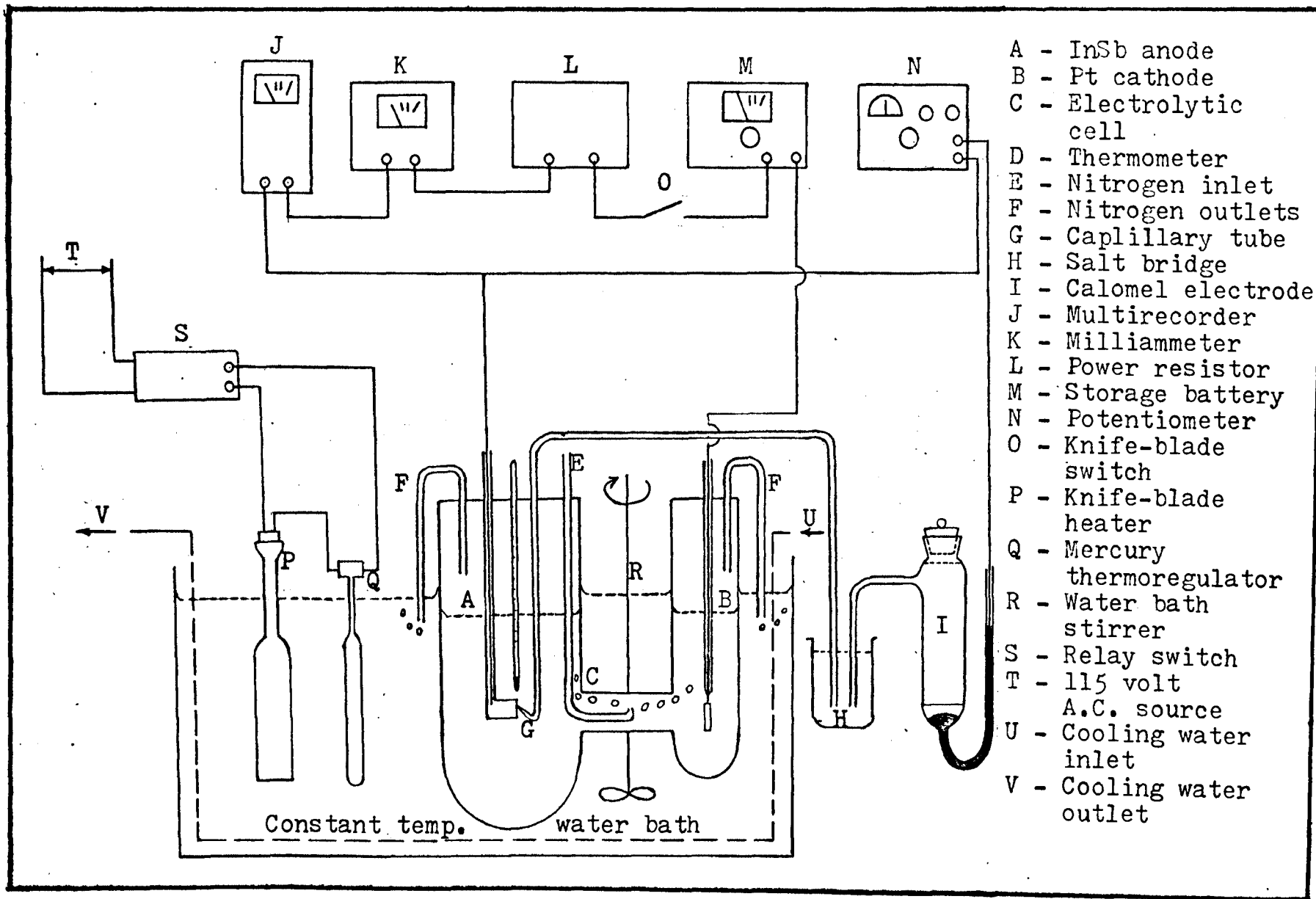


Fig. 16. Sketch of the apparatus used for potential measurements or electron number determinations of InSb single crystals undergoing anodic dissolution.

The electrolyte was purged by prepuried nitrogen gas. The flowing gases stirred the electrolyte during the experiment. At the end of each run, the InSb single crystal was removed from the anode, rinsed in distilled water and then acetone, and dried to constant weight in a dessicator. Finally the weight loss was determined.

Since the single crystal during the run dissolved not only anodically but also showed some self-dissolution (chemical reaction), the rate of the latter reaction in various aqueous solutions was determined separately by the weight loss method. The apparatus was essentially the same as described before except that no anodic current was passed and only the InSb single crystal electrode was placed into the cell for 24 hours or longer. The weight losses found are shown in Table I. In 2 N HCl no detectable weight loss occurred. In 1 N HNO₃-1 N H₂C₄H₄O₆, 2 N HCl-0.005 N Fe³⁺ and 2 N HCl-0.01 N Fe³⁺, the self-dissolution rates were very small compared to the anodic dissolution rates. Therefore, for the apparent electron number measurements, the very small amount of the weight loss due to self-dissolution was neglected.

The apparent electron number which corresponds to the sum of the absolute values of the oxidation number of both In and Sb was calculated from the expression:

$$V = \frac{ItA}{F(W-w)} \quad (1)$$

where,

I - the current in amperes,

t - the time in seconds,

A - the molecular weight of InSb = 236.57 g,

F - Faraday's constant = 96,500 coulombs/g equivalent,

W - the weight loss of the electrode in grams,

w - the weight loss of the electrode in grams due to self-dissolution.

If the value of w is small as compared to the value of W, the weight w can be neglected. There results only a very small deviation of the value V, and Equation (1) becomes

$$V = \frac{ItA}{FW} \quad (2)$$

C. Results

1. Self-dissolution rates of InSb in various electrolytes. The rates are shown in Table I.

2. Apparent electron number of InSb in various electrolytes.

a. In 2 N HCl. The InSb electrode was anodically dissolved in a 2 N HCl electrolyte. The current densities were adjusted from ~1 to ~90 ma/cm² for both inverse {111} planes and also for the {110} and {100} planes. The data are shown in Tables II through V and plotted in Fig. 17.

TABLE I
 THE WEIGHT LOSS OF InSb ELECTRODE IN VARIOUS ELECTROLYTES
 AT 25°C WITH ZERO EXTERNAL CURRENT APPLIED

Electrode	Electrolyte	Time (hr)	Weight Loss (mg)	Self-dissolution Rate (mg/cm ² ·24 hrs)
In {111}	2 N HCl	24	0.00	0.00*
Sb {111}	2 N HCl	24	0.00	0.00*
In {111}	1 N H ₂ C ₄ H ₄ O ₆ ⁻ 1 N HNO ₃	30	0.05	0.07*
Sb {111}	1 N H ₂ C ₄ H ₄ O ₆ ⁻ 1 N HNO ₃	30	0.04	0.04**
In {111}	2 N HCl- 0.005 N Fe ³⁺	45	1.63	1.06**
Sb {111}	2 N HCl- 0.005 N Fe ³⁺	45	1.51	1.33*
In {111}	2 N HCl- 0.01 N Fe ³⁺	37	2.10	2.25*
Sb {111}	2 N HCl- 0.01 N Fe ³⁺	37	2.43	2.60*

*Exposed surface area of the electrode = 0.60 cm²

**Exposed surface area of the electrode = 0.82 cm²

TABLE II
 THE APPARENT ELECTRON NUMBER OF AN InSb SINGLE CRYSTAL WITH
 THE In {111} FACE IN 2 N HCl AT 25°C

Time (sec)	Electrode Surface Area (cm ²)	Current Density (ma/cm ²)	Weight Loss (mg)	Apparent Electron No.
36,000	0.60	0.995	8.74	6.08
6,000	0.82	9.15	18.40	6.00
12,300	0.353	9.91	17.62	5.99
3,600	0.353	19.8	10.21	6.05
3,600	0.60	28.9	25.52	6.05
2,700	0.306	39.2	13.15	6.00
3,600	0.353	56.6	29.11	6.07
2,100	0.353	62.4	18.41	6.01
2,500	0.306	71.8	24.74	5.45*
1,500	0.353	90.6	22.03	5.34*
Average				6.06

*Excluded.

TABLE III

THE APPARENT ELECTRON NUMBER OF AN InSb SINGLE CRYSTAL WITH
THE Sb{ $\bar{1}\bar{1}\bar{1}$ } FACE IN 2 N HCl AT 25°C

Time (sec)	Electrode Surface Area (cm ²)	Current Density (ma/cm ²)	Weight Loss (mg)	Apparent Electron No.
76,000	0.60	1.00	18.64	6.05
40,000	0.60	1.35	13.59	5.92
7,200	0.353	9.91	10.41	5.93
14,400	0.353	12.05	25.20	5.95
7,200	0.353	14.2	14.70	6.00
5,400	0.353	22.6	17.53	6.04
3,600	0.306	36.0	16.15	6.01
2,000	0.353	48.2	14.40	5.79*
1,200	0.605	52.9	17.35	5.42*
2,100	0.306	58.8	16.82	5.51*
1,500	0.353	70.8	16.92	5.43*
1,500	0.353	90.6	21.47	5.48*
Average				6.01

*Excluded.

TABLE IV
 THE APPARENT ELECTRON NUMBER OF AN InSb SINGLE CRYSTAL WITH
 THE {110} FACE IN 2 N HCl AT 25°C

Time (sec)	Electrode Surface Area (cm ²)	Current Density (ma/cm ²)	Weight Loss (mg)	Apparent Electron No.
40,000	0.60	1.35	13.33	6.03
12,000	0.60	4.96	14.54	6.07
3,600	0.60	9.92	8.73	6.07
3,600	0.353	19.8	10.46	5.91
1,800	0.353	48.2	12.52	5.99
1,800	0.353	57.5	17.11	5.42*
1,200	0.60	71.1	23.55	5.37*
1,500	0.353	90.6	21.35	5.51*

Average 6.01

*Excluded.

TABLE V
 THE APPARENT ELECTRON NUMBER OF AN InSb SINGLE CRYSTAL WITH
 THE {100} FACE IN 2 N HCl AT 25°C

Time (sec)	Electrode Surface Area (cm ²)	Current Density (ma/cm ²)	Weight Loss (mg)	Apparent Electron No.
46,000	0.6	1.35	15.36	6.02
9,000	0.6	5.78	12.75	6.06
3,600	0.353	9.91	5.17	5.97
3,600	0.353	19.8	10.28	6.01
2,700	0.353	39.6	14.97	6.19
1,800	0.353	48.2	13.24	5.67*
1,800	0.353	59.4	17.10	5.42*
1,200	0.60	70.3	23.11	5.41*
1,500	0.353	90.6	22.16	5.31*

Average 6.05

*Excluded.

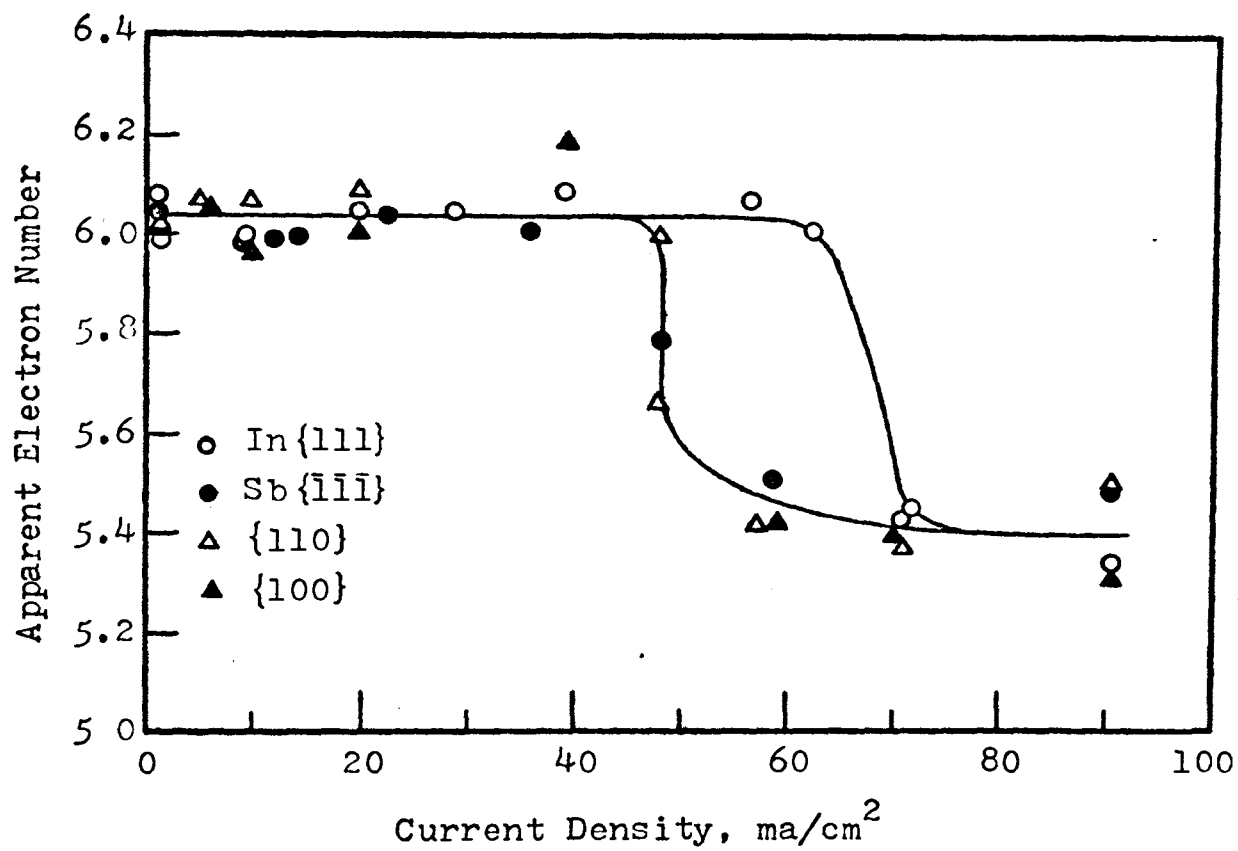


Fig. 17

Calculated electron number of InSb single crystals as a function of current density of the faces In{111}, Sb{ $\bar{1}\bar{1}\bar{1}$ }, {110} and {100} dissolving anodically in 2 N HCl.

From the above measurements (Tables II through V), it appears that the apparent electron numbers among the anodes of various planes are close to each other. The calculated electron numbers of InSb single crystal in 2 N HCl are close to the value of 6 at current densities below $\sim 40 \text{ ma/cm}^2$ (for In{111} below $\sim 60 \text{ ma/cm}^2$), and then rapidly decrease to a value of $\sim 5.4 \pm 0.1$ with further increasing current densities up to $\sim 90 \text{ ma/cm}^2$. The critical current density varies with the plane used as an anode as shown in Tables II through V and in Fig. 17. Furthermore, the valence number below the critical density is found the same for both inverse {111} planes (Table II and III) and also for the {110} and {100} planes (Tables IV and V).

b. In 1 N HNO₃-1 N H₂C₄H₄O₆. The InSb electrodes were anodically dissolved in this electrolyte at a current density of $\sim 10 \text{ ma/cm}^2$. Both inverse {111} planes were used as anodes. The data are shown in Table VI.

TABLE VI

THE APPARENT ELECTRON NUMBER OF InSb SINGLE CRYSTAL IN
1 N HNO₃-1 N H₂C₄H₄O₆ AT 25°C

Face	Time (sec)	Electrode Surface Area (cm ²)	Current Density (ma/cm ²)	Weight Loss (mg)	Apparent Electron No.*
In {111}	3,600	0.60	9.91	8.82	6.00
Sb {111}	7,500	0.353	9.91	10.88	5.92

*Calculated by Equation (2).

c. In 2 N HCl with Fe³⁺ additions. The InSb electrode was anodically dissolved in 2 N HCl with an addition of 0.005 N Fe³⁺ at a current density of ~ 10 ma/cm². Both of the inverse {111} planes were used for the measurements. The data are shown in Table VII.

TABLE VII

THE APPARENT ELECTRON NUMBER OF InSb SINGLE CRYSTAL IN
2 N HCl-0.005 N Fe³⁺ AT 25°C

Face	Time (sec)	Electrode Surface Area (cm ²)	Current Density (ma/cm ²)	Weight Loss (mg)	Apparent Electron No.*
In {111}	3,600	0.353	9.91	5.20	5.96
Sb {111}	7,200	0.353	9.91	10.36	5.98

*Calculated by Equation (1).

From the above measurements (Tables VI and VII), it appears that at a moderate current density of ~ 10 ma/cm² (where no visible anodic film is formed), the apparent electron number of both inverse {111} faces is close to the value of 6. No effect on the apparent electron number is found by the small addition of Fe³⁺.

3. Reason for the decline of the valency number at increased current densities. The surface of InSb mostly turned dark under anodic dissolution in 2 N HCl. Of the four faces investigated usually only In {111} remained shiny at current densities lower than ~ 30 ma/cm², although etch pits appeared, visible even to the naked eye.

At current densities higher than $\sim 40 \text{ ma/cm}^2$ a thicker and continuous black film was observed on the surface of the anode for all four faces. This film could usually be removed from the crystal a soft brush. Microscopic examination revealed that a section through the flakes, obtained from either the $\text{In}\{111\}$ or the $\text{Sb}\{\bar{1}\bar{1}\bar{1}\}$ face, consisted of parallel layers as shown in Fig. 18. The side that previously stuck to the substrate (Fig. 19) appeared more even than the other side (Fig. 20). Interference colors were observed on both sides.

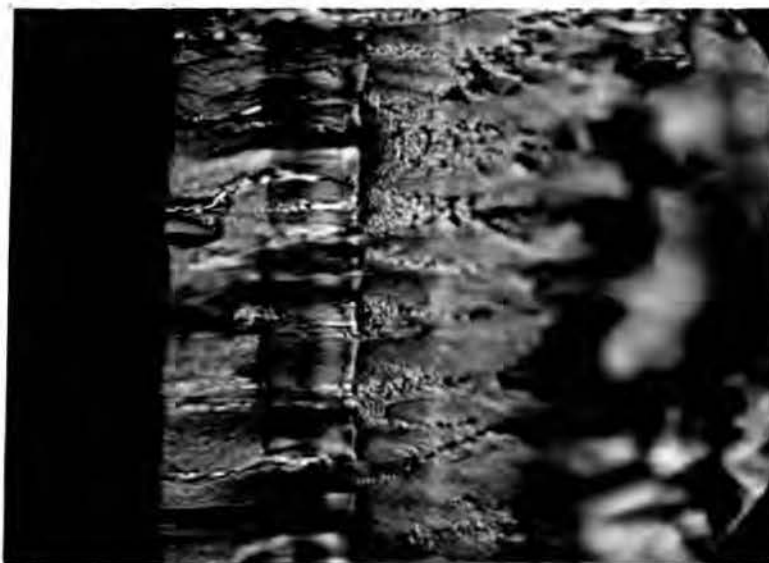


Fig. 18

Cross section of the black film normally to its surface. The flakes resulted from anodic dissolution of the $\text{In}\{111\}$ face of InSb in 2 N HCl at 70 ma/cm^2 . 970X.

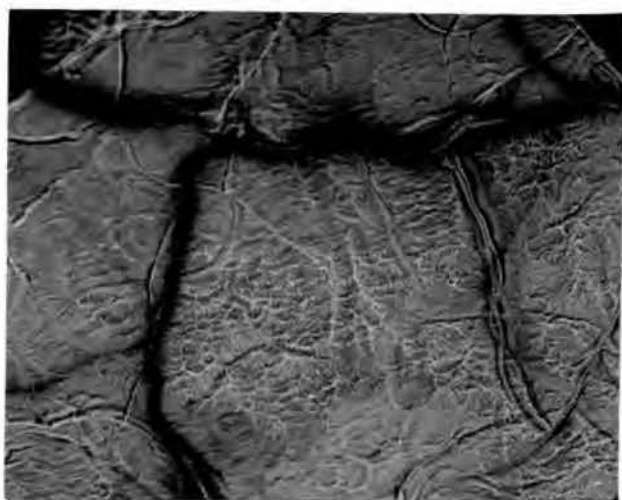


Fig. 19

A piece of black film resulting from anodic dissolution of In{111} of InSb in 2 N HCl at 70 ma/cm^2 .

Substrate side. 970X.

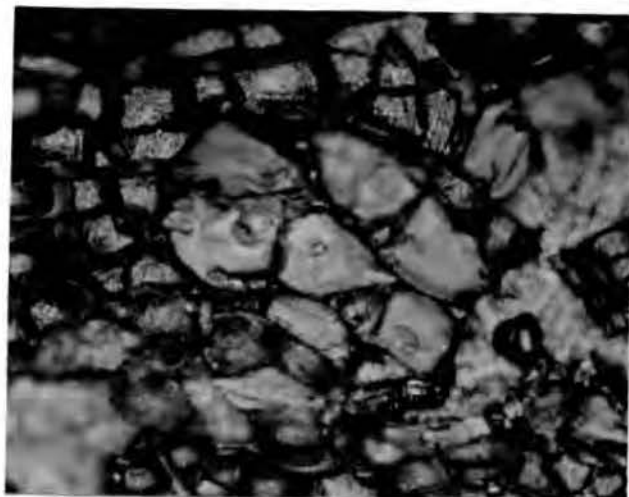


Fig. 20

The same as in Fig. 19. Electrolyte side. 970X.

The black film collected from the anode, resulting from anodic dissolution at 70 ma/cm^2 for 30 minutes, was used to make an X-ray diffraction picture. The black film is colloidal in nature. However, if the black film were transferred to a glass tubing, which was then evacuated, sealed and heated to 350°C for ~ 2 hours, a clear X-ray diffraction picture was obtained with the powder showing many diffraction rings. They coincided with the diffraction pattern of the grey-colored film which resulted from anodic dissolution of pure metallic antimony in 2 N HCl electrolyte at $\sim 15 \text{ ma/cm}^2$ for ~ 1 hour. Therefore, the black film of InSb contained in a finely dispersed form is the same

compound which resulted from anodic dissolution of pure Sb in 2 N HCl. To determine the nature of the compound X-ray patterns were made of a white powder prepared as follows: 2 grams of SbCl_3 (crystals, reagent grade) were dissolved in 20 milliliters of 4 N HCl and 20 milliliters of water were added. Hydrolysis occurred and a white turbid solution was obtained. The precipitate was separated, dried in a vacuum and powdered. Mellor's "A Comprehensive Treatise on Inorganic and Theoretical Chemistry"²⁴⁾ states that solid SbCl_3 when dissolves in a large amount of water hydrolyzes, forming an oxychloride of the composition $\text{Sb}_4\text{O}_5\text{Cl}_2$. A transition from SbOCl to $\text{Sb}_4\text{O}_5\text{Cl}_2$ may occur in solutions more dilute than 2.5 N HCl.

The d spacings calculated from the X-ray patterns of this oxychloride, identified as $\text{Sb}_4\text{O}_5\text{Cl}_2$, agree with those of the vacuum heated black deposit. Since the Sb in the oxychloride is trivalent, it appears certain that the InSb single crystal undergoes anodic dissolution with the formation of trivalent indium and trivalent antimony, which altogether adds to a valence number of 6 for the compound InSb.

In order to find out why an apparent electron number lower than 6 results at current densities higher than $\sim 40 \text{ ma/cm}^2$ (for In{111} higher than $\sim 60 \text{ ma/cm}^2$, see Fig. 17), further X-ray pictures were made.

The black film spalling off the substrate, resulting from anodic dissolution at 70 ma/cm^2 , was annealed in

evacuated glass tubing at 350°C for ~ 2 hours. The grey particles in the glass tubing were observed under the microscope with reflected and transmitted light (Fig. 21 and 22). They appeared to contain both metallic and colloidal matter.

If the above-mentioned film were annealed in evacuated glass tubing at 650°C for ~ 2 hours, a layer of white material stuck to the wall of the glass tubing and the residue clustered as grey particles. Microscopic observation of this white material revealed it to be transparent under the transmitted light (Fig. 23 and 24). This suggests no metallic particles present in the white material. X-ray diffraction pictures prepared from opaque particles (Fig. 25 and 26) selected from the residue revealed intense diffraction rings of metallic antimony. This proves that surface disintegration of the anode does occur when InSb single crystals undergo anodic dissolution in aqueous 2 N HCl electrolyte at a higher current density (above $\sim 40 \text{ ma/cm}^2$). The total apparent electron number of less than 6 can thus be explained.

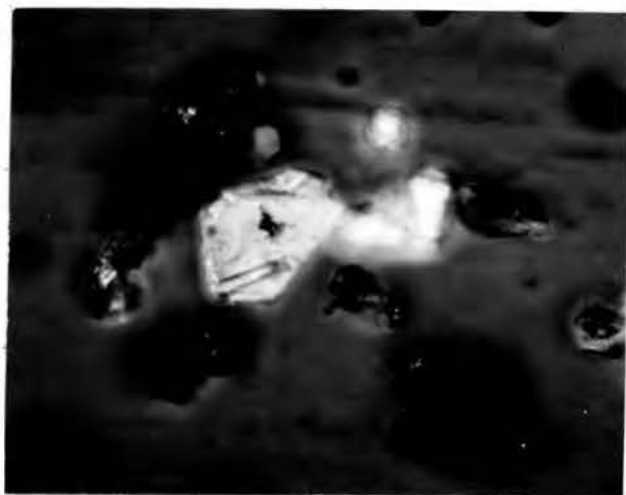


Fig. 21

The particles of annealed (350°C , ~ 2 hrs) black film, resulting from anodic dissolution in 2 N HCl at 70 ma/cm^2 . Reflected light. 405X.

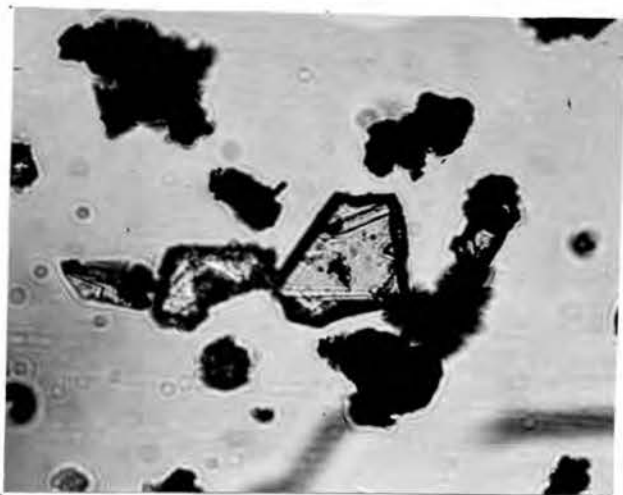


Fig. 22

Same as shown in Fig. 21 but in transmitted light. 405X.

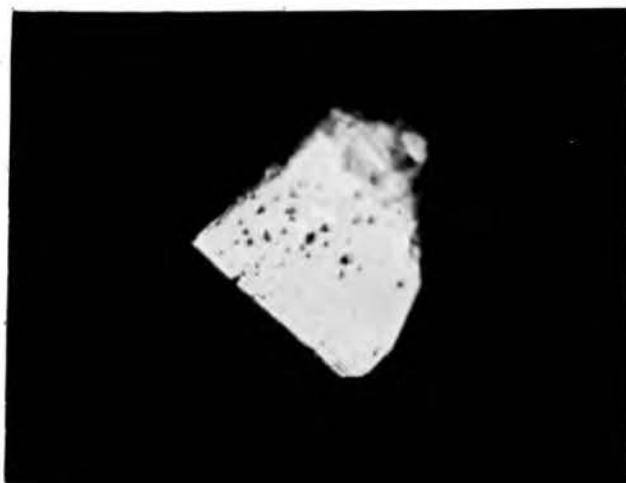


Fig. 23

The white material sticking to the wall of the glass tubing after the InSb black film was annealed at 650°C for ~ 2 hrs. Reflected light. 405X.

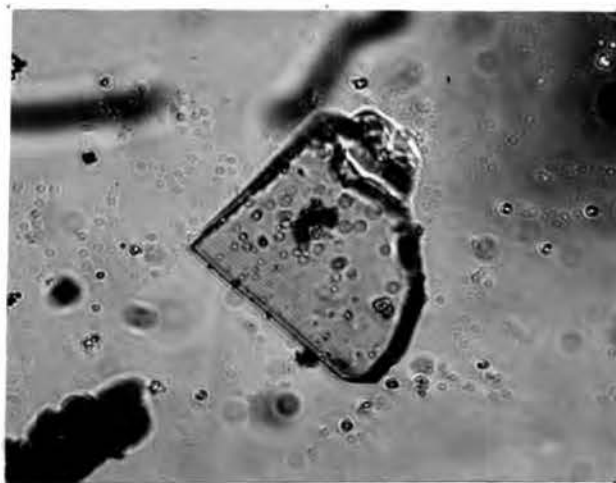


Fig. 24

Same as shown in Fig. 23 but in transmitted light. 405X.

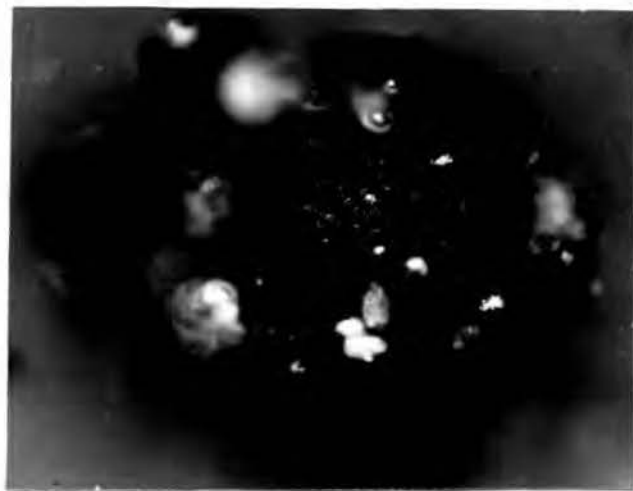


Fig. 25

A selected particle of the residue of the annealed (650°C , ~ 2 hrs) black film of InSb, resulting from anodic dissolution in 2 N HCl at 70 ma/cm^2 . Reflected light. 405X.



Fig. 26

The same as in Fig. 25 but in transmitted light. 405X.

V. MEASUREMENTS OF DISSOLUTION POTENTIALS OF InSb SINGLE CRYSTALS

A. Materials

The materials were the same as described in Section III.

B. Dissolution Potential Without Anodic Current

1. Apparatus and procedure. The apparatus was the same as described in Section IV, except that a calomel electrode (1: N KCl) was used for reference. A salt bridge (~3.5 N KCl) and a Luggin capillary (Fig. 27) eliminated the liquid junction potentials and prevented the electrolyte in the cell from contacting the electrolyte of the calomel electrode. The potential difference was measured with a precision potentiometer. A sketch of the arrangement is shown in Fig. 16. The readings for the potential difference of the circuit were taken as soon as possible after the electrode was immersed into the electrolyte. Then the intervals were extended to 5 minutes for the first 15 minutes and then to 15 minutes.

2. Data and results.

a. Measurements of dissolution potential without anodic current of the inverse {111} faces of an InSb single crystal in aqueous HCl solution. The dissolution potential E_H' was expressed on the standard hydrogen scale (SHE) by adding 0.281 volt to the potential as measured against the calomel electrode. The results are tabulated in Tables VIII to X, Appendix C. Plots of the E_H' versus time in

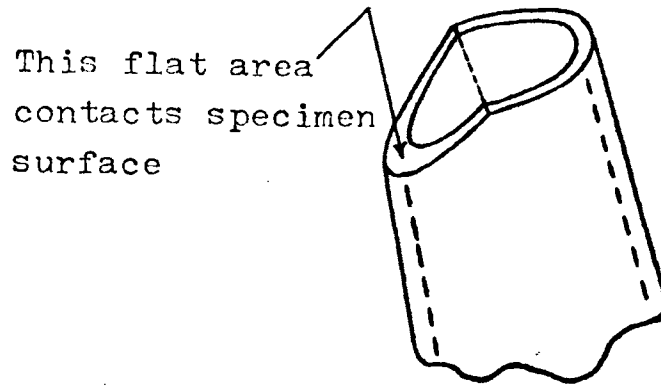


Fig. 27

Sketch showing the end of capillary tube in detail

various concentrations of HCl are shown in Fig. 28. It is found that:

(1) The E_H 's of both inverse {111} faces in the same concentration of HCl are close to each other, the potential difference being less than ± 10 mv.

(2) For both inverse {111} faces, the higher the concentration of HCl, the less noble the E_H '. There is no significant potential difference between the In{111} and Sb{ $\bar{1}\bar{1}\bar{1}$ } faces.

(3) Time has no particular influence on the E_H '. Steady potentials are usually obtained after 15 minutes in most cases. This may result from the chemical pre-etching (CP-4) of the specimen surface.

(4) The dissolution potentials without anodic current (or the zero-potentials) are reproducible within a deviation of roughly ± 10 mv.

b. Measurements of dissolution potential without anodic current of the inverse {111} faces of an InSb single crystal in various concentrations of HCl with 0.1 N Fe^{3+} additions. The Fe^{3+} was prepared from purified anhydrous $FeCl_3$. The dissolution potentials E_H ' were expressed on SHE. The results are tabulated in Tables XI to XII, Appendix C. Plots of the E_H ' versus time in various concentrations of HCl with 0.1 N Fe^{3+} additions are shown in Fig. 29. For comparison a curve in pure 2 N HCl is also shown. It is found that:

(1) In the presence of Fe^{3+} the E_H ' of Sb{ $\bar{1}\bar{1}\bar{1}$ }

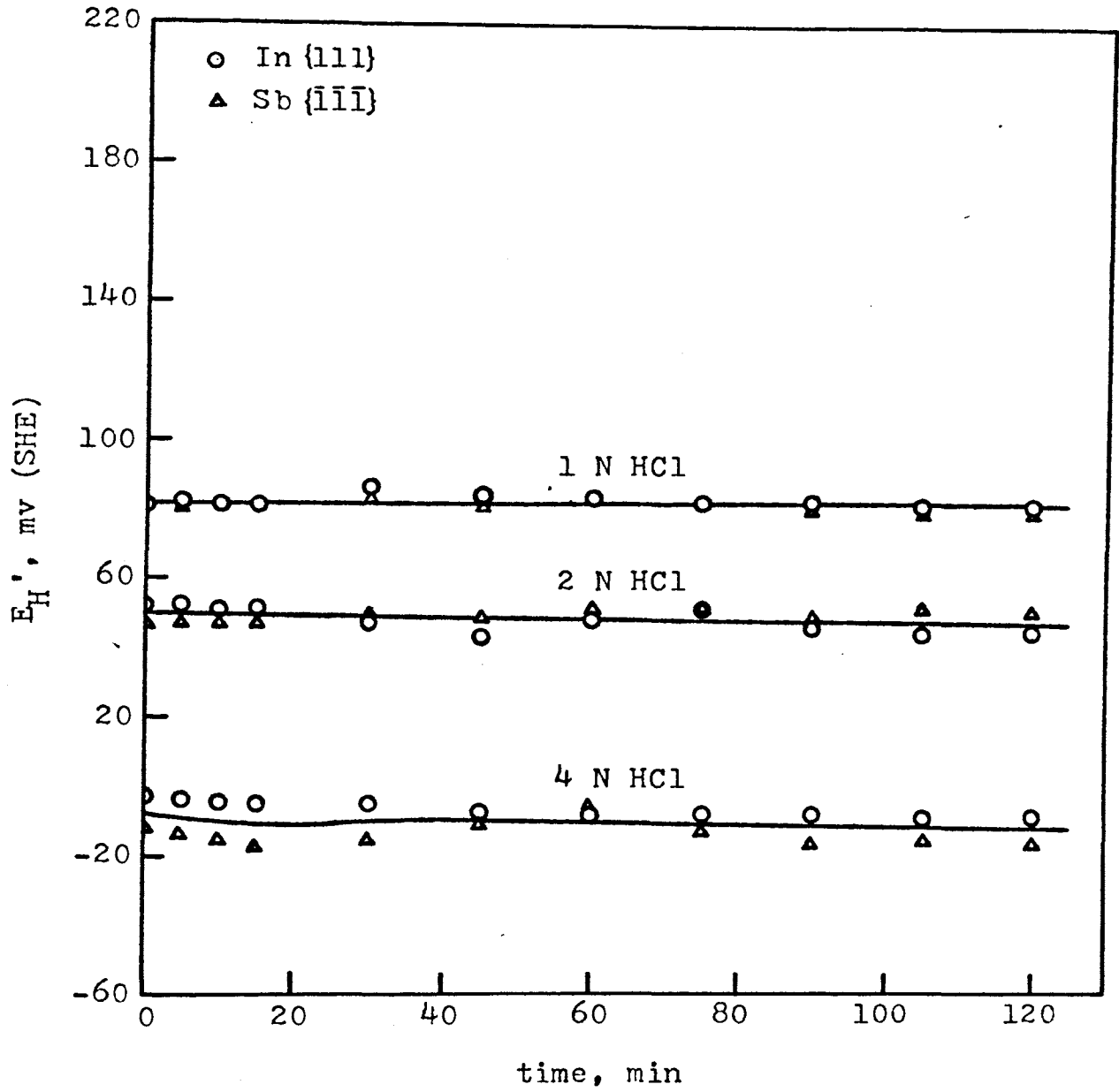


Fig. 28

Dissolution potentials without anodic current of the inverse {111} faces of InSb versus time in various concentrations of HCl at 25°C.

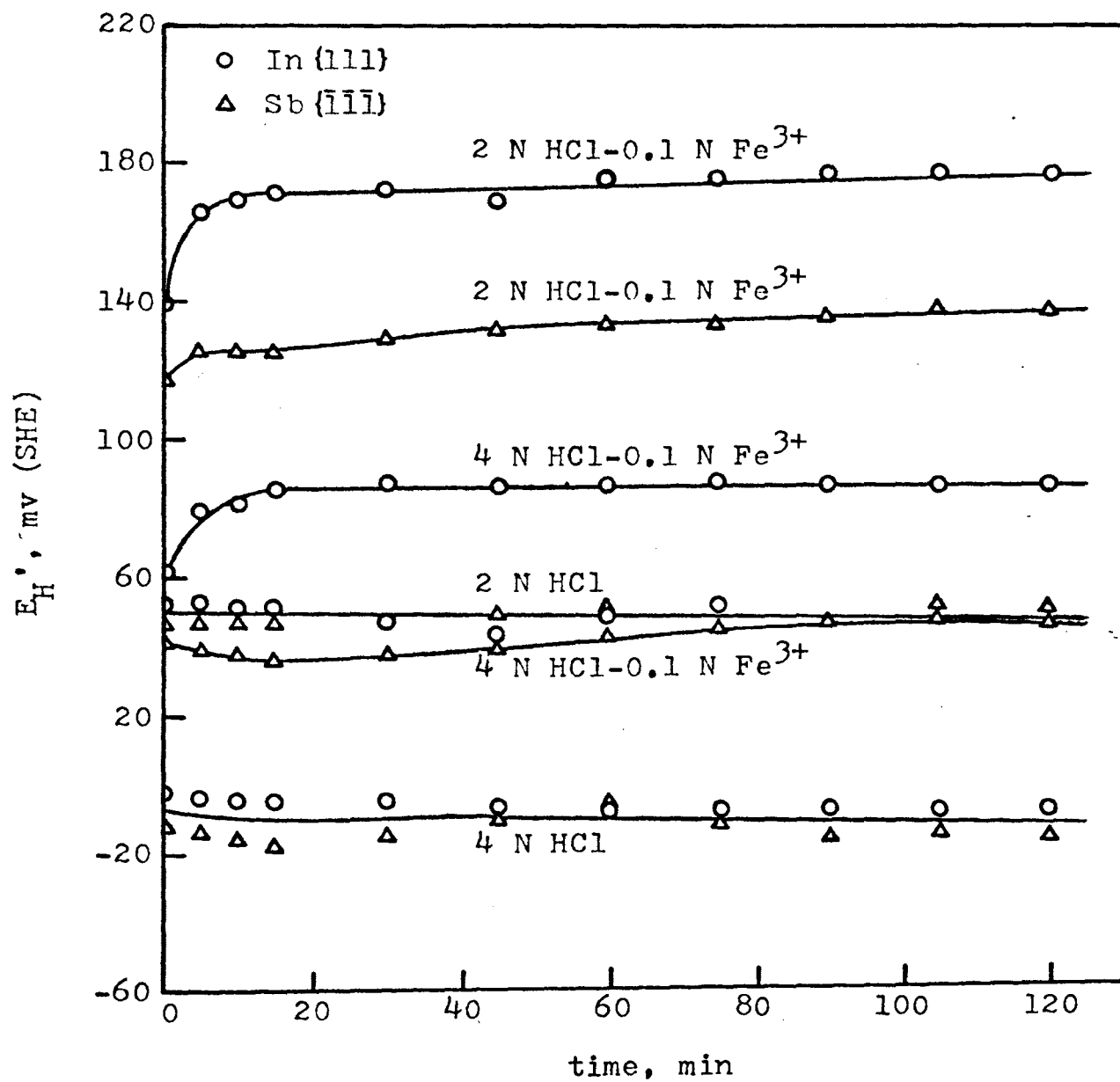


Fig. 29

Dissolution potentials without anodic current of the inverse {111} faces of InSb versus time in various concentrations of HCl with Fe^{3+} additions at 25°C.

is always less noble than that of In {111} in the same solution.

(2) With 0.1 N Fe^{3+} additions the E_H' of both {111} faces becomes less noble with increasing concentration of HCl. The potential difference between the two inverse faces is ~ 40 mv in both 2 N HCl-0.1 N Fe^{3+} and 4 N HCl-0.1 N Fe^{3+} solutions.

(3) Keeping the concentration of HCl constant, the addition of Fe^{3+} shifts the E_H' of both inverse {111} faces to more noble potentials without changing the sequence in potentials of In {111} and Sb {111}.

C. The Anodic Potential-Current Density Relationship for an InSb Single Crystal

The electrode surface preparation and the apparatus were the same as described in Section III and IV. The potential measurements were carried out as previously described (Fig. 16). However, the platinized platinum electrode used in the apparent valency measurements was coupled with the InSb electrode. The capillary (Fig. 27) provided a close contact with the dissolving specimen and thus reduced its shielding effect and the IR drop. During the run, the time, ammeter reading (current density) and potentiometer reading were recorded. Since time was not of particular importance, each potentiometer reading was taken after 5 minutes at each ammeter setting. All the current densities are plotted against the measured anodic potential (SHE) as Gerischer did^{18,19,25}, and not against

the overpotential (or polarization potential).

The results are as follows:

1. In 2 N HCl. Polarization curves of In{111}, Sb{ $\bar{1}\bar{1}\bar{1}$ }, {110} and {100} faces of InSb single crystal undergoing anodic dissolution in 2 N HCl are shown in Fig. 30. The respective data are listed in Tables XIII to XVI, Appendix C. It is found that:

(1) The anodic dissolution potential E_H' of the 4 different faces becomes less noble in the sequence: In{111}, {100}, {110}, Sb{ $\bar{1}\bar{1}\bar{1}$ }. The potential difference between In{111} and Sb{ $\bar{1}\bar{1}\bar{1}$ } is ~ 44 mv (at 10 ma/cm^2).

(2) All 4 anodic polarization curves obey the Tafel relation over about three decades of current density, roughly within the range of 3×10^{-2} to 30 ma/cm^2 .

(3) Within the above mentioned range of current density, the 4 anodic polarization curves give nearly parallel Tafel lines, with a slope of ~ 56 mv/log i for In{111}, and ~ 48 mv/log i for the last three planes.

2. In 1 N HNO₃-1 N H₂C₄H₄O₆: Polarization curves of In{111} and Sb{ $\bar{1}\bar{1}\bar{1}$ } faces dissolving anodically in this solution are traced in Fig. 31. The data are summarized in Tables XVII to XVIII, Appendix C. It is found that:

(1) The anodic dissolution potentials E_H' of both inverse {111} faces coincide at a current density lower than $\sim 10 \text{ ma/cm}^2$. At higher current densities the E_H' of Sb{ $\bar{1}\bar{1}\bar{1}$ } becomes less noble than that of In{111}.

(2) The anodic polarization curves of the two

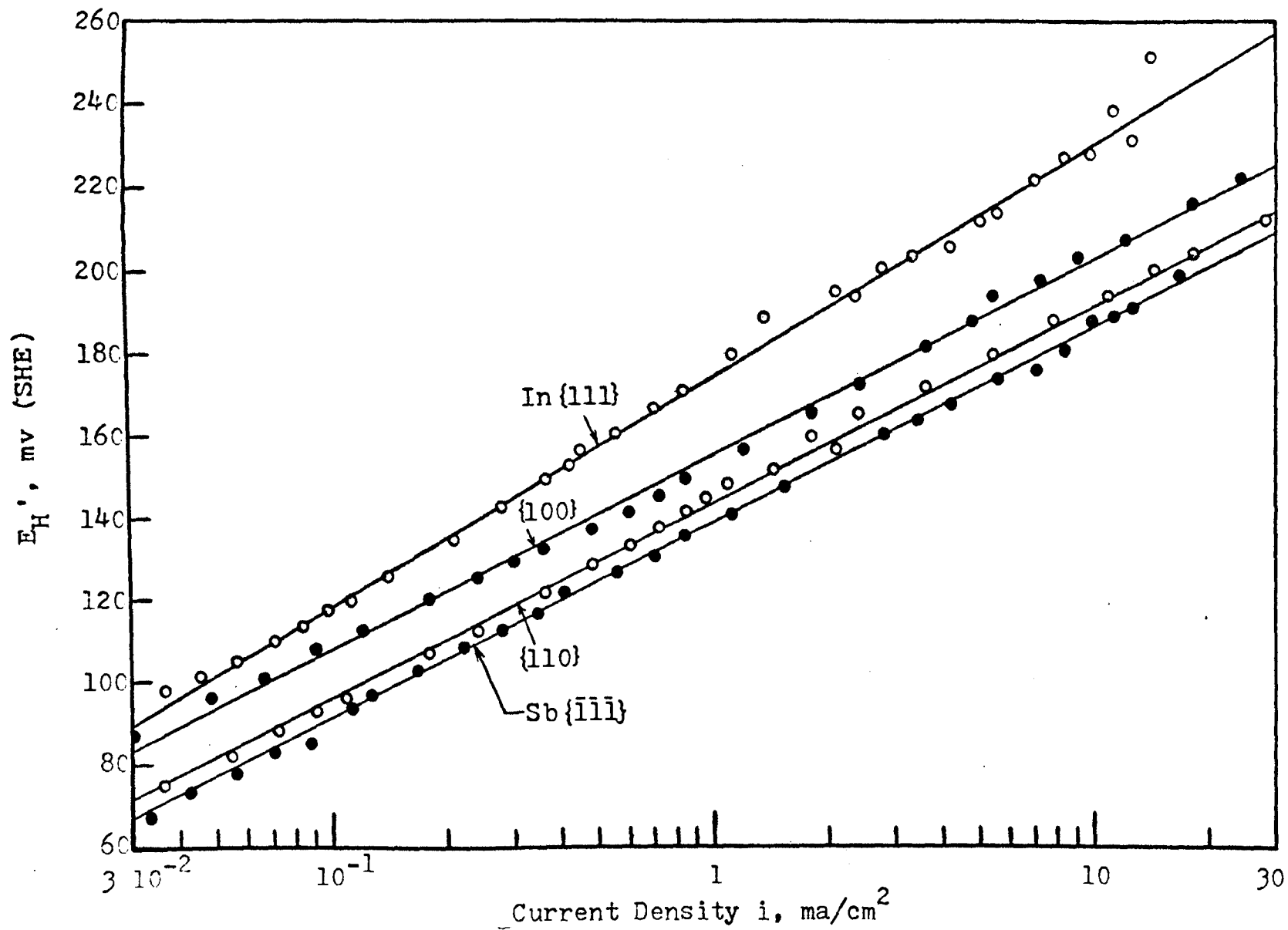


Fig. 30 Anodic dissolution potentials E_H' of InSb versus log of current density i of the planes In{111}, Sb{111}, {110} and {100} at 25°C.

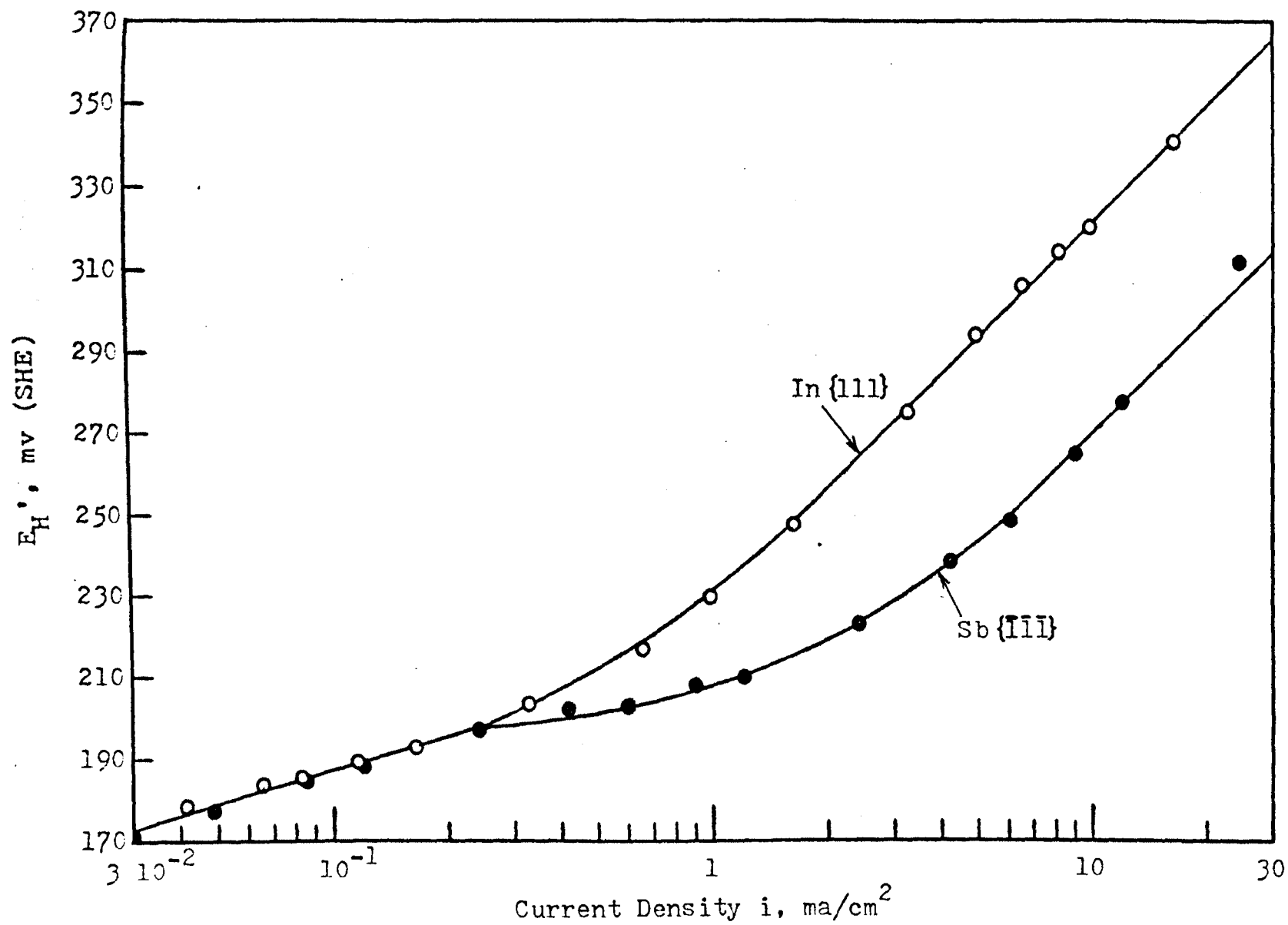


Fig. 31. Anodic dissolution potentials E_H' of the inverse {111} faces of InSb versus log of current density i in 1 N HNO_3 -1 N $\text{H}_2\text{C}_4\text{H}_4\text{O}_6$ at 25°C .

inverse {111} faces obey the Tafel relation within the range of $\sim 10^{-3}$ to $\sim 10^{-1}$ ma/cm² and ~ 3 to ~ 30 ma/cm². Within the former range the Tafel lines of the inverse {111} faces coincide with each other with a slope of ~ 26 mv/log i. Within the latter range the Tafel lines of the inverse {111} faces are parallel with a slope of ~ 92 mv/log i.

(3) The potential difference between the two inverse {111} faces within the range of 3 to 30 ma/cm² is ~ 50 mv.

(4) When an InSb single crystal dissolves anodically at current densities lower than 30 ma/cm² (where no visible anodic film is formed), the In{111} surfaces always remains more even and shiny than the Sb{ $\bar{1}\bar{1}\bar{1}$ } surfaces.

From (3), it is indicated that the anodic reaction of InSb in 1 N HNO₃-1 N H₂C₄H₄O₆ has two consecutive steps with Tafel slopes of ~ 26 and ~ 92 mv/log i (the former step referred to as step I and the latter as step II). According to Conway's explanation²⁶⁾, at high current density (in this case higher than ~ 3 ma/cm²) process I with a smaller electrochemical rate constant (large Tafel slope) is rate controlling, while at a lower current density step II is rate-controlling. The potential difference between the inverse {111} faces is shown only at higher current densities where the Tafel line has a large slope, the potential of Sb{ $\bar{1}\bar{1}\bar{1}$ } being less noble.

3. In 2 N HCl with Fe³⁺ additions. Polarization curves of In{111} and Sb{ $\bar{1}\bar{1}\bar{1}$ } undergoing anodic dissolution in

2 N HCl-0.0004 M Fe^{3+} and in 2 N HCl-0.002 M Fe^{3+} (Fe^{3+} was prepared from purified anhydrous FeCl_3) are shown in Fig. 32. For comparison the curves in pure 2 N HCl are also shown. The data are tabulated in Tables XIX to XXII, Appendix C. It is found that:

(1) In HCl- Fe^{3+} solutions the E_H' of Sb{ $\bar{1}\bar{1}\bar{1}$ } is, as in the absence of Fe^{3+} , less noble than that of In{111}.

(2) Keeping the concentration of HCl constant, the addition of Fe^{3+} shifts the dissolution potential E_H' of the inverse {111} faces to less noble potentials.

(3) The nobility of the anode decreases with increasing Fe^{3+} concentration. (In dilute solutions of oxidants, less than 0.01 g-equiv/liter, the dissolution obeys diffusion kinetics²⁷).

(4) The polarization curves obey the Tafel relation within the range of ~ 1 to ~ 10 ma/cm². The slope of the Tafel line of In{111} in both 2 N HCl-0.0004 M Fe^{3+} and 2 N HCl-0.002 M Fe^{3+} is ~ 62 mv/log i and that of Sb{ $\bar{1}\bar{1}\bar{1}$ } in the same solution is ~ 58 mv/log i . The potential difference between the inverse {111} faces in this region is ~ 37 mv in 2 N HCl-0.002 M Fe^{3+} and ~ 33 mv in 2 N HCl-0.0004 M Fe^{3+} .

Because of Fe^{3+} being a comparatively powerful oxidizing reagent the self-dissolution rate in 2 N HCl in the presence of Fe^{3+} was much higher than that in 2 N HCl in absence of Fe^{3+} (Table I). This self-dissolution along with anodic dissolution might break down a possible deposit formed on the InSb surface. Thus, the resistance between

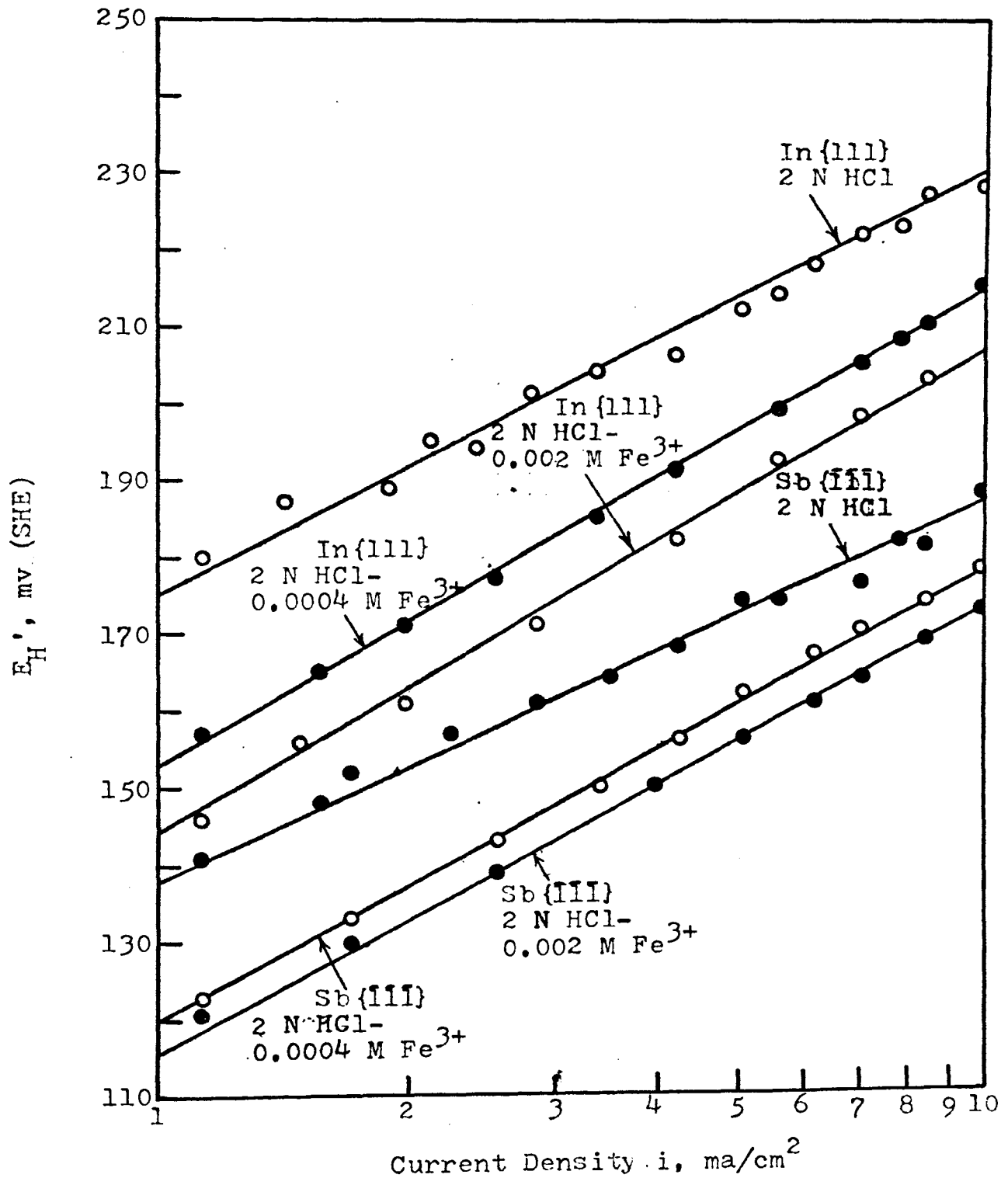


Fig. 32

Anodic dissolution potentials E_H' of the inverse (111) faces of InSb versus log of current density i in 2 N HCl with Fe^{3+} additions at 25°C.

the InSb bulk and solution would decrease with increasing Fe^{3+} concentration which would finally result in E_H' becoming less noble (depolarization).

4. In 2 N HCl with Fe^{2+} additions. Polarization curves of In{111} and Sb{ $\bar{1}\bar{1}\bar{1}$ } while dissolving anodically in 2 N HCl-0.002 M Fe^{2+} (Fe^{2+} was prepared from FeCl_2) are drawn in Fig. 33. For comparison the curves in pure 2 N HCl are also shown. The data are listed in Tables XXIII to XXIV, Appendix C. It is found that:

(1) The E_H' of Sb{ $\bar{1}\bar{1}\bar{1}$ }, as it was in pure HCl in the absence of Fe^{2+} , is less noble than that of In{111}. The potential difference between the inverse {111} faces is ~ 26 mv (at 10 ma/cm^2).

(2) At a constant concentration of HCl, the addition of Fe^{2+} shifts the E_H' of both inverse {111} planes to less noble potentials (as for Fe^{3+} additions).

(3) The polarization curves of both inverse {111} faces obey the Tafel relation within the range of ~ 1 to $\sim 10 \text{ ma/cm}^2$ with a slope of $\sim 80 \text{ mv/log } i$ for In{111} and $\sim 66 \text{ mv/log } i$ for Sb{ $\bar{1}\bar{1}\bar{1}$ }.

(4) No deposit is observed on both inverse {111} surfaces up to a current density of $\sim 20 \text{ ma/cm}^2$.

In a 2 N HCl-0.002 M Fe^{2+} solution exposed to air during its preparation, an appreciable amount of Fe^{3+} was formed because of the oxidation of Fe^{2+} by oxygen. The presence of Fe^{3+} caused the the anodic dissolution potential to become less noble (Fig. 32). Thus the action of Fe^{2+} additions

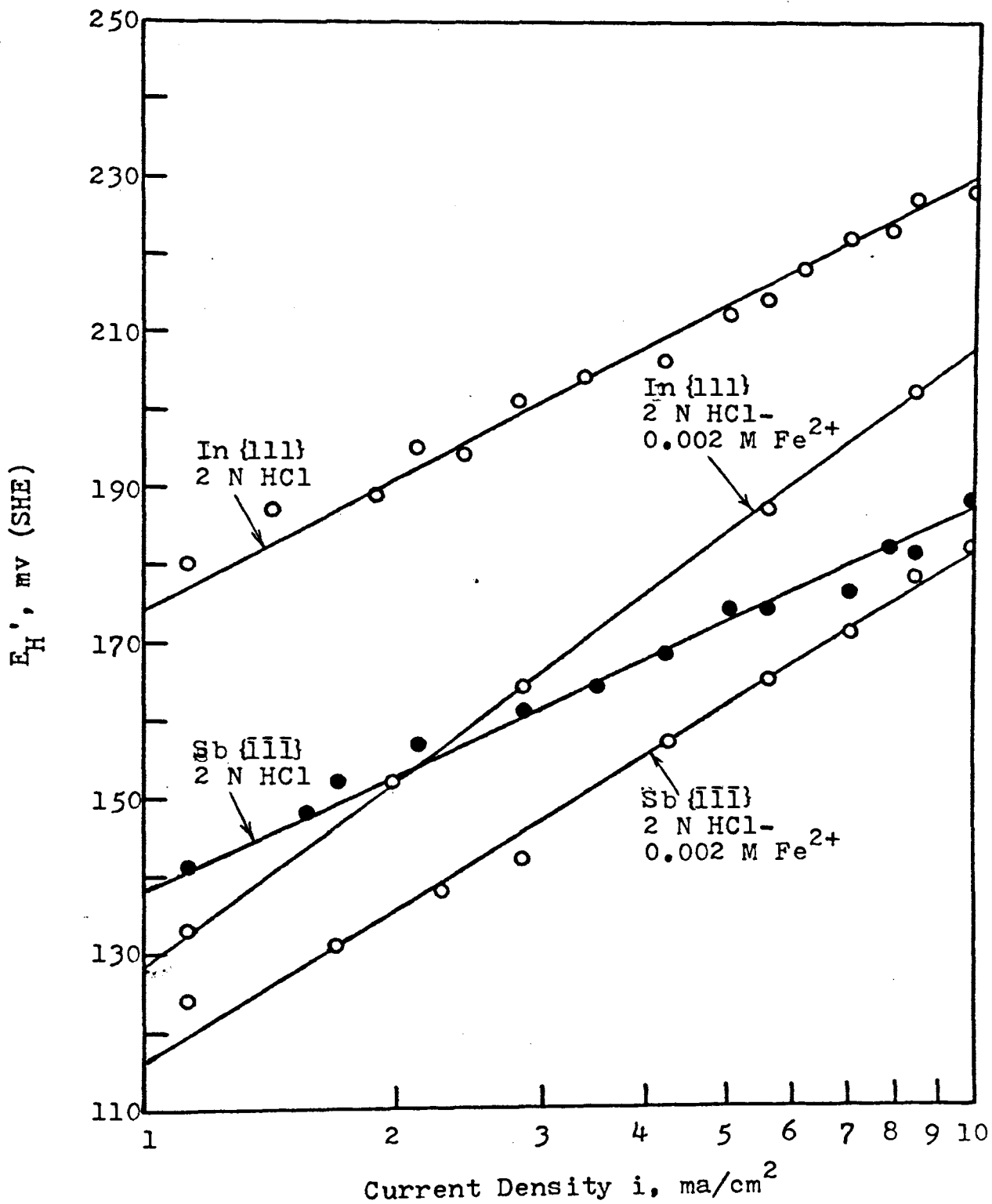


Fig. 33

Anodic dissolution potentials E_H' of the inverse {111} faces of InSb versus current density i in 2 N HCl at 25°C.

in HCl during anodic dissolution of InSb can be explained.

However, at a current density of 10 ma/cm^2 the potential difference between the inverse $\{111\}$ faces in $2 \text{ N HCl}-0.002 \text{ M Fe}^{2+}$ is $\sim 26 \text{ mv}$ and that in $2 \text{ M HCl}-0.002 \text{ M Fe}^{3+}$ is $\sim 37 \text{ mv}$, indicating the effect of Fe^{3+} in the former is smaller than that in the latter solution. It is quantitatively related to the Fe^{3+} contained in the solution.

5. In 2 N HCl with $\text{K}_3\text{Fe}(\text{CN})_6$ and $\text{K}_4\text{Fe}(\text{CN})_6$ additions.

Polarization curves for In $\{111\}$ and Sb $\{\bar{1}\bar{1}\bar{1}\}$ faces undergoing anodic dissolution in $2 \text{ N HCl}-0.00125 \text{ M K}_3\text{Fe}(\text{CN})_6$ and in $2 \text{ N HCl}-0.00125 \text{ M K}_4\text{Fe}(\text{CN})_6$ are shown in Fig. 34. The data are summarized in Tables XXV to XXVII, Appendix C. It is found that:

(1) In 2 N HCl containing $\text{K}_3\text{Fe}(\text{CN})_6$ or $\text{K}_4\text{Fe}(\text{CN})_6$ the E_H' of Sb $\{\bar{1}\bar{1}\bar{1}\}$ at lower current densities ($< \sim 4 \text{ ma/cm}^2$), is as in pure HCl, less noble than that of In $\{111\}$. The potential difference of the inverse $\{111\}$ faces in $2 \text{ N HCl}-0.00125 \text{ M K}_3\text{Fe}(\text{CN})_6$ is $\sim 13 \text{ mv}$ and that in $2 \text{ N HCl}-0.00125 \text{ M K}_4\text{Fe}(\text{CN})_6$ is $\sim 21 \text{ mv}$.

(2) At current densities lower than $\sim 4 \text{ ma/cm}^2$, keeping the concentration of HCl constant, the addition of $\text{K}_3\text{Fe}(\text{CN})_6$ shifts the E_H' of the inverse $\{111\}$ faces to less noble potentials, and the addition of $\text{K}_4\text{Fe}(\text{CN})_6$ to more noble potentials.

(3) Within the range of ~ 0.1 to $\sim 1 \text{ ma/cm}^2$ Tafel lines are obtained for the inverse $\{111\}$ faces only in 2 N HCl with $\text{K}_3\text{Fe}(\text{CN})_6$ additions with a Tafel slope of

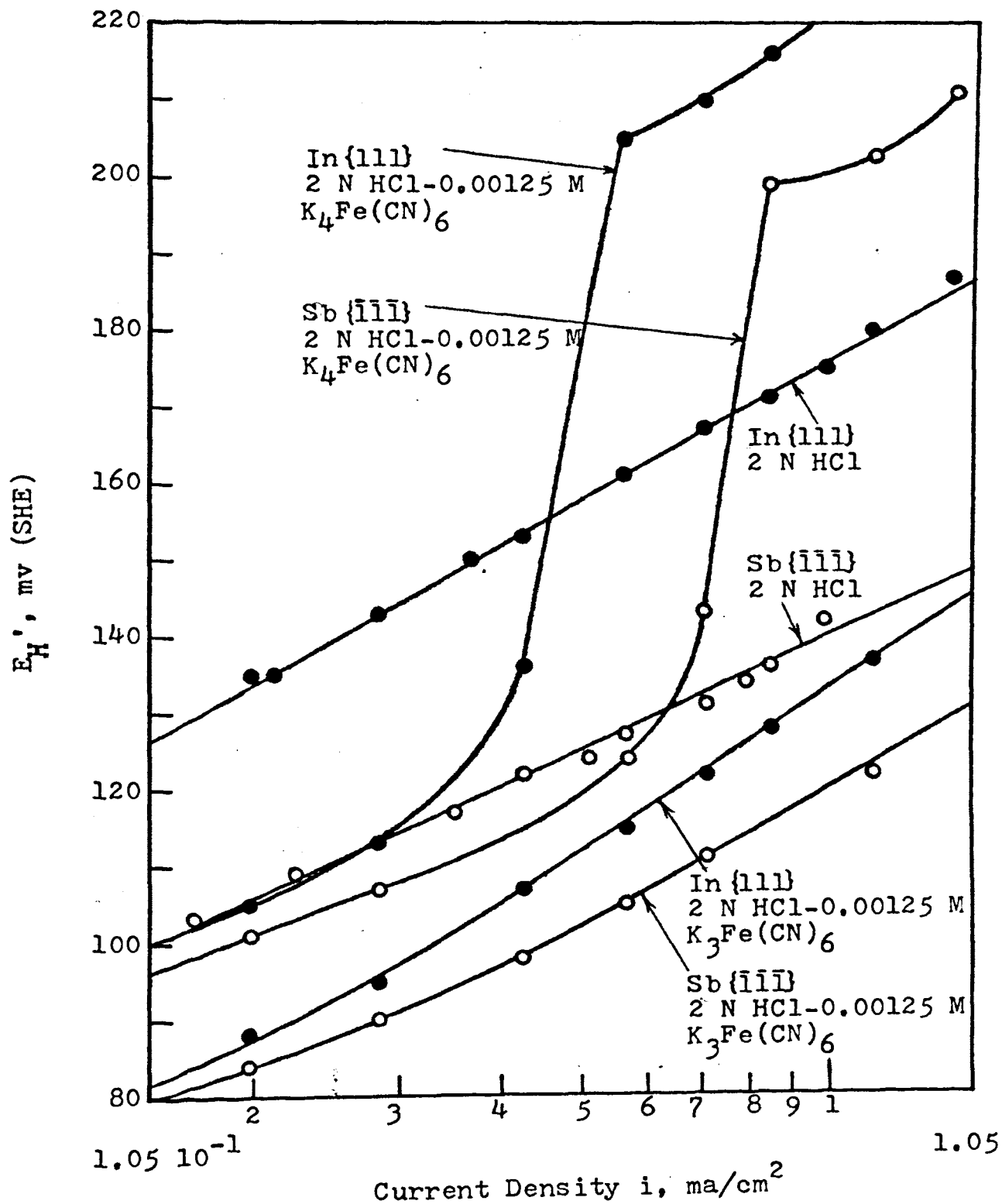


Fig. 34

Anodic dissolution potentials E_H' of the inverse {111} faces of InSb versus log of current density i in 2 N HCl with $\text{K}_3\text{Fe}(\text{CN})_6$ and $\text{K}_4\text{Fe}(\text{CN})_6$ additions at 25°C .

~ 70 mv/log i for In {111} and ~ 60 mv/log i for Sb {111}.

(4) A white colloidal layer is observed on both inverse {111} surfaces when InSb is dissolved anodically in 2 N HCl-0.00125 M $K_4Fe(CN)_6$ at a current density higher than ~ 1 ma/cm². The layer can be removed by rinsing with water. No deposit is observed in 2 N HCl-0.00125 M $K_3Fe(CN)_6$ even at a current density higher than ~ 10 ma/cm².

Mellor's "A Comprehensive Treatise on Inorganic and Treoretical Chemistry"²⁸⁾ mentions that $K_4Fe(CN)_6$ gives with In^{3+} a white precipitate, but no precipitate with solutions of $K_3Fe(CN)_6$. $K_3Fe(CN)_6$ can also be reduced by metallic Sb. $SbCl_3$ gives a white precipitate with $K_4Fe(CN)_6$, but no precipitate with a solution of $K_3Fe(CN)_6$. These statements were confirmed experimentally. Thus, the E_H' of the inverse {111} faces abrupt shift to more noble potentials in 2 N HCl-0.00125 M $K_4Fe(CN)_6$ (Fig. 34) was due to the formation of a white colloidal layer starting at a certain current density on the InSb surface. This layer increased the resistance between the InSb bulk and the solution, and as a consequence the potential became more noble when measured galvanostatically.

In a 2 N HCl-0.00125 M $K_3Fe(CN)_6$ solution, $K_3Fe(CN)_6$ reacted as an oxidant and was reduced by Sb. Therefore, during anodic dissolution of InSb, this oxidation reaction increased the dissolution rate and removed the layer possibly formed on the InSb surface. Thus the resistance between the InSb bulk and the electrolyte decreased and the E_H' became less noble in comparision with E_H' in pure 2 N HCl (Fig.34).

At higher current densities ($> \sim 8 \text{ ma/cm}^2$), the reduction reaction along with anodic dissolution became serious and an appreciable amount of $\text{K}_4\text{Fe}(\text{CN})_6$ was produced which possibly reacted with In^{3+} or Sb^{3+} to give a white precipitate. This white precipitate formed as a thin colloidal layer on the InSb surface as observed in the solution of 2 N HCl-0.00125 M $\text{K}_4\text{Fe}(\text{CN})_6$. This resulted in the potential increasing from a less noble to a more noble potential in comparison with E_{H} in pure 2 N HCl and also inverted the sequence in the potentials of In 111 and Sb 111 (see Tables XXV and XXVI).

VI. EFFECT OF TEMPERATURE ON THE DISSOLUTION POTENTIAL-CURRENT DENSITY RELATIONSHIP OF InSb SINGLE CRYSTALS DISSOLVING ANODICALLY IN 2 N HCl

A. Materials

The materials were the same as described in Section III.

B. Apparatus and Procedure

1. Galvanostatic experiments. The apparatus and procedure used here were the same as described in Section V. A sketch of the arrangement is shown in Fig. 16. The water bath temperature was maintained by adjusting the thermostat (P).

2. Potentiostatic experiments. A Wenking potentiostat (N) was used to maintain a constant potential of the anode (A). A Keithley electrometer (M) measured the potential difference between the anode and reference electrode (I). The current was recorded on a Bausch & Lomb graphic ammeter (L). The rest of the apparatus was the same as that for the galvanostatic measurements. A sketch of the arrangement is shown in Fig. 35. Adjusted at a specific anodic potential, the temperature of the water bath could be set by the thermostat between 25°C to 45°C at an increment of ~5 degrees for working at various temperatures.

C. Data and Results

1. The dissolution potential-current density relationship for InSb single crystals dissolving anodically at various temperatures. The polarization curves of In{111}

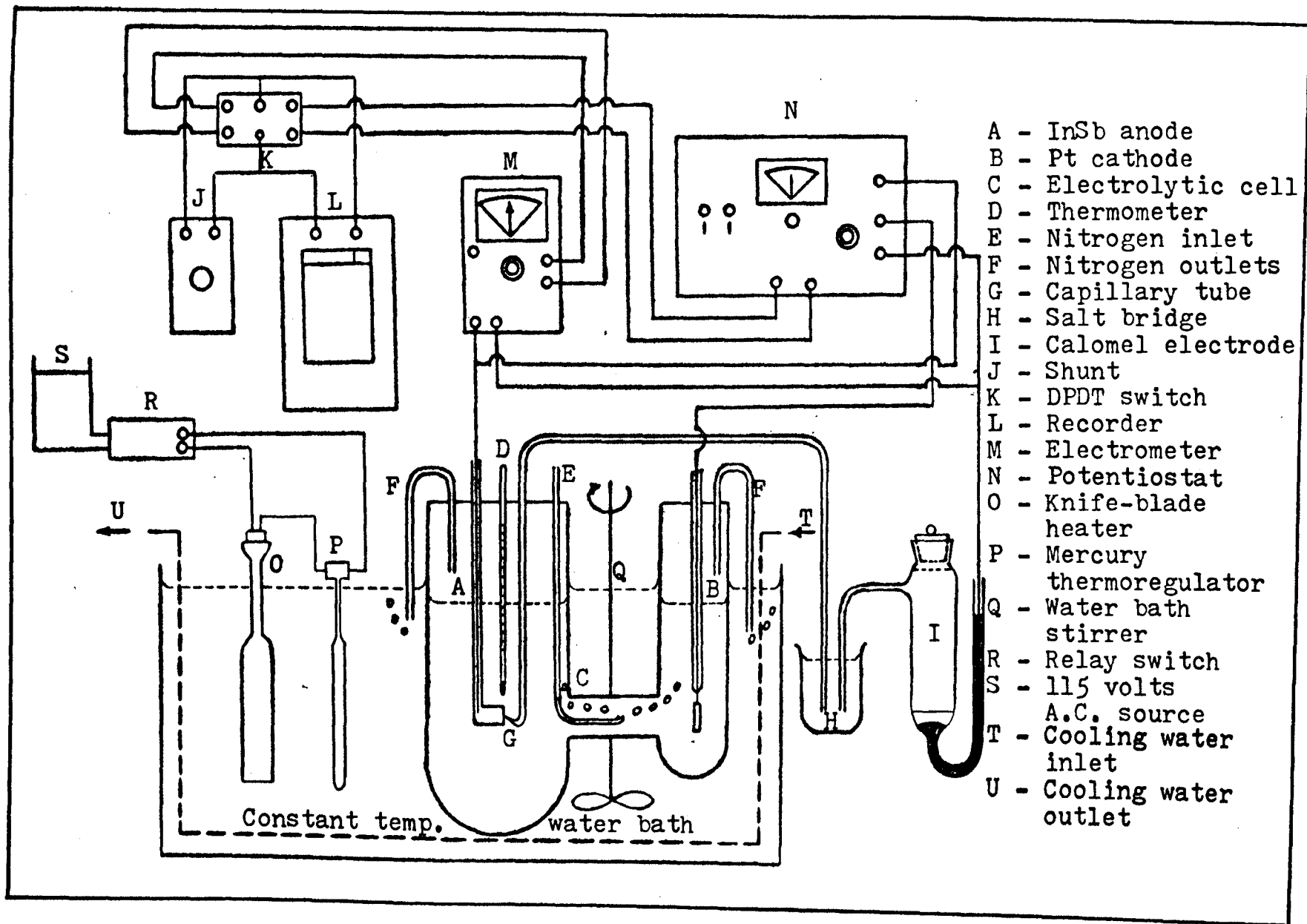


Fig. 35. Sketch of the apparatus used for potentiostatic studies of InSb single crystals undergoing anodic dissolution.

and Sb{ $\bar{1}\bar{1}\bar{1}$ } faces of InSb single crystals undergoing anodic dissolution in 2 N HCl at 25°C, 35°C, and 45°C are traced in Fig. 36 and 37. The data are listed in Tables XIII to XIV and XXIX to XXXII, Appendix C. It is found that:

(1) At the same current density, the anodic dissolution potential E_H' for both inverse {111} faces becomes less noble with increasing temperature.

(2) All the anodic polarization curves of both inverse {111} faces at different temperatures obey the Tafel relation over at least two decades of current density, roughly within the range of 10^{-1} to 10 ma/cm² for In{111} face (Fig. 36) and 10^{-1} to 30 ma/cm² for the Sb{ $\bar{1}\bar{1}\bar{1}$ } face (Fig. 37).

(3) Within the above mentioned ranges of current density, the three anodic polarization curves give nearly parallel Tafel lines, with slopes of ~ 56 mv/log i for the In{111} face (Fig. 36) and ~ 48 mv/log i for the Sb{ $\bar{1}\bar{1}\bar{1}$ } face (Fig. 37).

(4) Within the Tafel region, the potential differences of the In{111} face are ~ 30 mv, and that of Sb{ $\bar{1}\bar{1}\bar{1}$ } ~ 23 mv for each 10 degrees of temperature change.

(5) The potential differences between In{111} and Sb{ $\bar{1}\bar{1}\bar{1}$ } are ~ 36 mv, ~ 27 mv and ~ 20 mv at 25°C, 35°C and 45°C respectively.

2. Activation energy calculations. To explain the effect of temperature on anodic current density (or dissolution rate), the Arrhenius equation was applied:

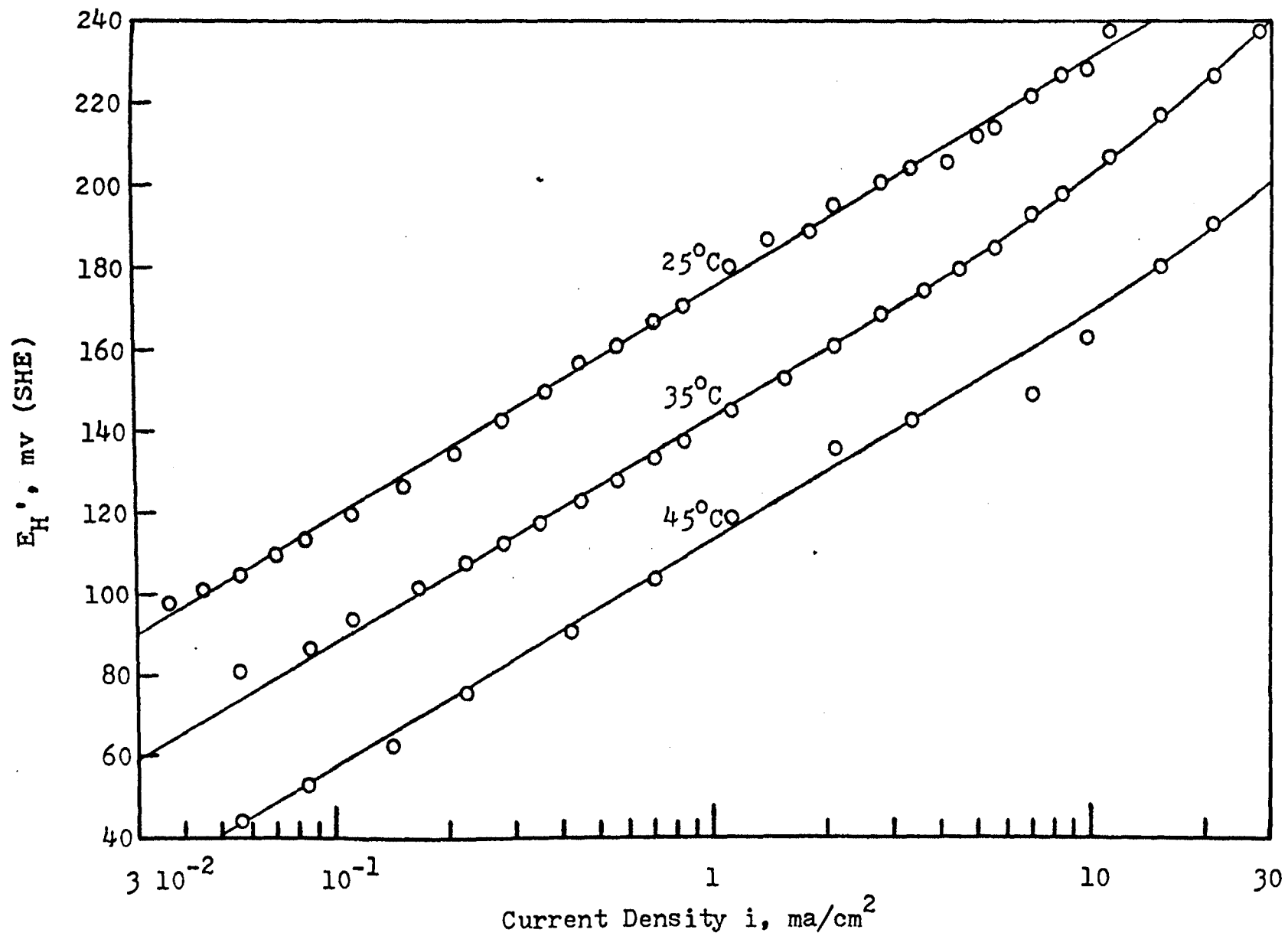


Fig. 36. Anodic dissolution potentials E_H' of the In(111) face of InSb versus current density i in 2 N HCl at three temperatures.

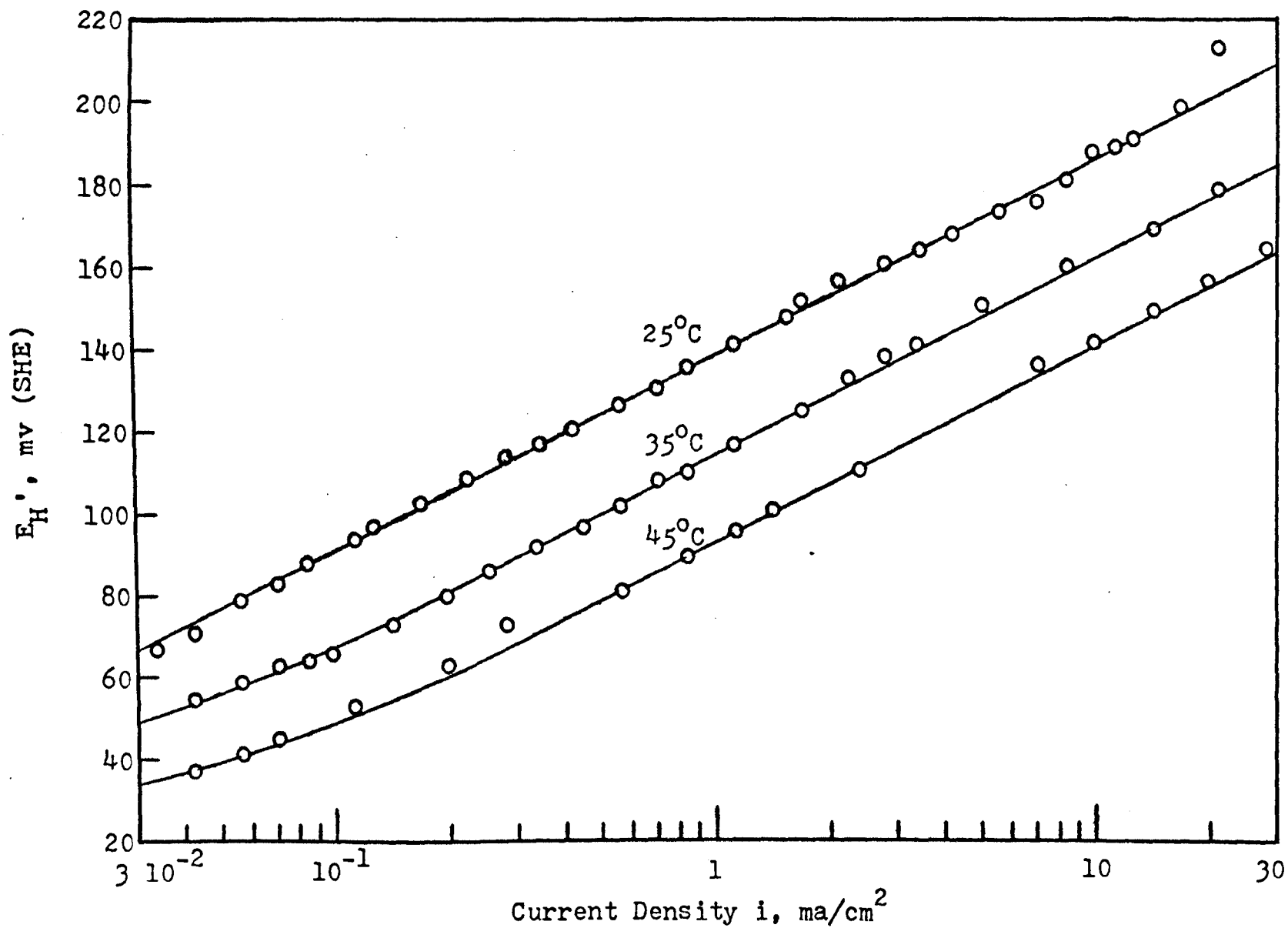


Fig. 37. Anodic dissolution potentials E_H' of the Sb{111} face of InSb versus current density i in 2 N HCl at three temperatures.

$$k = A e^{-E_a/RT} \quad (3)$$

where k is the reaction or dissolution rate constant related to the anodic current density i ²⁸, A a frequency factor, E_a the energy of activation of the reaction, R the gas constant and T the absolute temperature. Replacing k by i , the logarithmic form of equation (3) is then as follows:

$$\log i = - \frac{E_a}{2.303 R} \frac{1}{T} + \log A' \quad (4)$$

A plot of $\log i$ verse $\frac{1}{T}$ should conform to a straight line, with the slope being related to the activation energy by

$$\text{slope} = - \frac{E_a}{2.303 R}$$

where E_a is expressed in cal/mole and R the gas constant in cal/mole-deg with a value of 1.987. The activation energy was calculated based on two different ways of measurement.

a. E_a from galvanostatic measurements. Arrhenius plots for the anodic dissolution of both inverse {111} faces of InSb in 2 N HCl were obtained with the arrangement of Fig. 35 at a potential of 101 mv (SHE). The data are summarized in Tables XXXIII-A and B. The plots are shown in Fig. 38.

The calculated slopes (Fig. 38) of In{111} and Sb{111} are equal to -5.24×10^3 and -4.65×10^3 respectively.

Thus,

$$\text{for In}\{111\}, \quad - 5.24 \times 10^3 = - \frac{E_a}{2.303 R}$$

$$E_a = 24.0 \text{ Kcal/mole}$$

$$\text{for Sb}\{\bar{1}\bar{1}\bar{1}\}, \quad - 4.65 \times 10^3 = - \frac{E_a}{2.303 R}$$

$$E_a = 21.3 \text{ Kcal/mole}$$

Therefore, the average value of E_a is 22.6 ± 1.4 Kcal/mole

TABLE XXXIII

DATA USED TO MAKE ARRHENIUS PLOT FOR THE ANODIC DISSOLUTION
OF InSb SINGLE CRYSTALS IN 2 N HCl

A. In {111}

$$E_H' = 101 \text{ mv (SHE)}$$

Temperature (°C)	(1/T) × 10 ³ (°K)	(1/T) × 10 ³ (°K ⁻¹)	i* (ma/cm ²)	log i (ma/cm ²)
25	298.16	3.354	4.8 × 10 ⁻²	-1.319
35	308.16	3.245	1.75 × 10 ⁻¹	-0.757
45	318.16	3.143	6.2 × 10 ⁻¹	-0.215

*Value from Fig. 36.

B. Sb {111}

$$E_H' = 101 \text{ mv (SHE)}$$

Temperature (°C)	(1/T) × 10 ³ (°K)	(1/T) × 10 ³ (°K ⁻¹)	i* (ma/cm ²)	log i (ma/cm ²)
25	298.16	3.354	1.6 × 10 ⁻¹	-0.796
35	308.16	3.245	5.2 × 10 ⁻¹	-0.284
45	318.16	3.143	1.45	0.161

*Value from Fig. 37.

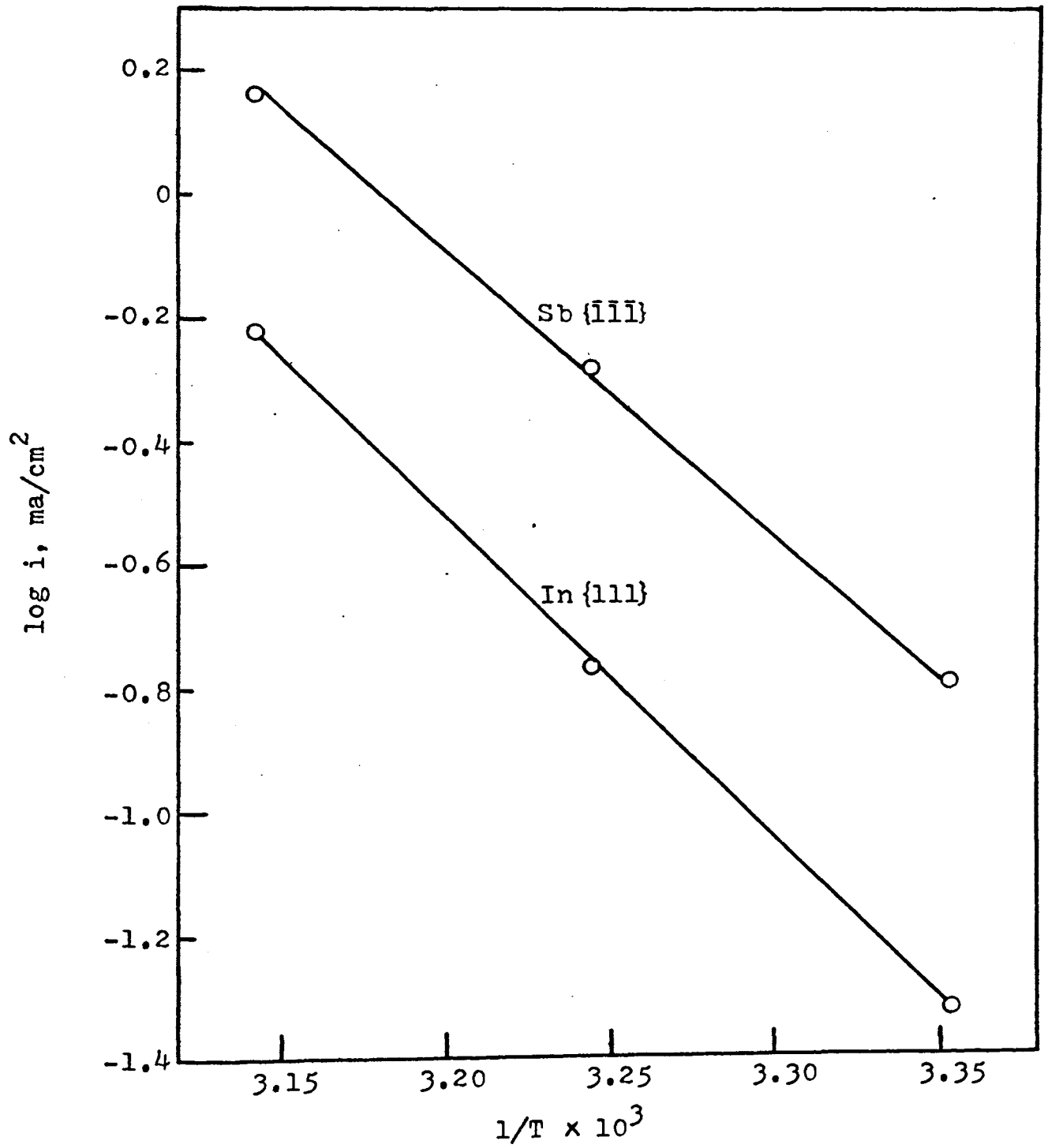


Fig. 38. Arrhenius plot of the anodic dissolution of InSb single crystals in 2 N HCl. Galvanostatic measurements.

b. E_a from potentiostatic measurements. The current density data at various temperatures for four different planes at a potential of 101 mv (SHE) can be found in Tables XXXIV A to D. The Arrhenius plots are shown in Fig. 39.

The calculated slopes (Fig 39) for In{111}, Sb{ $\bar{1}\bar{1}\bar{1}$ }, {110} and {100} are -4.65×10^3 , -4.40×10^3 , -4.43×10^3 and -4.05×10^3 respectively. Thus,

$$\text{for In}\{111\}, \quad -4.65 \times 10^3 = -\frac{E_a}{2.303 R}$$

$$E_a = 21.3 \text{ Kcal/mole}$$

$$\text{for Sb}\{\bar{1}\bar{1}\bar{1}\}, \quad -4.40 \times 10^3 = -\frac{E_a}{2.303 R}$$

$$E_a = 20.1 \text{ Kcal/mole}$$

$$\text{for}\{110\}, \quad -4.43 \times 10^3 = -\frac{E_a}{2.303 R}$$

$$E_a = 20.3 \text{ Kcal/mole}$$

$$\text{for}\{100\}, \quad -4.05 \times 10^3 = -\frac{E_a}{2.303 R}$$

$$E_a = 18.5 \text{ Kcal/mole}$$

Therefore, the average value of E_a is 20.0 ± 0.8 Kcal/mole

This investigation shows that (1) there are no appreciable differences among the apparent activation energies of different planes and (2) that the apparent activation energies obtained from both galvanostatic and potentiostatic measurements are fairly close to each other. The close

TABLE XXXIV

DATA USED TO MAKE ARRHENIUS PLOT FOR THE ANODIC DISSOLUTION
OF InSb SINGLE CRYSTALS IN 2 N HCl AT A POTENTIAL
OF 101 mv (SHE). POTENTIOSTATIC MEASUREMENTS.

A. In {111}

Temperature (°C)	(°K)	$(1/T) \times 10^3$ (°K ⁻¹)	i^* (ma/cm ²)	log i (ma/cm ²)
25.8	298.96	3.345	4.96 10^{-2}	-1.305
30.8	303.96	3.290	8.98 10^{-2}	-1.047
35.25	308.41	3.242	1.50 10^{-1}	-0.824
40.3	313.46	3.190	2.60 10^{-1}	-0.585
44.8	317.96	3.145	4.76 10^{-1}	-0.322

*Value from potentiostatic measurements.
Exposed surface area of the electrode = 0.353 cm².

B. Sb {111}

Temperature (°C)	(°K)	$(1/T) \times 10^3$ (°K ⁻¹)	i^* (ma/cm ²)	log i (ma/cm ²)
25.5	298.66	3.348	1.57 10^{-1}	-0.803
30.35	303.51	3.295	2.88 10^{-1}	-0.541
35.2	308.36	3.243	4.94 10^{-1}	-0.306
39.8	312.96	3.195	8.29 10^{-1}	-0.081
44.6	317.76	3.147	1.280	0.107

*Value from potentiostatic measurements.
Exposed surface area of the electrode = 0.82 cm².

C. {110}

Temperature		$(1/T) \times 10^3$ ($^{\circ}\text{K}^{-1}$)	i*		log i
($^{\circ}\text{C}$)	($^{\circ}\text{K}$)		(ma/cm 2)		(ma/cm 2)
25.75	298.91	3.345	1.53	10^{-1}	-0.815
30.85	304.01	3.290	2.72	10^{-1}	-0.565
35.2	308.36	3.243	4.16	10^{-1}	-0.381
40.15	313.31	3.192	7.37	10^{-1}	-0.133
44.65	317.81	3.147	1.444		0.160

*Value from potentiostatic measurements.

Exposed surface area of the electrode = 0.353 cm 2 .

D. {100}

Temperature		$(1/T) \times 10^3$ ($^{\circ}\text{K}^{-1}$)	i*		log i
($^{\circ}\text{C}$)	($^{\circ}\text{K}$)		(ma/cm 2)		(ma/cm 2)
25.3	298.46	3.351	1.28	10^{-1}	-0.893
30.3	303.46	3.295	2.17	10^{-1}	-0.664
35.0	308.16	3.245	2.87	10^{-1}	-0.542
39.7	312.86	3.196	5.49	10^{-1}	-0.260
44.4	317.56	3.149	8.41	10^{-1}	-0.075

*Value from potentiostatic measurements.

Exposed surface area of the electrode = 0.82 cm 2 .

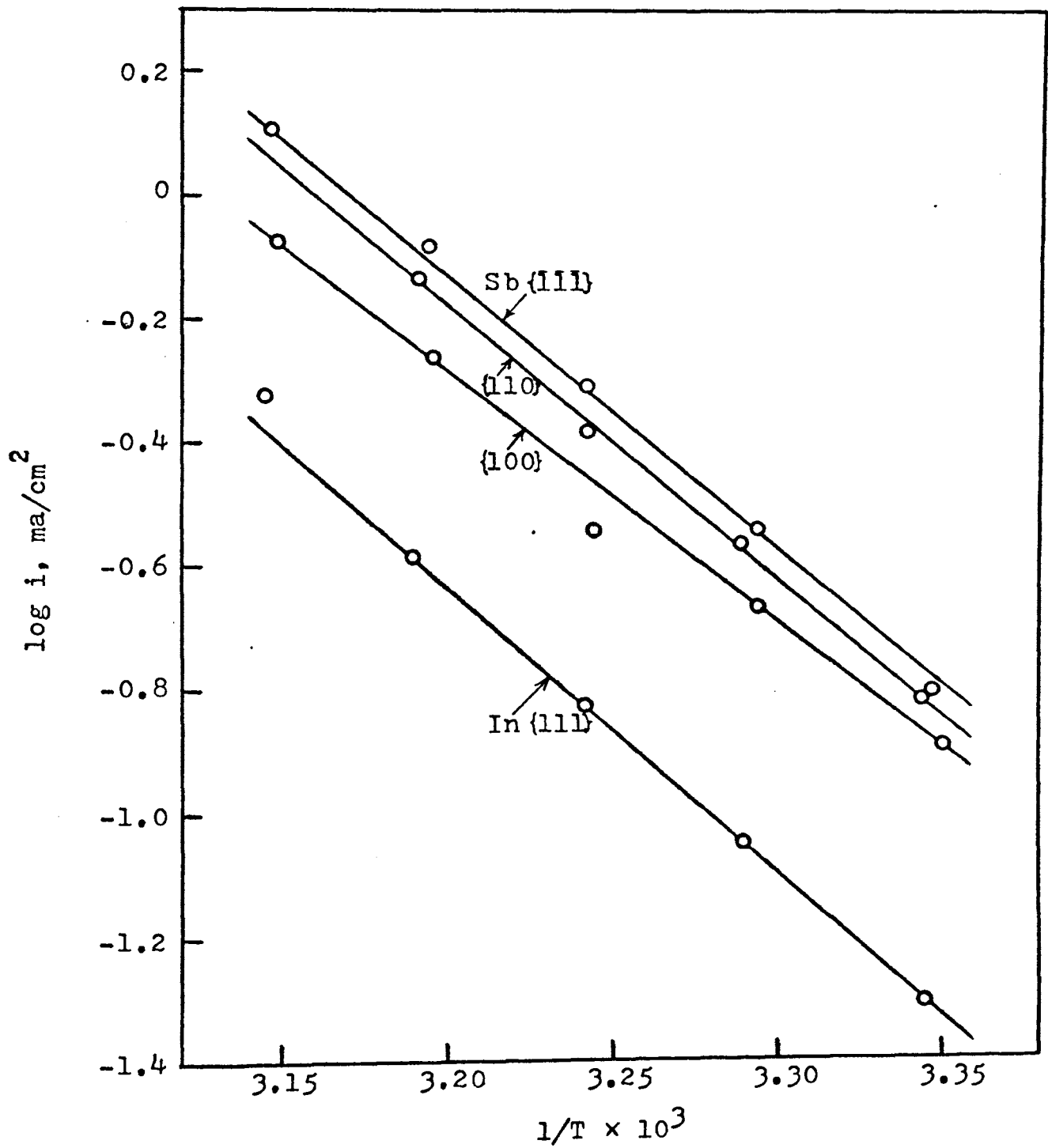


Fig. 39. Arrhenius plot of the anodic dissolution of InSb single crystals in 2 N HCl. Potentiostatic measurements.

agreement of the E_a values for the faces measured suggests that the mechanism of dissolution (r.d.s.) is the same regardless of the crystal plane and that the anodic dissolution of the planes is under chemical activation control. Finally, the inclination of the potential-current density slopes suggests a one electron discharge for the slow step of InSb anodic dissolution in HCl, similarly as for GaAs in KOH²¹⁾.

VII. DISCUSSION

The discussion of results regarding InSb is presented in three parts; (1) anodic dissolution and potentials, (2) etching behavior of the $\{111\}$ faces, and (3) coulometric measurements and disintegration.

A. Anodic Dissolution and Potentials

From the Tafel curves of the 4 planes of InSb undergoing anodic dissolution in 2 N HCl, it appears that the nobility decreases in the sequence: In $\{111\}$, $\{100\}$, $\{110\}$ and Sb $\{111\}$. The largest deviation of anodic dissolution potentials is observed between the inverse $\{111\}$ planes, the potential of In $\{111\}$ being always nobler. This is also true for InSb dissolving anodically in some other electrolytes, such as $\text{HNO}_3\text{-H}_2\text{C}_4\text{H}_4\text{O}_6$, HCl-Fe^{3+} , HCl-Fe^{2+} , $\text{HCl-K}_3\text{Fe(CN)}_6$ and $\text{HCl-K}_4\text{Fe(CN)}_6$. Thus, it is found that the addition of either oxidizing or reducing agent does not shift the sequence of nobility of the inverse $\{111\}$ planes. As to the rest potential of the inverse $\{111\}$ planes, that of In $\{111\}$ in HCl-Fe^{3+} is significantly nobler. In order to explain the differences in dissolution potentials between the inverse $\{111\}$ planes, it is better to begin with crystal structure and molecular configuration.

It has been mentioned in the literature review that InSb with a noncentrosymmetric center is polar and, therefore, not all directions in the crystal are equivalent. Taking the $\{111\}$ direction as an example (Fig. 40), each

surface atom (for instance, In) is attached by three bonds to the layer of the Sb atoms beneath. Each of the Sb atoms in turn is attached to the surface layer by three bonds, but to the layer beneath by only one bond. Therefore, if the surface layer of In atoms is removed by dissolution, in the uncovered layer of Sb there are three free bonds at each atom. This configuration is considered as highly unstable. Thus, the removal of material occurs immediately in two layers and after dissolution the surface layer again consists of In atoms¹⁴). For this reason, the opposite face, Sb{ $\bar{1}\bar{1}\bar{1}$ }, always consists of atoms of Sb and this situation is maintained during dissolution.

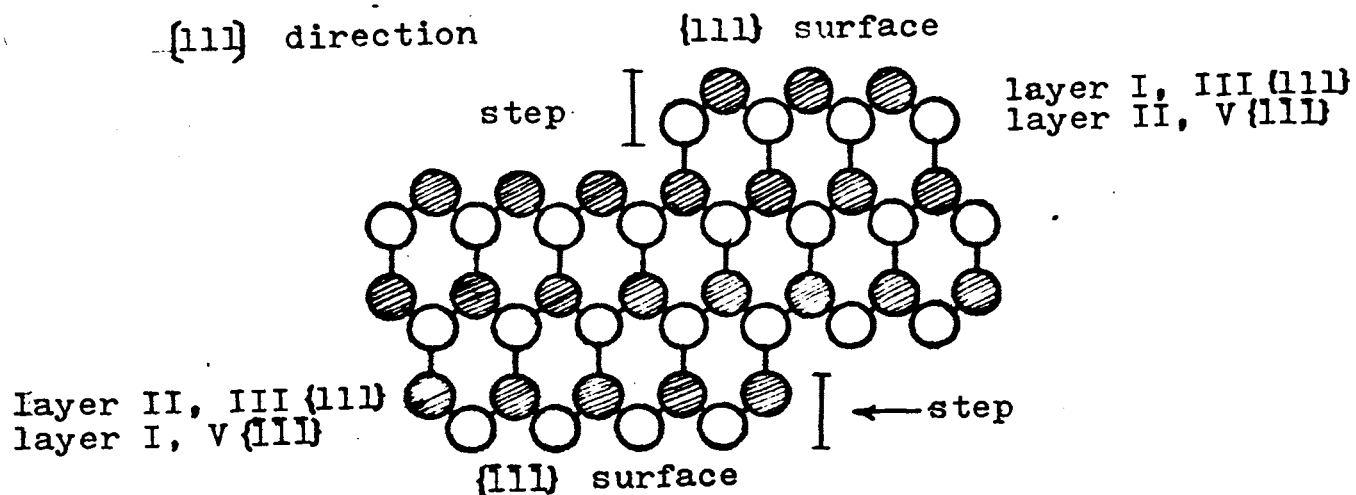


Fig. 40

Two-dimensional representation of the zinc-blende structure
with surface steps

For further explaining the differences in behavior between the inverse {111} faces of InSb, the electronic structure of the surface atoms of In and Sb is sketched in Fig. 41. This structure is considered as the most likely to occur as it leads to electrically neutral surfaces⁷⁾. Since the atoms of In are triply bonded to the surface layer of the Sb atoms and the former atoms are normally trivalent, therefore all the valency electrons are used in covalent bonds with Sb atoms. The Sb atoms are triply bonded to the surface layer of the In atoms, but the normal valence of Sb is five. Therefore, the Sb atoms have an unshared pair of electrons available for reaction and should be more reactive than the In atoms.

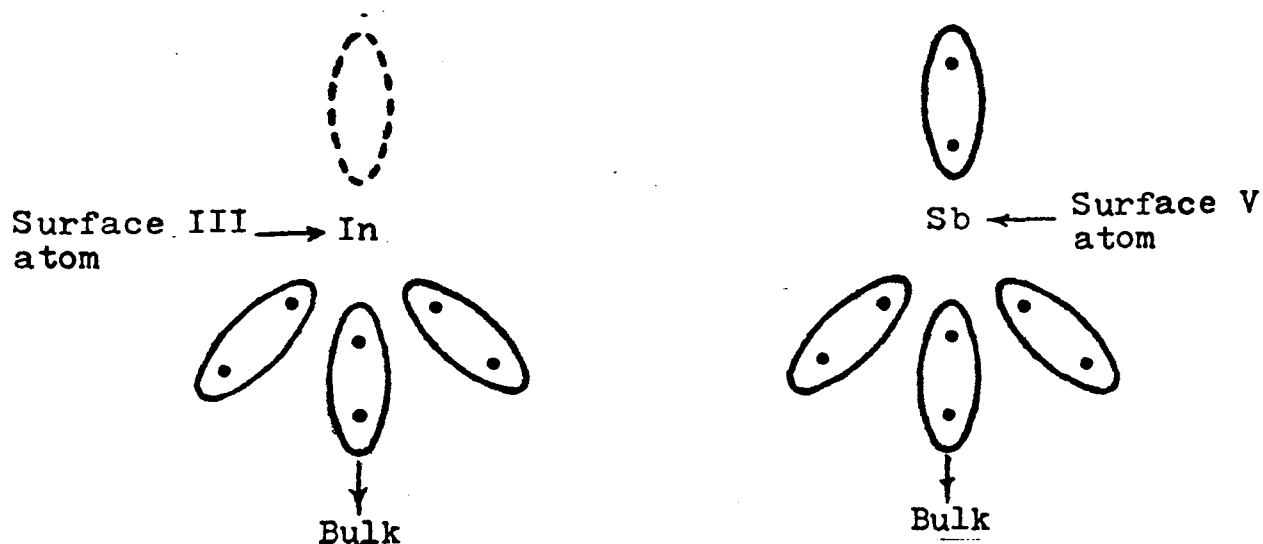


Fig. 41

Schematic diagram of the electronic structure of a single InSb crystal

However, this condition does not show up in the dissolution potentials of metallic In and Sb. Therefore, the anodic potential (E_H')-current density (i) relationship of both metallic In and Sb in 2 N HCl (at 25°C) was investigated. The results are tabulated in Tables XXXV to XXXVI, Appendix C, and plotted in Fig. 42. For comparison, the results for the inverse {111} faces are also shown. It can be seen that E_H' of metallic Sb is much more noble (~600 mv) than that of metallic In. Contrariwise, the Sb{ $\bar{1}\bar{1}\bar{1}$ } face, which upon dissolution leaves more Sb atoms present (In goes into solution easier), has a less noble potential than the In{111} face. If the chemical properties of the two inverse {111} faces are determined by the properties of the respective dominating atoms, take Sb{ $\bar{1}\bar{1}\bar{1}$ } for example, the E_H' should be more noble than that of In{111}. However, this is not so (Fig. 42). Evidently on In{111} surface, In goes into solution faster and Sb remains. A dense protective layer of $Sb_4O_5Cl_2$ is formed and hence, the potential becomes nobler than that of the inverse side where the protective layer may be thinner. Thus, the protective layers explain the decreased rate of In{111} (Fig. 30). Generally, the dissolution potentials of the two inverse {111} faces are much closer to that of metallic Sb than to metallic In, indicating that the latter undergoes a larger chemical change during the InSb formation than Sb. It is also interesting to note that pure Sb becomes passive at a current density of ~15 ma/cm² while Sb{ $\bar{1}\bar{1}\bar{1}$ } does not passivate even at

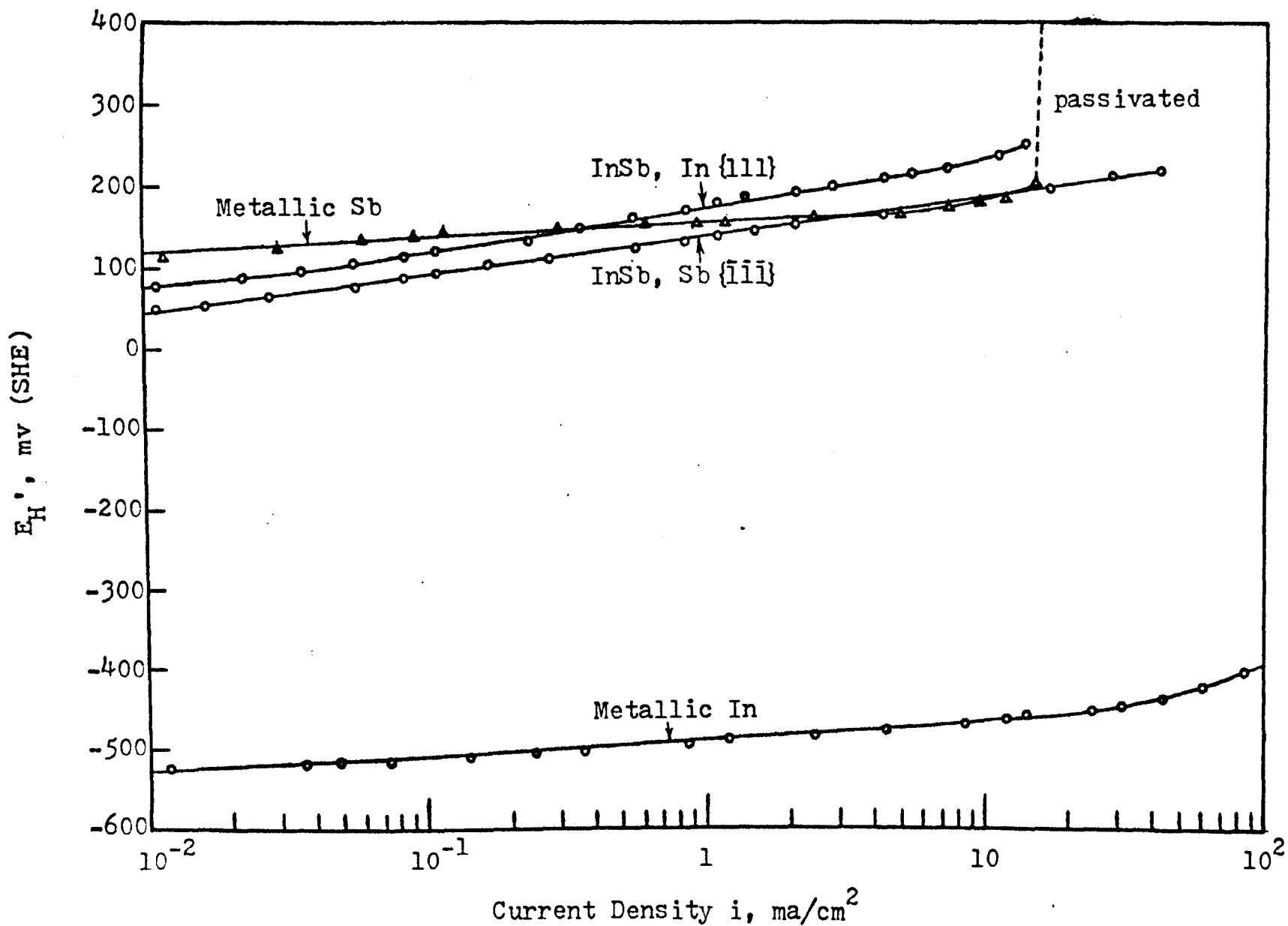


Fig. 42. Anodic dissolution potentials E_H' of metallic In, metallic Sb and the inverse {111} faces of an InSb single crystal versus log of current density i in 2 N HCl at 25°C.

$\sim 40 \text{ ma/cm}^2$ (Fig. 42). From the above investigation, it can be concluded that a single InSb crystal behaves quite differently than the pure metallic components, whereby the chemical activity of the Sb{111} face is greater than that of the In{111} face, which applies also in the presence of oxidizing and reducing agents such as Fe^{3+} , $\text{K}_3\text{Fe}(\text{CN})_6$, Fe^{2+} and $\text{K}_4\text{Fe}(\text{CN})_6$.

B. Etching Behavior of the {111} Surfaces

The growth and dissolution of crystals are generally considered to proceed through the propagation of atomic or molecular steps along the exposed surface¹⁴⁾. In the case of the III-V compounds like InSb, such steps are considered to be diatomic layers as shown in Fig. 40. The surface configuration with simply bonded atoms is considered unstable; if it were stable, both inverse {111} faces would behave alike. Thus, the rate determining step of the dissolution process is primarily associated with the binding between layers I and II instead of breaking the single bonds between the atoms of layer II and the substrate. According to Gatos et al.'s¹⁴⁾ explanation, atomic pits are created by the removal of one atom from layer I and the kinks are created by the removal of the adjacent atoms also from layer I such as shown in Fig. 43. Those pits and kinks can be considered as nucleation points for further forming pits and also for merging pits. (This etching behavior is shown by this investigation in Section III). Furthermore, it may be assumed that the formation of etch pits is due to

the relative magnitudes of the rate of dissolution of the diatomic steps (indicated by V_s) and the rate of formation of atomic pits or kinks (indicated by V_n)¹⁴). Taking an In{111} face etched chemically in modified CP-4 for instance, the rate of formation of atomic pits or kinks exceeds that of dissolution of the diatomic steps, therefore the etch pits are formed on the In{111} face. Etching the Sb{ $\bar{1}\bar{1}\bar{1}$ } face, V_n does not exceed V_s , thus no pits are observed on it and as a result of etching the Sb{ $\bar{1}\bar{1}\bar{1}$ } face becomes polished. When InSb is etched anodically in 2 N HCl or 1 N HNO₃-1 N H₂C₄H₄O₆, the rate of formation of atomic pits and kinks of both inverse {111} faces exceeds that of dissolution of the diatomic steps; therefore the dislocation etch pits are observed on both planes.

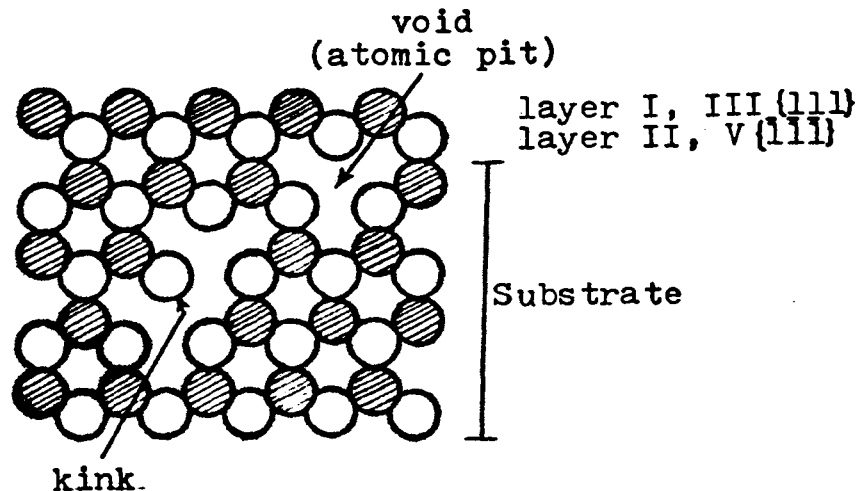


Fig. 43

Representation of a {111} face with an atomic pit and kink

According to Gatos and Lavine¹⁴), in some instances virtually all of the dislocations can be revealed individually by employing slow etchants. In general, however, an etchant which develops dislocation etch pits does not necessarily reveal all of the dislocations terminating at a given surface. The fact that distinct dislocation etch pits have not been observed on the $\{111\}$ planes certainly does not imply that these surfaces are not intersected by dislocation lines. They also point out the etching difference between the two inverse $\{111\}$ faces is due to the much higher overall etch rate of $V\{\bar{1}\bar{1}\bar{1}\}$ faces, which must be greatly reduced by addition of an inhibitor to allow regular etch pits to be formed.

In the present investigation of anodic dissolution, however, etch pits are observed on both inverse $\{111\}$ faces. After anodic etching in acidic solutions (at a lower current density where no visible anodic film is formed), it is found that the In $\{111\}$ surface is always shinier than that of the Sb $\{\bar{1}\bar{1}\bar{1}\}$ surface. Thus the surface appearance gives another way to distinguish the inverse $\{111\}$ faces of InSb.

The HNO_3 -HF etchant produces round etch pits on the In $\{111\}$ faces and a few triangular etch pits on the Sb $\{\bar{1}\bar{1}\bar{1}\}$ faces. In the HCl- Fe^{3+} etchant, the etch figures on the In $\{111\}$ and the Sb $\{\bar{1}\bar{1}\bar{1}\}$ faces are strikingly different. The etch figures on the In $\{111\}$ faces form arrays of well defined or overlapping equilateral triangles (Fig. 7). The

etch figures on the Sb $\{\bar{1}\bar{1}\bar{1}\}$ faces are irregular or regular hexagons but usually less well-defined than those on the inverse planes. Both etch figures are bounded along the $\{110\}$ direction¹⁴⁾. These two etch patterns of the inverse $\{111\}$ planes observed by this investigation (Fig. 7 and 8) are different from those observed by Gatos and Lavine (see Fig. 2 of their publication¹⁴⁾). The overlapping equilateral triangular etch figures do appear on the In $\{111\}$ face instead of the Sb $\{\bar{1}\bar{1}\bar{1}\}$ face. This is further shown by Fig. 15. Thus, the identification of the two inverse $\{111\}$ faces of InSb by chemical etching is also possible using $\text{HNO}_3\text{-HF}$ or HCl-Fe^{3+} as etchant. It shows that the characteristic etch patterns can thus be developed under anodic or chemical etching by employing several kinds of etchants, as indicated above, without the addition of an inhibitor.

C. Coulometric Measurements and Disintegration

The coulometric measurements show that InSb undergoes anodic dissolution in 2 N HCl at a lower current density (less than $\sim 40 \text{ ma/cm}^2$) with the formation of In^{3+} and Sb^{3+} , which explains the apparent electron number of 6. At a higher anodic current density (above $\sim 40 \text{ ma/cm}^2$) the total apparent electron number is less than 6. The present investigation proves that this is due to partial disintegration of InSb. During electrolysis a dark film consisting of antimony hydroxyl chloride is formed on the surface of the anode, identified by X-ray diffraction to be $\text{Sb}_4\text{O}_5\text{Cl}_2$.

Sb particles, colloidal in origin and embedded in this corrosion product, are responsible for the dark color.

As the products of anodic dissolution of the III-V intermetallic compound are insoluble or only slightly soluble in the electrolyte, they are deposited on the surface, as for metallic electrodes. Under certain conditions anodic films can grow to a considerable thickness provided that there is adequate ionic conduction through the film to carry the current for continued film growth. For one or another reasons these films do not cover the anodes uniformly and the anodic current will follow the path of least resistance. At places where the film is thin or not formed at all, the current density will be high and anodic dissolution will occur around such spots, undermining them. After some time the respective spot still containing some metallic compound adhering to the anodic layer, may drop out. If the anodic layer is difficultly soluble in the electrolyte, the metallic particles will appear embedded in the film. That is why metallic antimony is found in the InSb anodic film after it is annealed to $\sim 650^{\circ}\text{C}$ in the evacuated glass tubing. The purpose of this annealing is to separate the metallic compound from the anodic film. This separation occurs by clustering of the original colloidal Sb particles to layer entities.

Metallic Sb and $\text{Sb}_4\text{O}_5\text{Cl}_2$ (the main composition of the anodic film) are insoluble in aqueous HCl, whereas metallic In and indium oxides or chlorides are easily dissolved in

HCl. As the X-ray diffraction pattern of the annealed anodic film is identical with that of the precipitate (prepared by dissolving SbCl_3 in HCl and diluting with water), it is, therefore, reasonable to assume that In and In compounds are not present in the anodic layer.

The ions (mainly In^{3+}) going anodically into solution exhibit some pressure on the Sb-salt film formed and it may slightly separate from the substrate. A new anodic film is then formed underneath on the places of separation. It is shown in Fig. 18 that such an anodic film results from both inverse $\{111\}$ faces, and grows layer by layer and continuously for the time of electrolysis, indicating that the film growth behavior of InSb is similar to that of most pure metals.

VIII. SUMMARY AND CONCLUSION

The etching behavior of single InSb crystals was studied in this investigation. The inverse $\{111\}$ faces can be identified by: (1) etch patterns developed by chemical etching with modified CP-4, $\text{HNO}_3\text{-HF}$ or HCl-Fe^{3+} etchants, (2) etch figures produced from anodic dissolution in acidic solutions, (3) open circuit potentials in HCl-Fe^{3+} solution or anodic dissolution potentials in acidic solutions, e.g. HCl , $\text{HNO}_3\text{-H}_2\text{C}_4\text{H}_4\text{O}_6$, as the potentials of $\text{In}\{111\}$ are always nobler than that of $\text{Sb}\{\bar{1}\bar{1}\bar{1}\}$, (4) surface appearance after anodic dissolution in acidic solutions (when no visible anodic film is formed), as the $\text{In}\{111\}$ surface is shinier than that of the $\text{Sb}\{\bar{1}\bar{1}\bar{1}\}$ surface.

It appears certain that InSb undergoes anodic dissolution in 2 N HCl at current densities below $\sim 40 \text{ ma/cm}^2$ with the formation of In^{3+} and Sb^{3+} , which adds to the valence number of 6. The stoichiometry is the same for both inverse $\{111\}$ faces and also for the $\{110\}$ and $\{100\}$ planes. At current densities higher than $\sim 40 \text{ ma/cm}^2$ (for $\text{In}\{111\}$, higher than $\sim 60 \text{ ma/cm}^2$) the total electron number drops below 6, due to surface disintegration. Sb particles, colloidal in origin, are embedded in the insoluble anodic film (dark in color) with a composition mainly of $\text{Sb}_4\text{O}_5\text{Cl}_2$.

The inverse $\{111\}$ faces exhibit significant differences in anodic dissolution potential in various acidic solutions, roughly with a value from ~ 30 to ~ 50 mv. The

addition of oxidizing or reducing agents does not shift the sequence in potentials of the inverse $\{111\}$ faces within certain ranges of current density as studied. The potential of $\text{In}\{111\}$ is always nobler than that of $\text{Sb}\{\bar{1}\bar{1}\bar{1}\}$. An appreciable difference in dissolution potential in the absence of an external anodic current is also found in HCl-Fe^{3+} , with a value of ~ 40 mv.

The anodic dissolution potential in 2 N HCl of the four low-indexed crystallographic planes becomes less noble in the sequence: $\text{In}\{111\}$, $\{100\}$, $\{110\}$, $\text{Sb}\{\bar{1}\bar{1}\bar{1}\}$. The polarization curves of the four different faces undergoing anodic dissolution obey the Tafel relation over about three decades of current density ($\sim 3 \times 10^{-2}$ to ~ 30 ma/cm^2). The Tafel slopes are all nearly parallel (~ 56 $\text{mv}/\log i$ for $\text{In}\{111\}$, ~ 48 $\text{mv}/\log i$ for the last three planes). The activation energies of all four faces are close to one another (20.0 ± 0.8 Kcal/mole). This behavior suggests that the rate determining step is a one electron discharge and is the same on all the crystallographic planes.

It is also found that the dissolution potentials of the two inverse $\{111\}$ faces of InSb are much closer to that of metallic Sb than to metallic In, indicating that the latter undergoes a large chemical change during the InSb formation than Sb.

BIBLIOGRAPHY

1. Hilsum, C. and Rose-Innes, A. C., "Semiconducting III-V Compounds", p. 2, Pergamon Press, New York, Oxford, London, Paris (1961).
2. Myamlin, V. A. and Pleskov, Yu. V., "Electrochemistry of Semiconductors" (Russian translation), p. 3-5, Plenum Press, New York (1967).
3. Hilsum and Rose-Innes, op.cit., p. 5.
4. Hilsum and Rose-Innes, op. cit., p. 8.
5. Warekois, E. P. and Metzgen, P. H., J. Appl. Phys., 30, 960 (1959).
6. White, J. G. and Roth, W. C., J. Appl. Phys., 30, 946 (1959).
7. Gatos, H. C. and Lavine, M. C., J. Electrochem. Soc., 107, 427 (1960).
8. Dewald, J. F., J. Electrochem. Soc., 104, 244 (1957).
9. Gatos, H. C., Moody, P. L. and Lavine, M. C., J. Appl. Phys., 31, 212 (1960).
10. Faust Jr., J. W. and Sagar, A., J. Appl. Phys., 31, 331 (1960).
11. Lavine, M. C., Gatos, H. C. and Finn, M. C., J. Electrochem. Soc., 108, 974 (1961).
12. Holmes, P. J., "The Electrochemistry of Semiconductors", p. 329-377, Academic Press, London and New York (1962).
13. Holmes, op. cit., p. 367-375.

14. Gatos, H. C. and Lavine, M. C., J. Phys. Chem. Solid, 14, 169 (1960).
15. Holmes, op. cit., p. 290-328.
16. Holmes, op. cit., p. 164.
17. Pleskov, Yu. V., Dokl. Aked. Nauk USSR, 143, 1399 (1962).
18. Gerischer, H., Z. Electrochem., 69, 578 (1965).
19. Gerischer, H., Z. Physik. Chem. N.F. 49, 112 (1966).
20. Harvey, W. W., J. Electrochem. Soc., 114, 472 (1967).
21. Straumanis, M. E., Krumme, J.-P. and James, W. J., J. Electrochem. Soc., 115, 1050 (1968).
22. Allen, J. W., Phil. Mag., 2, 1475 (1957).
23. Holmes, op. cit., p. 345.
24. Mellor, J. W., "A Comprehensive Treatise on Inorganic and Theoretical Chemistry", Vol. IX, p. 469-484, Longmans, Green and Co., London, New York, Bombay, Calcutta, and Madras (1922).
25. Beck, F. and Gerischer, H., Z. Elektrochem., 63, 943 (1959).
26. Conway, B. E., "Theory and Principles of Electrode Process", p. 110, The Ronald Press Company, New York (1965).
27. Myamlin and Pleskov, op. cit., p. 363.
28. Mellor, op. cit., Vol. V, p. 393-397; Vol. IX, p. 378-388 and 503-509.
29. Uhlig, H. H., "Corrosion and Corrosion Control", p. 38, John Wiley & Sons, Inc., New York, London (1963).

APPENDICES

Three appendices are included in this thesis. Appendix A contains a list of materials. Appendix B contains a list of equipment and Appendix C contains the experimental data.

A. Materials

The following is a list of the materials and reagents used in this investigation:

1. InSb Single Crystals. (See p. 11).
2. Indium. High-purity (99.99+%), Cominco American Inc., Spokane, Wash.
3. Antimony. High-purity (99.99+%), American Smelting and Refining Co., South Plainfield, N. J.
4. Acid, Hydrochloric. Reagent grade, Mallinckrodt Chemical Works, St. Louis, New York, Los Angeles, Montreal.
5. Acid, Nitric. Reagent grade, Mallinckrodt Chemical Works, St. Louis, New York, Los Angeles, Montreal.
6. Acid, Acetic. Reagent grade, Mallinckrodt Chemical Works, St. Louis, New York, Los Angeles, Montreal.
7. Acid, Hydroflouric. Reagent grade, Fisher Scientific Company, Fairlawn, N. J.
8. Acid, Tartaric (Granular). Reagent grade, Mallinckrodt Chemical Works, St. Louis, New York, Los Angeles, Montreal.
9. Ferric Chloride. Purified, anhydrous-sublimed grade, Fisher Scientific Company, Fairlawn. N. J.
10. Ferrous Chloride. Reagent grade, Fisher Scientific Company, Fairlawn, N. J.
11. Potassium Ferricyanide. Reagent grade, Mallinckrodt Chemical Works, St. Louis, New York, Los Angeles, Montreal.
12. Potassium Ferrocyanide. Reagent grade, Allied Chemical & Dye Corp., New York, N.Y.

B. Equipment

The following is a list of the major components of the equipment and apparatus used in this investigation.

1. Surface preparation of InSb wafers.

a. Hand grinder. Handimet, 4-stage, Buehler No. 1470, Buehler Ltd., Evanston, Ill.

b. Polishing wheel. 2-speed. Polishing cloth: silk or nylon. Polisher: Silicon Carbide Powder (to make 3 micron slurry); Gamma Micropolish, 0.05 micron; Buehler Ltd., Evanston, Ill.

2. Apparatus for the electrolysis and potential measurements.

a. Ammeter. 3 ranges, 0-1.5 ma, 0-15 ma, 0-150 ma. Daystrom, Inc., Weston Instruments Division, Newark, N. J.

b. Multirecorder. Model 604, Simpson Electric Co., Chicago, Ill.

c. Battery, Storage. 12-volt.

d. Heater, Immersion. Knife-blade type, 115 v, 500 w, A.C., Central Scientific Co., Chicago, Ill.

e. Motor, Stirrer. 110 v, A.C.-D.C., Palo Laboratory Supplies, New York, N. Y.

f. Resistance Box. Graduated from 0-9999 ohms in 1 ohm divisions, Leeds & Northrup Co., Philadelphia, Pa., and Model DRC, graduated from 0-100Kohms in 10 Kohm divisions, Cornell-Dubilier Electronics Division, Federal Pacific Electric Co., (Fuquay, Virginia), N. C.

- g. Switch, Relay. 115 v, A.C., Fisher Scientific Co., Pittsburgh, Pa.
- h. Voltage Controller. Model 2600, Cole Parmer Co., Chicago, Ill.
- i. Thermoregulator. Graduated from 0°C-100°C in 1 degree divisions, JUMO-MS, D. B. DP., West Germany.
- j. Potentiometer. Rubicon Co., Philadelphia, Pa.
- k. Electrometer. Model 610B, Keithley Instruments, Inc., Cleveland, Ohio.
- l. Potentiostat. Wenking, ac. Brinkman Instruments, Westbury, N. Y.
- m. Recorder. Laboratory Recorder V.O.M.-5, Bausch & Lomb Incorp., Rochester, N. Y.

C. Experimental Data (Tables VIII-XXXII and XXXV-XXXVI)

TABLE VIII
 DISSOLUTION POTENTIAL OF THE INVERSE {111} FACES OF AN
 InSb SINGLE CRYSTAL VERSUS TIME WITHOUT ANODIC CURRENT
 IN 1 N HCl AT 25°C

In {111}		Sb { $\bar{1}\bar{1}\bar{1}$ }	
t (min)	E_H' (mv)*	t (min)	E_H' (mv)*
0	81	0	81
5	82	5	81
10	81	10	81
15	81	15	81
30	86	30	84
45	84	45	81
60	83	60	84
75	82	75	81
90	82	90	80
105	81	105	79
120	81	120	79

*SHE

TABLE IX
 DISSOLUTION POTENTIAL OF THE INVERSE {111} FACES OF AN
 InSb SINGLE CRYSTAL VERSUS TIME WITHOUT ANODIC CURRENT
 IN 2 N HCl AT 25°C

In {111}		Sb {111}	
t (min)	E_H' (mv)*	t (min)	E_H' (mv)*
0	52	0	47
5	52	5	47
10	51	10	47
15	51	15	47
30	47	30	49
45	43	45	49
60	48	60	51
75	51	75	51
90	46	90	49
105	44	105	51
120	44	120	50

*SHE

TABLE X
 DISSOLUTION POTENTIAL OF THE INVERSE {111} FACES OF AN
 InSb SINGLE CRYSTAL VERSUS TIME WITHOUT ANODIC CURRENT
 IN 4 N HCl AT 25°C

In {111}		Sb { $\bar{1}\bar{1}\bar{1}$ }	
t (min)	E_H' (mv)*	t (min)	E_H' (mv)*
0	-3	0	-12
5	-4	5	-14
10	-5	10	-16
15	-5	15	-18
30	-5	30	-15
45	-7	45	-11
60	-8	60	-7
75	-8	75	-13
90	-8	90	-17
105	-9	105	-16
120	-9	120	-17

*SHE

TABLE XI
 DISSOLUTION POTENTIAL OF THE INVERSE {111} FACES OF AN
 InSb SINGLE CRYSTAL VERSUS TIME WITHOUT ANODIC CURRENT
 IN 2 N HCl-0.1 N Fe³⁺ AT 25°C

In {111}		Sb ($\bar{1}\bar{1}\bar{1}$)	
t (min)	E _H ' (mv)*	t (min)	E _H ' (mv)*
0	139	0	117
5	165	5	125
10	169	10	125
15	171	15	125
30	172	30	129
45	169	45	131
60	175	60	133
75	175	75	133
90	177	90	135
105	177	105	137
120	177	120	137

*SHE

TABLE XII
 DISSOLUTION POTENTIAL OF THE INVERSE {111} FACES OF AN
 InSb SINGLE CRYSTAL VERSUS TIME WITHOUT ANODIC CURRENT
 IN 4 N HCl-0.1 N Fe³⁺ AT 25°C

In {111}		Sb {111}	
t (min)	E _H ' (mv)*	t (min)	E _H ' (mv)*
0	61	0	41
5	79	5	39
10	81	10	37
15	85	15	35
30	87	30	37
45	86	45	39
60	86	60	42
75	87	75	44
90	86	90	46
105	86	105	47
120	86	120	46

*SHE

TABLE XIII

ANODIC DISSOLUTION POTENTIAL OF THE In {111} FACE OF AN
InSb SINGLE CRYSTAL IN 2 N HCl AT 25°C

Run No. 1

i (ma/cm ²)*	E_H (mv)**	i (ma/cm ²)*	E_H (mv)**
1.42×10^{-3}	43	3.68×10^{-1}	150
2.83	54	4.53	157
5.66	65	5.66	161
8.5	74	7.1	167
1.13×10^{-2}	79	8.5	171
1.7	87	1.13×10^0	180
2.26	90	1.42	187
2.83	93	2.12	195
3.68	98	2.83	201
4.53	101	4.25	206
5.66	105	5.66	214
7.1	110	7.1	222
8.5	114	8.5	227
1.13×10^{-1}	120	1.13×10	238
1.56	127	1.42	251
2.12	135	2.26	286
2.83	143	3.4	329

*Electrode surface area = 0.353 cm^2

**SHE

Run No. 2

i (ma/cm ²)*	E_H' (mv)**	i (ma/cm ²)**	E_H' (mv)**
7.09×10^{-3}	69	9.91×10^{-1}	175
1.42×10^{-2}	81	1.84×10^0	189
1.98	86	2.41	194
4.25	100	3.4	204
5.1	102	5.1	212
9.91	118	6.23	218
1.42×10^{-1}	126	7.93	223
1.98	135	9.92	228
4.25	153	1.27×10	231
7.93	168		

*Electrode surface area = 0.353 cm^2

**SHE

TABLE XIV

ANODIC DISSOLUTION POTENTIAL OF THE Sb {111} FACE OF AN
InSb SINGLE CRYSTAL IN 2 N HCl AT 25°C

Run No. 1

i (ma/cm ²)*	E_H' (mv)**	i (ma/cm)*	E_H' (mv)**
2.83×10^{-3}	42	5.66×10^{-1}	127
5.66	47	7.1	131
8.5	49	8.5	136
1.13×10^{-2}	49	1.13×10^0	141
1.7	55	1.56	148
2.83	64	2.12	157
4.25	71	2.83	161
5.66	78	4.25	168
7.1	83	5.66	174
8.5	88	7.1	176
1.13×10^{-1}	94	8.5	181
1.7	103	1.13×10	189
2.26	109	1.7	199
2.83	114	2.83	212
4.25	122	4.25	219

*Electrode surface area = 0.353 cm^2

**SHE

Run No. 2

i (ma/cm ²)*	E_H' (mv)**	i (ma/cm ²)*	E_H' (mv)**
7.09×10^{-3}	47	3.5×10^{-1}	117
1.42×10^{-2}	53	5.1	124
1.98	60	7.94	134
3.4	67	9.91	142
4.25	73	1.7×10^0	152
5.1	75	3.5	164
9.91	90	5.1	174
1.27×10^{-1}	97	7.94	182
1.98	104	9.91	188
2.55	110	1.27×10	191

*Electrode surface area = 0.353 cm^2

**SHE

TABLE XV
ANODIC DISSOLUTION POTENTIAL OF THE {110} FACE OF AN
InSb SINGLE CRYSTAL IN 2 N HCl AT 25°C

i (ma/cm ²)*	E_H' (mv)**	i (ma/cm ²)*	E_H' (mv)**
1.22×10^{-3}	31	6.1×10^{-1}	134
2.44	37	7.32	138
3.66	41	8.55	142
6.1	48	9.75	145
8.55	52	1.1×10^0	149
1.1×10^{-2}	56	1.46	152
1.83	63	1.83	160
2.44	69	2.44	166
3.66	75	3.66	172
5.49	82	5.49	180
7.32	88	7.93	188
9.15	93	1.1×10	194
1.1×10^{-1}	96	1.46	200
1.83	107	1.83	204
2.44	113	3.05	214
3.66	122	3.66	220
4.88	129	4.88	225

*Electrode surface = 0.82 cm^2

**SHE

TABLE XVI
 ANODIC DISSOLUTION POTENTIAL OF THE {100} FACE OF AN
 InSb SINGLE CRYSTAL IN 2 N HCl AT 25°C

i (ma/cm ²)*	E_H' (mv)**	i (ma/cm ²)*	E_H' (mv)**
1.22×10^{-3}	39	6.10×10^{-1}	142
2.44	45	7.32	146
3.66	50	8.55	150
4.88	59	1.22×10^0	157
8.55	66	1.83	166
1.22×10^{-2}	75	2.44	173
1.83	81	3.66	182
2.44	83	4.88	188
3.05	87	5.50	194
4.88	96	7.32	198
6.70	101	9.15	203
9.15	108	1.22×10	207
1.22×10^{-1}	113	1.83	216
1.83	121	2.44	222
2.44	126	3.66	229
3.05	130	4.88	242
3.66	133	6.10	261
4.88	138		

*Electrode surface area = 0.82 cm²

**SHE

TABLE XVII
 ANODIC DISSOLUTION POTENTIAL OF THE In{111} FACE OF AN
 InSb SINGLE CRYSTAL IN 1 N HNO₃-1 N H₂C₄H₄O₆
 AT 25°C

i (ma/cm ²)*	E_H' (mv)**	i (ma/cm ²)*	E_H' (mv)**
1.65×10^{-3}	139	6.61×10^{-1}	217
3.31	152	8.26	224
4.96	158	9.91	230
6.61	162	1.65×10^0	248
9.91	168	3.31	275
1.65×10^{-2}	173	4.96	294
2.48	175	6.61	306
4.14	178	8.26	314
6.61	183	9.91	320
8.26	185	1.65×10	340
1.16×10^{-1}	189	3.31	369
1.65	193	4.96	393
3.31	203	6.61	435
4.96	210		

*Electrode surface area = 0.60 cm²

**SHE

TABLE XVIII
ANODIC DISSOLUTION POTENTIAL OF THE Sb{111} FACE OF AN
InSb SINGLE CRYSTAL IN 1 N HNO₃-1 N H₂C₄H₄O₆
AT 25°C

i (ma/cm ²)*	E_H' (mv)**	i (ma/cm ²)*	E_H' (mv)**
1.22 × 10 ⁻³	131	2.44 × 10 ⁻¹	197
2.44	141	4.26	202
3.66	148	6.10	203
4.88	153	9.15	208
8.55	162	1.22 × 10 ⁰	210
1.22 × 10 ⁻²	165	2.44	223
1.83	168	4.26	238
2.44	169	6.10	248
3.05	171	9.15	265
4.88	177	1.22 × 10	277
8.55	185	2.44	311
1.22 × 10 ⁻¹	188		

*Electrode surface area = 0.82 cm²

**SHE

TABLE XIX
 ANODIC DISSOLUTION POTENTIAL OF THE In{111} FACE OF AN
 InSb SINGLE CRYSTAL IN 2 N HCl-0.0004 M Fe³⁺
 AT 25°C

i (ma/cm ²)*	E_H' (mv)**	i (ma/cm ²)*	E_H' (mv)**
2.83×10^{-3}	45	1.56×10^0	165
7.1	50	1.98	171
1.13×10^{-2}	53	2.55	177
2.83	62	3.4	185
5.66	74	4.25	191
8.5	84	5.66	199
1.13×10^{-1}	92	7.1	205
1.98	108	7.93	208
2.55	116	8.5	210
3.4	125	9.92	215
4.25	131	1.13×10	220
5.66	140	1.42	228
7.1	145	1.7	236
8.5	149	1.84	240
1.13×10^0	157	1.98	243

*Electrode surface area = 0.353 cm²

**SHE

TABLE XX
 ANODIC DISSOLUTION POTENTIAL OF THE Sb {111} FACE OF AN
 InSb SINGLE CRYSTAL IN 2 N HCl-0.0004 M Fe³⁺
 AT 25°C

i (ma/cm ²)*	E_H' (mv)**	i (ma/cm ²)*	E_H' (mv)**
2.83×10^{-2}	61	4.25×10^0	156
5.66	66	5.1	162
8.5	73	6.24	167
1.13×10^{-1}	76	7.1	170
1.98	86	8.5	174
2.83	92	9.92	178
4.25	101	1.13×10	182
5.66	106	1.27	185
7.1	112	1.42	187
8.5	116	1.56	191
1.13×10^0	123	1.70	193
1.7	133	1.84	195
2.55	143	1.98	197
3.4	150		

*Electrode surface area = 0.353 cm²

**SHE

TABLE XXI
 ANODIC DISSOLUTION POTENTIAL OF THE In{111} FACE OF AN
 InSb SINGLE CRYSTAL IN 2 N HCl-0.002 M Fe³⁺
 AT 25°C

i (ma/cm ²)*	E_H' (mv)**	i (ma/cm ²)*	E_H' (mv)**
2.83×10^{-3}	61	1.13×10^0	146
5.66	61	1.98	161
1.13×10^{-2}	62	2.83	171
5.66	71	4.25	182
1.13×10^{-1}	76	5.66	192
2.83	109	7.1	198
4.25	121	8.5	203
5.66	127	1.13×10	210
7.1	135	1.98	228
8.5	138		

*Electrode surface area = 0.353 cm^2

**SHE

TABLE XXII
 ANODIC DISSOLUTION POTENTIAL OF THE Sb{ $\bar{1}\bar{1}\bar{1}$ } FACE OF AN
 InSb SINGLE CRYSTAL IN 2 N HCl-0.002 M Fe³⁺
 AT 25°C

i (ma/cm ²)*	E_H' (mv)**	i (ma/cm ²)*	E_H' (mv)**
2.83×10^{-2}	68	1.13×10^0	121
5.66	71	1.7	130
1.13×10^{-1}	78	2.55	139
1.56	82	3.97	150
2.12	86	5.1	156
2.83	91	6.24	161
4.25	99	7.1	164
5.66	104	8.5	169
7.1	114	9.92	173
8.5	114	1.13×10	177
		1.98	191

*Electrode surface area = 0.353 cm²

**SHE

TABLE XXIII
 ANODIC DISSOLUTION POTENTIAL OF THE In {111} FACE OF AN
 InSb SINGLE CRYSTAL IN 2 N HCl-0.002 M Fe²⁺
 AT 25°C

i (ma/cm ²)*	E_H' (mv)**	i (ma/cm ²)*	E_H' (mv)**
1.13×10^{-2}	65	1.98×10^0	152
2.83	68	2.83	164
5.66	71	5.66	187
8.50	74	8.5	202
1.13×10^{-1}	76	1.13×10	213
2.83	93	1.98	238
5.66	109	2.83	257
8.50	124	4.25	281
1.13	133	5.66	305

*Electrode surface area = 0.353 cm²

**SHE

TABLE XXIV
 ANODIC DISSOLUTION POTENTIAL OF THE Sb {111} FACE OF AN
 InSb SINGLE CRYSTAL IN 2 N HCl-0.002 M Fe²⁺
 AT 25°C

i (ma/cm ²)*	E_H' (mv)**	i (ma/cm ²)*	E_H' (mv)**
2.83×10^{-2}	68	2.83×10^0	142
5.66	75	4.25	157
8.5	80	5.66	165
1.13×10^{-1}	83	7.1	171
1.98	90	8.5	178
2.83	96	9.92	182
4.25	104	1.13×10	185
7.1	114	1.7	198
1.13×10^0	124	2.26	207
1.7	131	2.83	215
2.27	138	4.25	237

*Electrode surface area = 0.353 cm²

**SHE

TABLE XXV

ANODIC DISSOLUTION POTENTIAL OF THE In{111} FACE OF AN
InSb SINGLE CRYSTAL IN 2 N HCl-0.00125 M $K_3Fe(CN)_6$
AT 25°C

i (ma/cm ²)*	E_H' (mv)**	i (ma/cm ²)*	E_H' (mv)**
1.13×10^{-2}	62	1.13×10^0	137
2.83	65	1.56	147
7.1	70	2.12	157
1.13×10^{-1}	76	2.83	166
1.98	88	4.25	182
2.83	95	5.66	193
4.25	107	7.1	207
5.66	115	8.5	218
7.1	122	9.92	232
8.5	128	1.13×10	265

*Electrode surface area = 0.353 cm^2

**SHE

TABLE XXVI
 ANODIC DISSOLUTION POTENTIAL OF THE Sb $\{\bar{1}\bar{1}\bar{1}\}$ FACE OF AN
 InSb SINGLE CRYSTAL IN 2 N HCl-0.00125 M $K_3Fe(CN)_6$
 AT 25°C

i (ma/cm ²)*	E_H' (mv)**	i (ma/cm ²)*	E_H' (mv)**
2.83×10^{-2}	65	1.98×10^0	138
7.1	71	2.83	149
1.13×10^{-1}	76	4.25	164
1.98	84	5.66	178
2.83	90	7.1	196
4.25	98	8.5	219
5.66	105	9.92	246
7.1	111	1.13×10	279
1.13×10^0	122		

*Electrode surface area = 0.353 cm^2

**SHE

TABLE XXVII

ANODIC DISSOLUTION POTENTIAL OF THE In{111} FACE OF AN
InSb SINGLE CRYSTAL IN 2 N HCl-0.00125 M $K_4Fe(CN)_6$
AT 25°C

i (ma/cm ²)*	E_H' (mv)**	i (ma/cm ²)*	E_H' (mv)**
1.13×10^{-2}	72	5.66×10^{-1}	205
2.83	81	7.1	210
5.66	87	8.5	216
8.5	91	1.13×10^0	229
1.13×10^{-1}	96	1.7	261
1.98	105	2.27	281
2.83	113	2.83	305
4.25	136	3.54	326

*Electrode surface area = 0.353 cm²

**SHE

TABLE XXVIII
 ANODIC DISSOLUTION POTENTIAL OF THE Sb {111} FACE OF AN
 InSb SINGLE CRYSTAL IN 2 N HCl-0.00125 M $K_4Fe(CN)_6$
 AT 25°C

i (ma/cm ²)*	E_H' (mv)**	i (ma/cm ²)*	E_H' (mv)**
1.13×10^{-2}	66	7.1×10^{-1}	143
2.83	76	8.5	199
5.66	82	1.13×10^0	203
8.5	88	1.42	211
1.13×10^{-1}	91	2.83	298
1.98	101	4.25	337
2.83	107	5.66	340
5.66	124		

*Electrode surface area = 0.353 cm²

**SHE

TABLE XXIX
 ANODIC DISSOLUTION POTENTIAL OF THE In{111} FACE OF AN
 InSb SINGLE CRYSTAL IN 2 N HCl AT 35°C

i (ma/cm ²)*	E_H' (mv)**	i (ma/cm ²)*	E_H' (mv)**
2.83×10^{-2}	73	2.83×10^0	169
5.66	81	3.68	175
8.5	87	4.53	180
1.13×10^{-1}	94	5.66	185
1.7	102	7.1	193
2.26	108	8.5	198
2.83	113	1.13×10	207
3.54	118	1.56	217
4.53	123	2.12	227
5.66	128	2.83	237
7.1	134	3.54	245
8.5	138	4.53	254
1.13×10^0	145	5.66	262
1.56	153	7.1	274
2.12	161		

*Electrode surface area = 0.353 cm^2

**SHE

TABLE XXX

ANODIC DISSOLUTION POTENTIAL OF THE In{111} FACE OF AN
InSb SINGLE CRYSTAL IN 2 N HCl AT 45°C

i (ma/cm ²)*	E_H' (mv)**	i (ma/cm ²)*	E_H' (mv)**
8.5×10^{-3}	21	2.12×10^0	136
1.42×10^{-2}	25	3.4	143
2.83	32	7.1	149
5.66	44	9.9	163
8.5	53	1.56×10	180
1.42×10^{-1}	63	2.12	191
2.26	76	3.4	213
4.25	91	3.97	217
7.1	104	4.53	219
1.13×10^0	119		

*Electrode surface area = 0.353 cm^2

**SHE

TABLE XXXI

ANODIC DISSOLUTION POTENTIAL OF THE Sb $\{\bar{1}\bar{1}\bar{1}\}$ FACE OF AN
InSb SINGLE CRYSTAL IN 2 N HCl AT 35°C

i (ma/cm ²)*	E_H' (mv)**	i (ma/cm ²)*	E_H' (mv)**
1.13×10^{-2}	42	7.1×10^{-1}	108
1.98	46	8.5	110
2.83	50	1.13×10^0	117
4.25	55	1.7	125
5.66	59	2.26	133
7.08	63	2.83	139
8.5	64	3.4	141
9.9	66	5.1	151
1.42×10^{-1}	73	8.5	160
1.98	80	1.42×10	169
2.55	86	2.12	178
3.4	92	4.25	194
4.53	97	5.66	200
5.66	102		

*Electrode surface area = 0.353 cm^2

**SHE

TABLE XXXII

ANODIC DISSOLUTION POTENTIAL OF THE Sb{ $\bar{1}\bar{1}\bar{1}$ } FACE OF AN
InSb SINGLE CRYSTAL IN 2 N HCl AT 45°C

i (ma/cm ²)*	E_H' (mv)**	i (ma/cm ²)*	E_H' (mv)**
4.25×10^{-3}	9	5.66×10^{-1}	81
5.66	12	8.5	90
8.5	15	1.13×10^0	96
1.13×10^{-2}	18	1.42	101
1.7	23	2.4	111
2.83	31	7.1	136
4.25	37	9.9	141
5.66	42	1.42×10	149
7.1	45	1.98	156
1.13×10^{-1}	53	2.83	164
1.98	63	3.97	172
2.83	73		

*Electrode surface area = 0.353 cm²

**SHE

TABLE XXXV
ANODIC DISSOLUTION POTENTIAL OF METALLIC INDIUM IN 2 N HCl
AT 25°C

i (ma/cm ²)*	E_H' (mv)**	i (ma/cm ²)*	E_H' (mv)**
1.22 × 10 ⁻²	-524	1.22 × 10	-465
3.66	-520	1.46	-462
4.88	-516	2.44	-454
7.32	-514	3.05	-447
1.46 × 10 ⁻¹	-510	3.66	-442
1.83	-508	4.27	-438
2.42	-505	4.88	-433
3.66	-502	5.49	-428
6.1	-499	6.1	-423
8.55	-494	6.7	-417
1.22 × 10 ⁰	-490	7.32	-414
2.44	-484	7.93	-409
4.27	-477	8.55	-405
6.1	-474	9.15	-402
8.55	-470	9.75	-398

*Electrode surface area = 0.353 cm²

**SHE

TABLE XXXVI
ANODIC DISSOLUTION POTENTIAL OF METALLIC ANTIMONY IN 2 N HCl
AT 25°C

i (ma/cm ²)*	E_H' (mv)**	i (ma/cm ²)*	E_H' (mv)**
6.1×10^{-3}	104	1.22×10^0	156
1.22×10^{-2}	114	2.44	163
3.05	127	4.88	169
6.1	136	7.32	175
9.15	140	9.75	180
1.22×10^{-1}	142	1.22×10	187
3.05	148	1.53	200
6.1	154	1.71	1,200***
9.15	155		

*Electrode surface area = 0.82 cm²

**SHE

***Fluctuated

VITA

The author, Lih-da Hu, was born on June 6, 1942 in Szuchuan, China. He received his elementary and high school education in Keelung, Taiwan. In June, 1963 he graduated from Chung-Yuan Christian College of Science and Engineering in Taiwan with the degree of Bachelor of Science in Chemical Engineering. After that he served in the Chinese Army for a period of one year. From October, 1964 to August, 1966 he was employed by the "Urea and Ammonia Plant, Mobil China Allied Chemical Industries Ltd." in Taiwan.

He entered the University of Missouri-Rolla in September, 1966 as a graduate student in the Chemical Engineering Department.